Modelling and Analysis of Peroxiredoxin Kinetics for Systems Biology Applications

---

Beatrice Demelza Eagling

BSc. (*Hons*) Genetics

Submitted in fulfilment of the academic requirements for the degree of Master of Science in the School of Life Sciences
University of KwaZulu-Natal
Pietermaritzburg

As the candidate's supervisor I have approved this dissertation for submission.

Signed: _____ Name: Dr C.S Pillay Date: _____

Preface

The experimental work described in this dissertation was carried out at School of Life Sciences, University of KwaZulu-Natal, Pietermaritzburg, from February 2014 to November 2015 under the supervision of Dr C.S. Pillay.

These studies represent original work by the author and have not otherwise been submitted in any form to another University. Where use has been made of the work by other authors it has been duly acknowledged in the text.

Signed:

_____

Beatrice Eagling

November 2015

College of Agriculture, Engineering and Science

Declaration of Plagiarism

I, Beatrice Eagling declare that:

1. The research reported in this thesis, except where otherwise indicated is my original research.
2. This thesis has not been submitted for any degree or examination at any other university.
3. This thesis does not contain other persons' data, pictures, graphs or other information, unless specifically acknowledged as being sourced from other persons.
4. This thesis does not contain other persons' writing, unless specifically acknowledged as being sourced from other researchers. Where other written sources have been quoted, then:
a. Their words have been re-written but the general information attributed to them has been referenced.
b. Where their exact words have been used, then their writing has been placed in italics and inside quotation marks, and referenced.
5. This thesis does not contain text, graphics or tables copied and pasted from the Internet, unless specifically acknowledged, and the source being detailed in the thesis and in the References sections.

Signed:

_____

November 2015

Abstract

Oxidative stress, caused by reactive oxygen species (ROS) such as hydrogen peroxide, can have harmful effects on important cellular components and processes which can lead to cell death. Cells have evolved extensive protein and non-protein antioxidant molecules to deal with hydrogen peroxide but it is now clear that hydrogen peroxide is also important signal molecule. It is not fully understood how cells maintain the balance between hydrogen peroxide detoxification and signal transduction. Peroxiredoxins are a ubiquitous family of antioxidant proteins that are the primary reductants of hydrogen peroxide and appear to be key molecules in mediating this balance. Using catalytic cysteines, peroxiredoxins reduce hydrogen peroxide and other ROS and in turn are reduced by thioredoxin and thioredoxin reductase. This coupled set of reactions collectively constitute the peroxiredoxin system and its precise role in redox signalling could be established using systems biology studies. However, there are some discrepancies on how peroxiredoxins should be described in these studies as three distinct kinetic models have been proposed for peroxiredoxin activity: the ping-pong enzyme, redox couple monomer and redox couple homodimer models. Further, different rate constants for hydrogen peroxide reduction by peroxiredoxins have been reported using steady state and competition assays and it is not clear which of these parameters should be used in computational models. In order to resolve these discrepancies, the three proposed peroxiredoxin kinetic models were simulated with core parameters and showed different responses to parameter changes. Computational modelling with *in vitro* datasets confirmed this result and also showed that many of the reported peroxiredoxin kinetic parameters have limited predictive value. Thus, the kinetic models for peroxiredoxin activity cannot be used interchangeably and computational models based on the reported peroxiredoxin kinetic parameters for hydrogen peroxide reduction should be viewed with caution. To confirm this result, the cytosolic peroxiredoxin thiol-specific antioxidant 1 (TSA1) from *Saccharomyces cerevisiae* was cloned, expressed and purified for *in vitro* analysis of this system. Data fitting of the peroxiredoxin kinetic models determined parameters that were able to predict independent datasets with increasing thioredoxin and peroxiredoxin concentrations using the ping-pong enzyme and redox couple monomer models but the redox couple homodimer model was unable to fit these datasets. A complex flux control pattern was also determined for the fitted models and whole system fitting to *in vitro* datasets is proposed to be a more accurate method for parameter determination for the peroxiredoxin system kinetic assays.

Acknowledgements

I would like to thank my supervisor, Dr. Ché Pillay, for your guidance, patience and support over the years. I am truly grateful for all of your help and encouragement which has allowed me to grow and improve tremendously as a scientist. I have enjoyed being a member of your lab and will cherish the time I spent there.

Thank you to the former and present members of Lab B23- Tersh, Lee, Mamoe, Nolyn, Scott, Nicky, Bianca, Bevika, Jezelle, Jess and Ryan. Working in the lab everyday was so much more enjoyable because of each of you. I would like to give a special mention to Tersh, who helped me enormously by sharing her thioredoxin clones with me and also many of the methods I used throughout my project. Thank you so much Tersh for being there for me, I'm not sure I would have got through it all without you! Also, thank you to Mamoe for sharing her thioredoxin reductase clones.

To Megan, thank you for all of your technical support in the department. To Goodman, thank you for all your help around the lab and for your positive attitude to all things. To Lauren Eyssen, thank you so much for taking the time to help us out with all your biochemistry knowledge. Thank you to the admin staff in the school of Life Sciences and in particular Patricia Joubert. To Mary, Bridget, Ashrenee, Courtnee, Sihle, Jimmy, Simba and all my other friends in the genetics department and in my life, thank you for your love and support.

I would like to thank the National Research Foundation for supplying me with funding to continue my postgraduate studies.

To my amazing parents, John and Jessie, your support throughout my studies has allowed me to pursue my dreams and I hope I have made you both proud. To my sisters Chaz and Angela, you may both be on the other side of the world but all your messages and phone calls gave me the strength to keep going. To my little brother Johannes, I have missed out on seeing you become the young man that you are but I hope I have at least been a good role model to you. To my niece and nephews, Raya, Nathan and new addition Benji, there is no greater joy in my life than being your Aunt. To Afam and his family, thank you for welcoming me into your family and for all your support during my time in South Africa.

List of Abbreviations

AEBSF	4-(2-aminoethyl) benzenesulfonyl fluoride hydrochloride
Ahp	alkyl hydroperoxide reductase
BN-PAGE	Blue native- polyacrylamide gel electrophoresis
BSA	Bovine serum albumin
DNA	Deoxyribonucleic acid
dNTPs	deoxyribonucleotides
DTNB	5, 5'-dithiobis (2-nitrobenzoic acid)
DTT	Dithiothreitol
EDTA	Ethylene diamine tetraacetic acid
Gpx3	Glutathione peroxidase-like protein 3
H_2O_2	Hydrogen peroxide
HRP	Horse radish peroxidase
IPTG	Isopropyl β-D-1-thiogalactopyranoside
k_{cat}	Turnover number
k_{cat}/K_m	Enzyme catalytic efficiency
K_m	Michaelis constant
LB	Luria Bertani
MsrA	Methionine sulfoxide reductase A
NADPH	β-nicotinamide adenine dinucleotide phosphate
Nox	NADPH oxidase
ODE	Ordinary Differential Equation
PAPS	3'-phosphoadenosine 5'-phosphosulfate
PCR	Polymerase Chain Reaction
Prdx	Peroxiredoxin
PRX	Peroxiredoxin
Prx_{SH}/Prx_{SS}	Reduced/Oxidised peroxiredoxin
PTP	Protein tyrosine phosphatase
PySCeS	Python Simulator of Cellular Systems
r^2	Regression coefficient
RNS	Reactive nitrogen species
RNR	Ribonucleotide reductase
ROS	Reactive oxygen species

SDS-PAGE	Sodium dodecyl sulfate-polyacrylamide gel electrophoresis
SRX	Sulfiredoxin
TEMED	*N*, *N*, *N*', *N*'-tetramethylethylenediamine
TPX	Thiol/thioredoxin peroxidase
TR	Thioredoxin reductase
TRR1	Thioredoxin reductase 1
TRX	Thioredoxin
Trxl1	Thioredoxin-like protein 1
Trx_{SH}/Trx_{SS}	Reduced/Oxidised thioredoxin
TSA1	Thiol-specific antioxidant 1
YPD	Yeast peptone dextrose

Table of Contents

List of Tables

List of Figures

μM thioredoxin reductase and 1 μM peroxiredoxin and 30 μM hydrogen peroxide in a reaction buffer pH 7.0. The results are representative of three replicate experiments and where standard errors are not visible they are smaller than the symbol (*n*=3).

Figure 4.4 Fitted peroxiredoxin kinetic models based on the ping-pong (A) and redox couple mechanisms (B) can predict independent *in vitro* datasets. Steady state assays were carried out with 150 μM NADPH, 0.5 μM thioredoxin reductase, 30 μM hydrogen peroxide in a reaction buffer pH 7.0 at varying thioredoxin (0-15 μM) and peroxiredoxin (0.5, 1 and 2 μM) concentrations. The standard errors for the datasets are shown (*n* =3).

Figure 4.5 The fitted ping-pong enzyme and redox couple monomer models show similar responses to increasing thioredoxin reductase (A) and peroxiredoxin concentrations (B). The ping-pong enzyme and redox couple monomer model datasets overlap in (B).

Figure 4.6 Simulation of the fitted ping-pong enzyme and redox couple monomer models yielded similar predictions on the redox state of thioredoxin with increasing thioredoxin reductase (A), peroxiredoxin (B) and hydrogen peroxide concentrations (C). The ping-pong enzyme and redox couple monomer model datasets overlap in (A), (B) and (C).

Figure 4.7 The fitted ping-pong enzyme and redox couple monomer models showed distinct responses to increasing hydrogen peroxide concentrations.

Figure 4.8 Flux control in the fitted redox couple monomer models was determined with varying thioredoxin concentrations for the human erythrocyte peroxiredoxin 2 (A), *C. crescentus* peroxiredoxin (B) and *S. cerevisiae* TSA1 (C) peroxiredoxin systems. At lower thioredoxin concentrations, peroxiredoxin reduction (reaction 3) was rate-limiting but as its concentration increased hydrogen peroxide reduction (reaction 2) became rate-limiting.

Figure S1 Standard curve for molecular weight sizing of native peroxiredoxin on a BN-PAGE 4-13% gradient gel using the molecular weight kit for non-denaturing PAGE (Sigma).

Chapter 1

1.1 Introduction

Aerobic life forms have evolved to utilise oxygen for respiration and other metabolic processes (Apel and Hirt, 2004; Halliwell, 2006; D'autreaux and Toledano, 2007; Weidinger and Kozlov, 2015). However, incomplete reduction of oxygen generates reactive free radical and non-radical species (ROS), such as the hydroxyl radical ($OH^{\cdot}$) and hydrogen peroxide which can damage lipids, protein and DNA (Figure 1.1, Apel and Hirt, 2004; D'autreaux and Toledano, 2007; Pham-Huy *et al.*, 2008a). Cells have evolved extensive protein and non-protein antioxidant systems to tackle ROS and maintain cellular redox homeostasis and an imbalance between ROS production and detoxification was proposed to be a central feature of many diseases including cancer (Schumacker, 2006; Liou and Storz, 2010) and aging (Liochev, 2013). Despite their toxicity, ROS have recently been identified as important signalling molecules in spite of these antioxidant systems and thus, the simple idea of a redox balance in oxidative stress is being modified (D'autreaux and Toledano, 2007; Veal *et al.*, 2007; Pham-Huy *et al.*, 2008a; Weidinger and Kozlov, 2015). The complexity of redox homeostasis and the necessity for low levels of ROS has also been shown by the failure of antioxidant therapies (Firuzi *et al.*, 2011) which may actually be detrimental and accelerate disease progression (Ristow *et al.*, 2009; Sayin *et al.*, 2014).

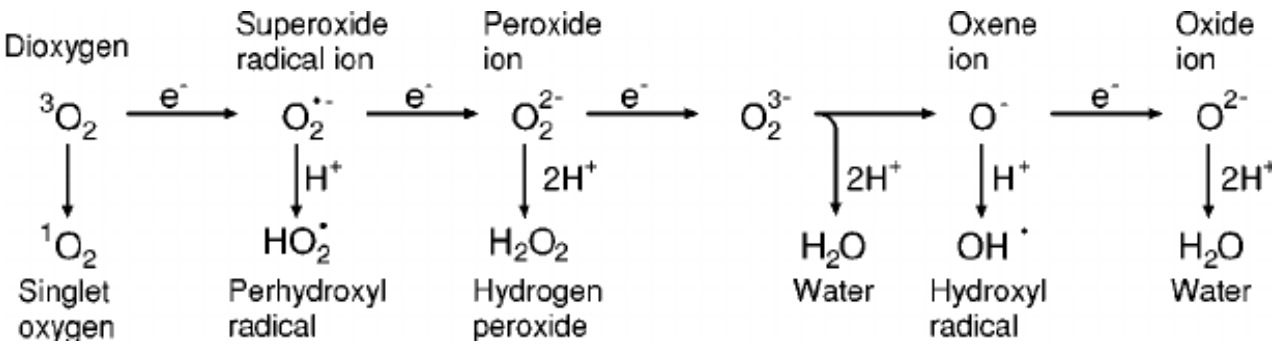

Figure 1.1 Ground state oxygen (O_2) is reduced sequentially through energy transfer and electron transfer reactions to more reactive species such as the highly reactive hydroxyl radical ($OH^{\cdot}$) (Taken from Apel and Hirt, 2004).

When compared to other ROS, hydrogen peroxide is less reactive but relatively stable with a half-life of ~10^{-3} s and appears to play a role in a number of important cellular processes such as activation of mitogen-activated protein kinases (MAPK) (Bhat and Zhang,

1999; Park *et al.*, 2005) and redox-dependent signalling (D'autreaux and Toledano, 2007; Veal *et al.*, 2007; Veal and Day, 2011; Boronat *et al.*, 2014). Intracellular hydrogen peroxide production results from oxidative phosphorylation in the mitochondria but can be specifically catalysed by a number of processes including growth factor stimulation of the membrane protein NADPH oxidase (Nox) (Figure 1.2, Finkel, 2011; Veal *et al.,* 2007). Hydrogen peroxide diffusion across membranes can also occur via aquaporins (Bienert *et al.*, 2006). Excessive hydrogen peroxide levels can lead to oxidative stress and causes damage to DNA (see for example Driessens *et al.*, 2009), proteins (see for example Cabiscol *et al.*, 2000) and lipids (see for example Siddique *et al.*, 2012). It is not clear how cells mediate the balance between hydrogen peroxide detoxification and hydrogen peroxide-dependent signalling.

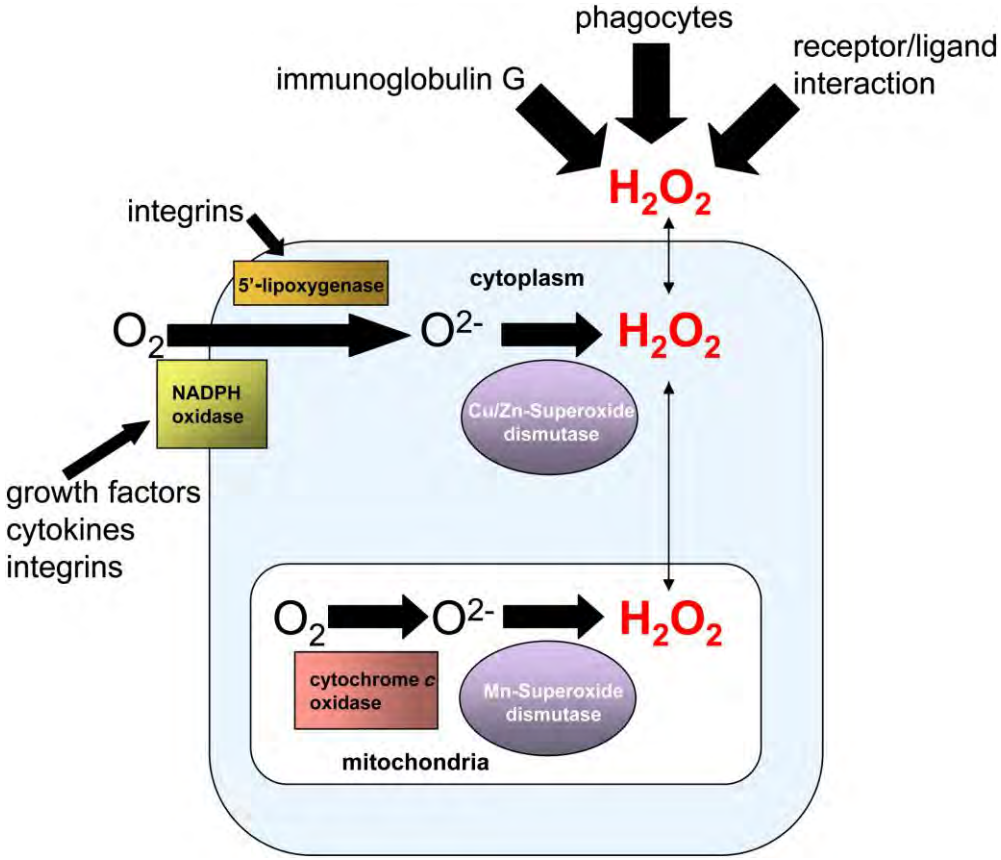

Figure 1.2 Intracellular and extracellular processes can result in hydrogen peroxide production. Growth factors and cytokines can purposefully stimulate intracellular hydrogen peroxide production. Oxygen diffusion into cells and partial oxygen reduction in mitochondria creates highly reactive superoxide molecules that are catalysed by superoxide dismutases into a less harmful hydrogen peroxide molecule. Phagocytic immune cell activity can produce hydrogen peroxide, which then diffuses across membranes into other cells (Taken from Veal *et al.,* 2007).

1.2 Cellular defences against hydrogen peroxide

Antioxidant activity can be classed as enzymatic and non-enzymatic (Young and Woodside, 2001; Pham-Huy *et al.*, 2008b). Non-enzymatic antioxidants include ascorbate and glutathione which are not considered primary hydrogen peroxide scavengers because of their low reactivity (Winterbourn, 2008). Catalases are one of the most well-studied enzymatic antioxidants and were long thought to be the most important catalysts for hydrogen peroxide detoxification (Masuoka *et al.*, 1996; Chelikani *et al.*, 2004) although it now recognised that they are more effective at relatively high hydrogen peroxide concentrations because they use a disproportion reaction mechanism (Mishra and Imlay, 2012). Peroxiredoxins are considered the primary reductants of hydrogen peroxide at the prevailing intracellular hydrogen peroxide concentrations. The cytosolic peroxiredoxin known as thiol-specific antioxidant 1 (TSA1) was first discovered in *Saccharomyces cerevisiae* (Chae and Rhee, 1994) and was the focus of this study.

1.2.1 Peroxiredoxins are part of the thioredoxin antioxidant superfamily

The redoxins, thioredoxin, glutaredoxin and peroxiredoxin, are members of the highly conserved thioredoxin antioxidant protein family and all contain a characteristic thioredoxin-fold in their structure (Martin, 1995). Thioredoxins are small, heat stable proteins that contain a highly conserved dithiol active site motif (Arner and Holmgren, 2000) and were first discovered for their role as electron donors to ribonucleotide reductase (RNR) in deoxyribonucleotide synthesis (Laurent *et al.*, 1964). In addition to RNR, thioredoxins reduce a number of protein and non-protein targets including peroxiredoxins and are subsequently reduced by thioredoxin reductase and β-nicotinamide adenine dinucleotide phosphate (NADPH) (Figure 1.3). Thioredoxins are also involved in redox signalling processes during non-stress conditions by inactivating apoptosis signal-regulating kinase-1 (ASK1) (Liu *et al.*, 2006), while during oxidative stress, thioredoxins interact with oxidative stress repair proteins such as methionine sulfoxide reductase A (MsrA) to facilitate repair (Olry *et al.*, 2004).

Glutaredoxins are structurally similar to thioredoxins as they are also small heat-stable proteins and are classed as monothiol or dithiol based on the number of cysteine residues in their active site (Holmgren, 1988; Lillig *et al.*, 2008). Although functionally similar to

thioredoxin, glutaredoxins uniquely interact with glutathione (GSH) via glutathione reductase to alter the activity of specific proteins through the glutathionylation/deglutathionylation cycle (Mieyal *et al.*, 2008; Grek *et al.*, 2013).

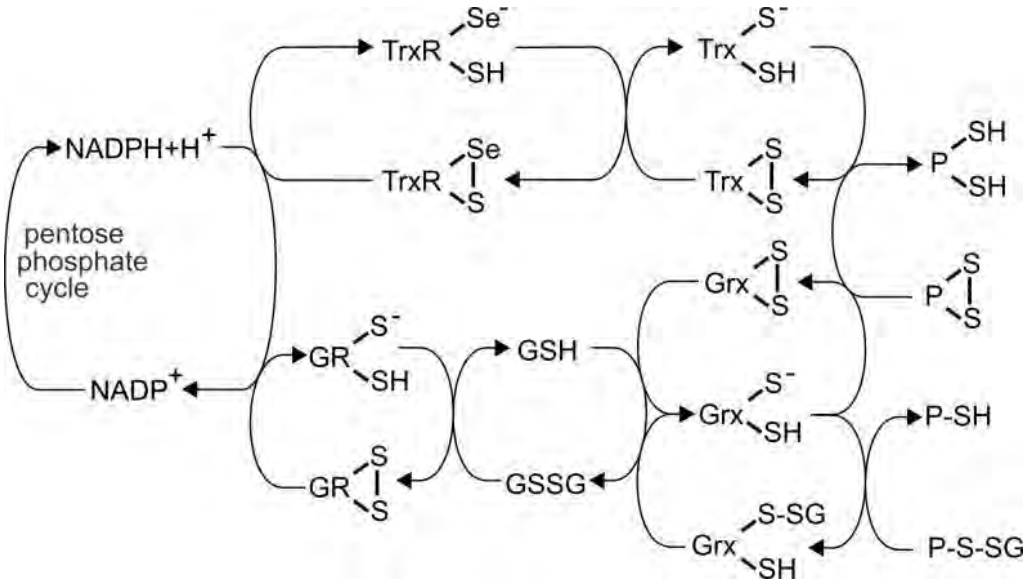

Figure 1.3 NADPH acts as an electron source for the thioredoxin system (Trx) via thioredoxin reductase (TrxR) and the glutaredoxin system (Grx) via glutaredoxin reductase (GR) and glutathione (GSH). Reduced thioredoxin and glutaredoxin then reduce a number of protein targets such as peroxiredoxins (Taken from Hanschmann *et al.*, 2013).

Peroxiredoxins are classed as 1-Cys or 2-Cys, depending on the number of highly conserved active site cysteine residues directly involved in their action (Wood *et al.*, 2003b; Hall *et al.*, 2009). As the primary cellular hydrogen peroxide reductants, peroxiredoxins play a key role in maintaining redox balance, in oxidative stress defence and can also reduce reactive nitrogen species (RNS) (Hall *et al.*, 2009; Poole *et al.*, 2011; Perkins *et al.*, 2015). Deletions of different peroxiredoxin genes have also revealed their role in a number of important cellular processes including regulating DNA damage checkpoints and maintaining genome stability (Chabes *et al.*, 2003; Iraqui *et al.*, 2009).

Although long considered enzymes in their own right, there is growing acceptance that redoxin activity and regulation depends on the kinetic linkages to their cognate systems (Figure 1.3). For example, in the peroxiredoxin system, reducing equivalents from NADPH are transferred to thioredoxin via thioredoxin reductase and in turn thioredoxin reduces peroxiredoxin which can than reduce a range of peroxide substrates (Chae *et al.*, 1994a). Disruption of thioredoxin reductase or thioredoxin can therefore effect peroxiredoxin activity

in vivo (Trotter *et al.*, 2008; Ragu *et al.*, 2014). The activity and functions of peroxiredoxins will be discussed below.

1.3 Peroxiredoxin kinetic mechanism and structure

As previously mentioned, the main role of peroxiredoxins is hydrogen peroxide degradation at physiological levels of hydrogen peroxide to maintain redox homeostasis. In addition, at high hydrogen peroxide levels (>1 mM), peroxiredoxins can become inactivated by hyperoxidation and undergo structural and functional changes to form high molecular weight super chaperones to defend against oxidative stress (Lim *et al.*, 2008; König *et al.*, 2013; Radjainia *et al.*, 2015).

Peroxiredoxins have also been found to be key mediators in redox signalling processes (Brown *et al.*, 2013; Park *et al.*, 2014; Sobotta *et al.*, 2015) and have also been linked with a number of pathologies including malaria (Kawazu *et al.*, 2008), tuberculosis (see for example Koshkin *et al.*, 2004) and cancer (see for example Wang *et al.*, 2005). Understanding the role of peroxiredoxins under normal and pathogenic conditions may therefore provide insight into redox signalling and pathologies associated with peroxiredoxin activity. The multifunctional activity of peroxiredoxins will be discussed in greater detail below.

1.3.1 Hydrogen peroxide reduction by peroxiredoxins

At physiological hydrogen peroxide concentrations (<1 mM), the peroxidatic cysteine residue of peroxiredoxin will form a sulfenic intermediate (-SOH) whilst reducing hydrogen peroxide to water (Figure 1.4). This cysteine residue will then form a disulfide bond with a resolving cysteine, before being reduced by thioredoxin to its active reduced form (-SH) (Wood *et al.*, 2003a).

In eukaryotic cells, peroxiredoxin activity is directly regulated by the prevailing hydrogen peroxide concentration (Figure 1.4). Eukaryotic peroxiredoxins have two modes of action based on 'normal' physiological or stress-inducing hydrogen peroxide concentrations (>1 mM) (Day *et al.*, 2012; Karplus and Poole, 2012). Disulfide bond formation between the peroxidatic cysteine and the resolving cysteine is a relatively slow reaction and at high hydrogen peroxide concentrations, in eukaryotic and some bacterial peroxiredoxins, the sulfenic acid can instead further react with hydrogen peroxide to form a hyperoxidised

sulfinic acid (-SO_2H). Efficient peroxiredoxin hyperoxidation by hydrogen peroxide has been reported to occur only in the presence of a recycling system (Cao *et al.*, 2014) and the resulting sulfinic acid cannot be regenerated by thioredoxin and instead requires an ATP-dependent reaction with sulfiredoxin (Biteau *et al.*, 2003). A further oxidation reaction of the sulfinic acid with hydrogen peroxide can also occur and irreversibly produces a sulfonic acid, which cannot be reduced (-SO_3H) (Lim *et al.*, 2008).

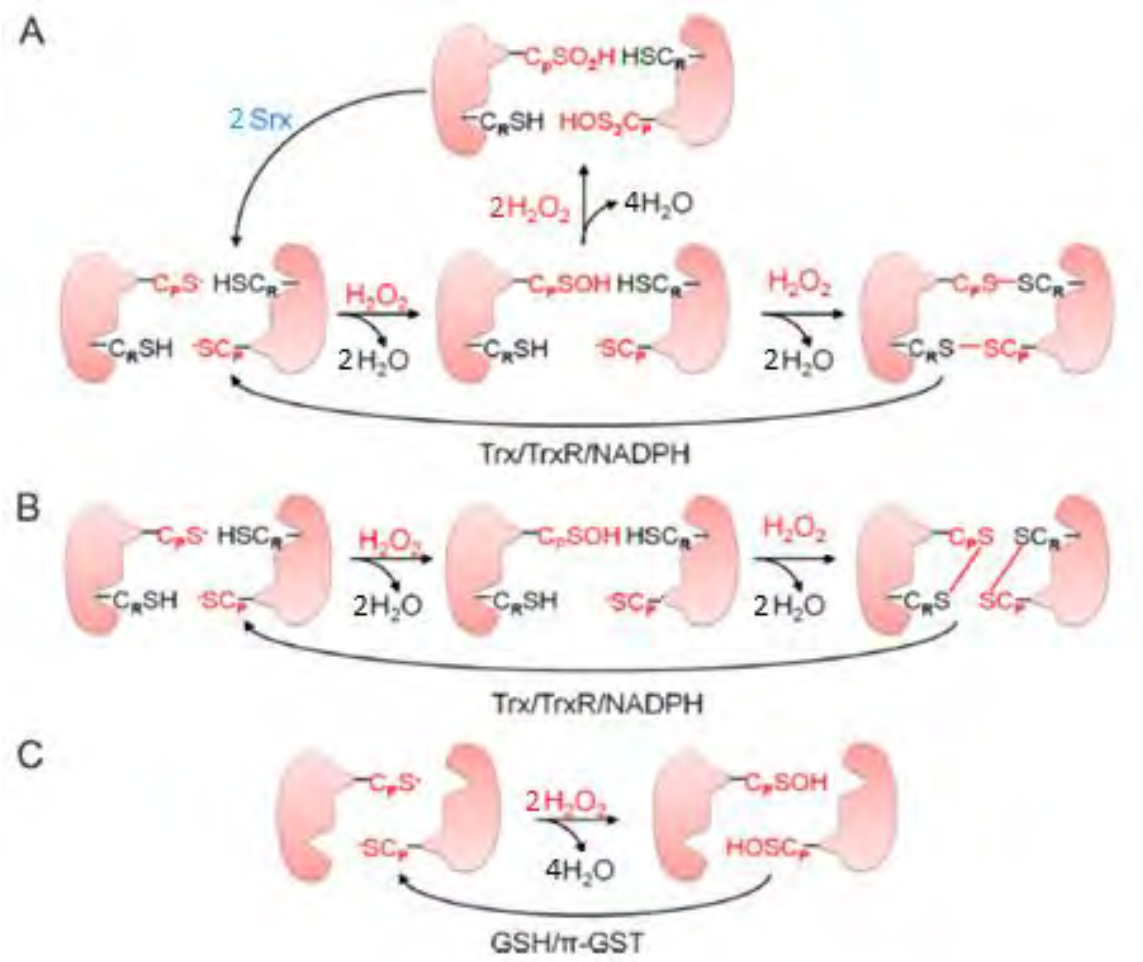

Figure 1.4 The catalytic cycle of a typical 2-Cys (A), atypical 2-Cys (B) and 1-Cys peroxiredoxin (C) which are normally resolved by the thioredoxin (Trx/TrxR/NADPH)/glutaredoxin (GSH/GST) system. Sulfiredoxin (SRX) may also be required to regenerate mammalian peroxiredoxins if they are hyperoxidised by high hydrogen peroxide concentrations (Taken from Rhee *et al.*, 2012).

1.3.2 Structural features of peroxiredoxins

2-Cys peroxiredoxins can be subdivided into two classes; typical and atypical (Wood *et al.,* 2003a). Most peroxiredoxins are typical 2-Cys and form homodimers in a head-tail arrangement with the peroxidatic and resolving cysteines on adjacent subunits. Atypical peroxiredoxins, such as mammalian Prdx V, are active as monomers and the peroxidatic and resolving cysteines are present on the same subunit (Seo *et al.*, 2000). Unlike thioredoxins and glutaredoxins, these peroxiredoxins can assemble into high molecular weight structures which have functional consequences for their activity.

Peroxiredoxins have typically been observed as decamers in their reduced form *in vivo* (De Oliveira *et al.*, 2007; Park *et al.*, 2011; Tairum *et al.*, 2012) and can dissociate into dimers upon oxidation (Parsonage *et al.*, 2005; Barranco-Medina *et al.*, 2009; Cao *et al.*, 2011). At high hydrogen peroxide concentrations, further oxidation to a hyperoxidised state yields monomers which can assemble into a dodecamer with chaperone activity (Jang *et al.*, 2004; Lim *et al.*, 2008; König *et al.*, 2013). Other factors affecting the oligomeric state of peroxiredoxins include pH (Morais *et al.*, 2015), protein and salt concentration (Matsumura *et al.*, 2008).

1.4 The role of peroxiredoxins in hydrogen peroxide redox signalling

Eukaryotic organisms have evolved to use hydrogen peroxide as an essential signal molecule by careful regulation of its production and localization (Veal *et al.*, 2007). Regulation of antioxidant activity is necessary to allow hydrogen peroxide to accumulate and function as a signal molecule but not accumulate to levels that can damage cellular components. Specific roles of peroxiredoxins in signalling processes will be discussed below.

1.4.1 Hyperoxidation causes inactivation of peroxiredoxins

There are two proposed biological explanations for why hyperoxidation occurs. Firstly, in the ‘floodgate’ hypothesis, hydrogen peroxide can accumulate by temporarily limiting peroxiredoxin activity through hyperoxidation, allowing for redox signalling (Wood *et al.*, 2003a). The second explanation suggests that the pool of reduced thioredoxin within the cell is preserved by peroxiredoxin hyperoxidation and is therefore available for other thioredoxin-dependent targets, such as MsrA, to repair proteins that may have been damaged by oxidative stress (Poole, 2005; Day *et al.*, 2012). Thus, the peroxiredoxin system is

‘sacrificed’ by inactivation in order to allow cells to recover from oxidative-stress induced damage. Collectively, these results suggest that the combined dynamics of the thioredoxin and peroxiredoxin systems result in a complex and differentiated oxidative stress response.

Hyperoxidised peroxiredoxins can also promote the repair of cellular proteins and structures damaged by oxidative stress by combining to form multimeric structures, typically dodecamers, which have a 4-fold increase in chaperone activity compared to reduced peroxiredoxin (Trotter *et al.*, 2008). These super chaperones are ribosome associated and help prevent protein misfolding and aggregation by binding to naked hydrophobic sites of unfolded proteins (Jang *et al.*, 2004; Trotter *et al.*, 2008), allowing cells to recover damaged structures found on ribosomes or protecting newly synthesized proteins during oxidative stress. Some peroxiredoxins are more susceptible to hyperoxidation and therefore it would seem that these peroxiredoxins play more of a protective role within the cell than other isoforms (Peskin *et al.*, 2013). For example, mammalian peroxiredoxins are relatively more susceptible to hyperoxidation than prokaryotic peroxiredoxins which seems appropriate as the levels of hydrogen peroxide that mammalian peroxiredoxins are subjected are different to those of free living bacteria and yeasts. Irreversibly hyperoxidised peroxiredoxins, which have a sulfonic acid peroxidatic cysteine ($-SO_3H$) permanently lose their peroxidase activity but have continued chaperone activity (Lim *et al.*, 2008). It has been suggested that measurement of this irreversibly hyperoxidised form of peroxiredoxin could be used as a marker for oxidative stress (Poynton and Hampton, 2014).

1.4.2 Inactivation of peroxiredoxins by phosphorylation allows an accumulation of hydrogen peroxide for signalling

Although inactivation of peroxiredoxins can occur by hyperoxidation, inactivation by phosphorylation has also been observed in some peroxiredoxins (Woo *et al.*, 2010). The mammalian peroxiredoxin PrxI, when membrane associated, was found to be phosphorylated on its Tyr^{194} residue and inactivated when the cell was stimulated by growth factors or immune receptors. Cellular hydrogen peroxide concentrations were then able to accumulate in this region and cause activation of phosphokinase signal pathways as hydrogen peroxide oxidizes redox-sensitive phosphatases (Figure 1.5, Finkel, 2011). Outside the periplasmic region, peroxiredoxins are still active and regulate hydrogen peroxide levels (Finkel, 2011; Woo *et al.*, 2010).

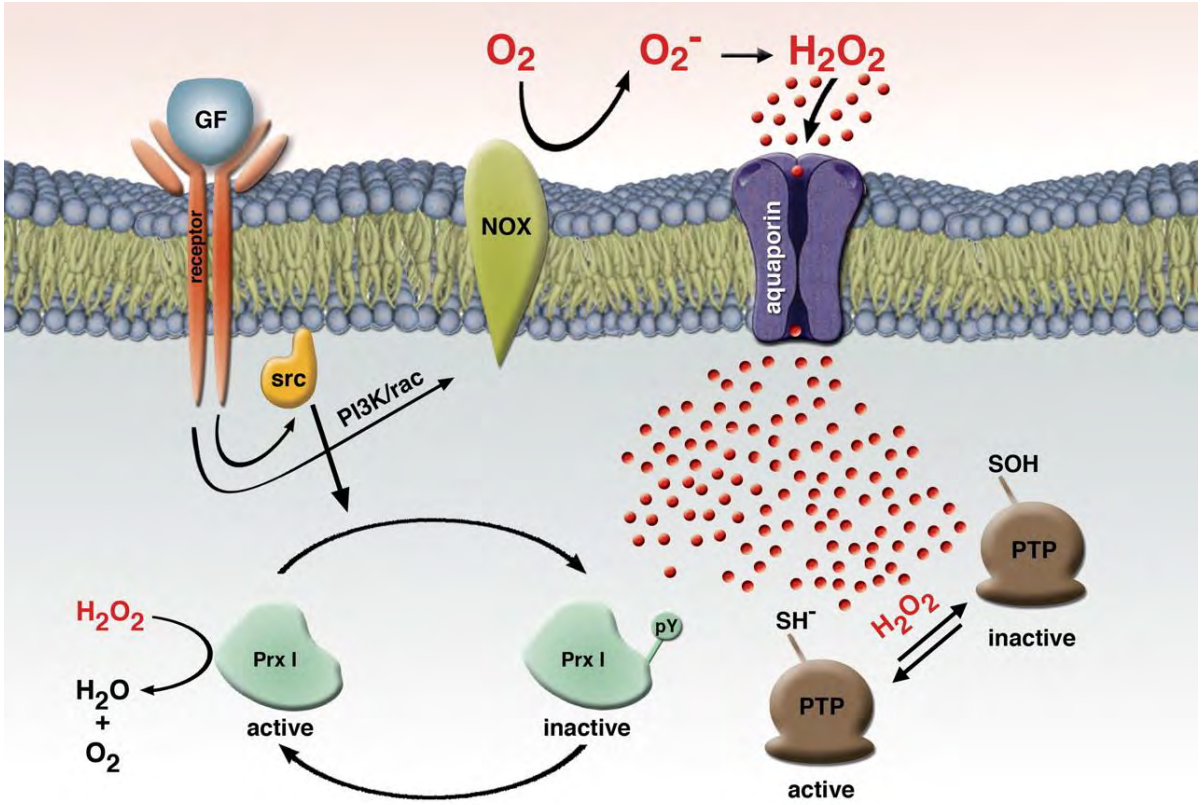

Figure 1.5 A growth factor (GF) signal is transmitted that inactivates peroxiredoxins (Prx1) by phosphorylation, allowing the intracellular hydrogen peroxide concentration to increase. Hydrogen peroxide then inactivates phosphatases (PTP), allowing for kinase-dependent signalling (Taken from Finkel, 2011).

1.4.3 Propagation of a redox signal by peroxiredoxin activity

Some peroxiredoxins can directly transmit redox signals by thiol-disulfide exchange. During their catalytic cycle, these peroxiredoxins become oxidised and in turn oxidise transcription facts such as YAP1 in budding yeast (Veal *et al.*, 2003; Tachibana *et al.*, 2009), STAT3 in mammalian cells (Sobotta *et al.*, 2015) and PAP1 in fission yeast (Brown *et al.*, 2013). To emphasise this function, the PAP1 system will be discussed in more detail below.

PAP1 is present in the cytosol in a reduced state under normoxic conditions (Brown *et al.*, 2013). If the extracellular hydrogen peroxide concentration is increased to 0.2 mM, the peroxiredoxin Tpx1 becomes oxidised and in turn oxidises PAP1, which accumulates in the nucleus and induces gene expression. PAP1 oxidation is absent in Δ*tpx1* cells and therefore Tpx1 acts as a signal transducer to activate PAP1-dependent gene expression at low hydrogen peroxide levels in *Schizosaccharomyces pombe* (Brown *et al.*, 2013). If extracellular

hydrogen peroxide reaches high levels (≥1 mM), peroxiredoxins are hyperoxidised and PAP1 is reduced to an inactive form by thioredoxin-like protein 1 (Trxl1) and PAP1-dependent gene expression is stopped.

Thus, it is clear that peroxiredoxins are more than simply hydrogen peroxide scavengers and the role of peroxiredoxins in signalling and hydrogen peroxide detoxification could be better understood through the use of systems biology tools such as computational modelling. The usefulness of these tools and the current limitation of their application in understanding peroxiredoxin networks will be discussed further below.

1.5 Systems biology studies for understanding the peroxiredoxin system

Determining the activity of biological systems is difficult, as their interactions and behaviour are typically too complex to be able to predict from the properties of the constituent components (Chiang *et al.*, 2014). *In silico* analyses of these complex systems are therefore necessary and have become feasible using systems biology tools. In particular, kinetic modelling with systems biology tools can describe each species and reaction in a system using ordinary differential equations (ODE) (Ideker *et al.*, 2001). These models can include information about which proteins in a system interact, their rates of interaction or if necessary their activation or degradation. Thus, a vast amount of data can be incorporated into a single computational model, which can provide insight into the behaviour of the system as a whole. A number of important system properties can also be predicted using system biology tools, such as the effect of perturbing some component on the system behaviour. Further, higher order tools such as control analysis, can be used to quantitatively describe the contribution of individual reactions to the flux and steady state concentrations of the system (Fell, 2005).

Unfortunately, there are some discrepancies as to how peroxiredoxins have been described in computational modelling studies (Table 1.1). These discrepancies involve differences in the kinetic models chosen to describe peroxiredoxin activity as well as the rate constants used for hydrogen peroxide reduction. These discrepancies will be described in detail below.

Table 1.1 Kinetic modelling in a number of published computational studies have made use of different kinetic expressions, structural descriptions and rate constants for peroxiredoxins.

Reference	Kinetic Expression	Structure	Rate constant for hydrogen peroxide reduction
Johnson *et al.* (2005)	Mass action	Monomer	10^5 M^{-1} s^{-1}
Adimora *et al.* (2010)	Mass action	Monomer	10^7 M^{-1} s^{-1}
Pillay *et al.* (2011)	Mass action	Monomer	10^4 M^{-1} s^{-1}
Aon *et al.* (2012)	Mass action	Monomer	10^7 M^{-1} s^{-1}
Benfeitas *et al.* (2014)	Mass action	Dimer	10^5-10^8 M^{-1} s^{-1}
Lim *et al.* (2015)	Mass action	Monomer	10^7 M^{-1} s^{-1}
Adolfsen and Brynildsen (2015)	Ping-Pong Enzyme	Monomer	10^5 M^{-1} s^{-1}

1.5.1 Distinct kinetic models for peroxiredoxin activity

The first unresolved discrepancy about peroxiredoxin activity is the choice of kinetic model to describe hydrogen peroxide reduction (Figure 1.6). These models represent a typical 2-Cys peroxiredoxin, as these are the most common isoform of peroxiredoxins *in vivo*. The first model (ping-pong enzyme model, Figure 1.6A), describes the traditional view that peroxiredoxins are enzymes with ping-pong kinetics (Baker and Poole, 2003; Adolfsen and Brynildsen, 2015). In the second model (redox couple monomer model, Figure 1.6B), peroxiredoxins have been treated as redox couples whose activity has been described with mass action kinetics (Johnson *et al.*, 2005; Lim *et al.*, 2015). Finally, in the third model (redox couple homodimer model, Figure 1.6C), peroxiredoxins are also considered redox couples and their activity is described with mass action kinetics. However, in this scheme each available active site can reduce hydrogen peroxide, affecting the stoichiometry of the reactions.

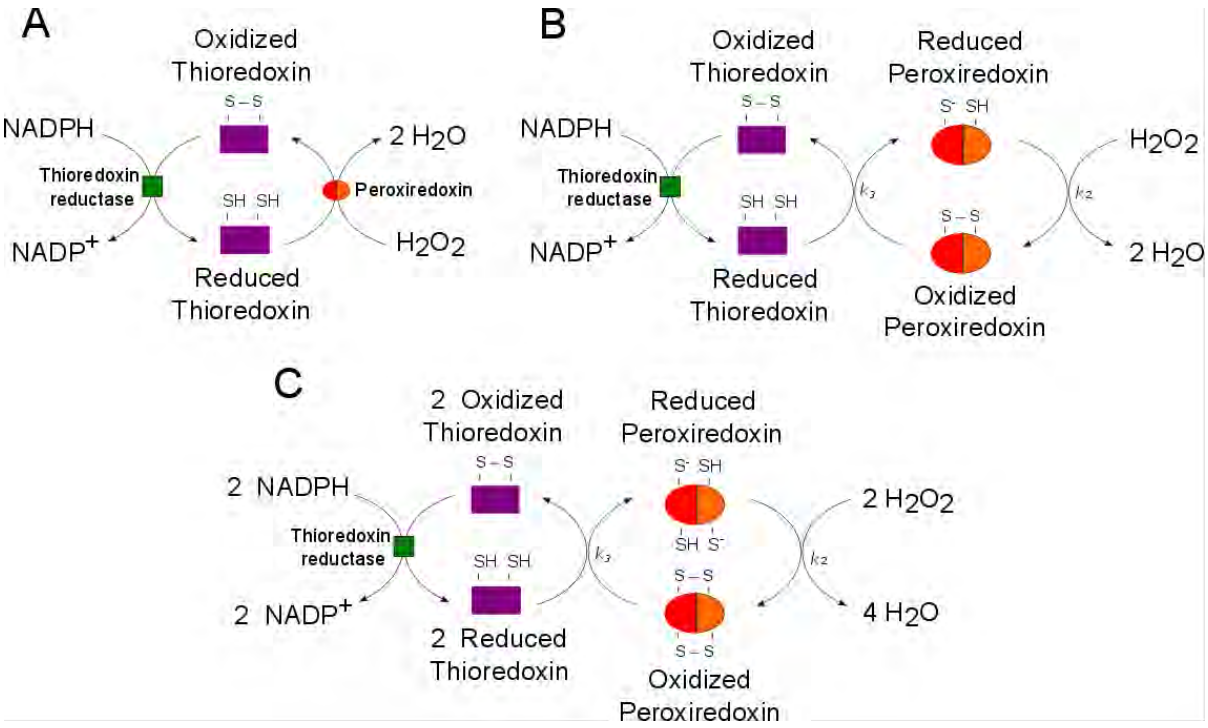

Figure 1.6 Peroxiredoxin activity has been described using ping-pong enzyme kinetics with hydrogen peroxide and thioredoxin as substrates (A) and mass action kinetics to model peroxiredoxins as redox couples (B). Peroxiredoxins have also been modelled in their homodimer form rather than as monomers (C). Each subunit in the homodimer is oxidised by hydrogen peroxide sequentially, which is represented by a statistical value of 2 in the computational models and Trx_{SS}/ Trx_{SH} refers to oxidised/reduced thioredoxin and Prx_{SS}/Prx_{SH} refers to oxidised/reduced peroxiredoxin

Systems biology studies based on these kinetic models may give different predictions about the system and would therefore affect our understanding of peroxiredoxin dependent processes. Meaningful analysis of peroxiredoxin activity would therefore benefit from determining which model should be used to describe the system.

1.5.2 Discrepancies with the rate constant for hydrogen peroxide reduction

A basic condition in most *in vitro* enzyme kinetic studies is that the substrate concentration in a reaction must greatly exceed that of the enzyme concentration for the Michaelis-Menten assumptions to be valid (Segel, 2013). Most *in vitro* kinetic analyses of peroxiredoxins have therefore typically been carried out with higher hydrogen peroxide concentrations than peroxiredoxin concentrations and kinetic parameters such as k_{cat} and K_m have been calculated under these conditions (see for example Jara *et al.*, 2007). However,

peroxiredoxins do not meet this basic assumption *in vivo* as the intracellular peroxiredoxin concentration observed is far greater than that of hydrogen peroxide (Huang and Sikes, 2014). The physiological relevance of results from such analyses is therefore questionable as the concentrations of the different species in these assays do not reflect the *in vivo* concentrations of these species. The *in vitro* kinetic behaviour of peroxiredoxins under physiological hydrogen peroxide and peroxiredoxin concentrations has not been described in the literature.

Another discrepancy that has been uncovered with previous studies of peroxiredoxin systems surrounds the rate of peroxiredoxin activity with hydrogen peroxide (Figure 1.7). In some analyses, NADPH oxidation of the coupled peroxiredoxin system has been used to determine the hydrogen peroxide reduction rate constant, while other studies have directly monitored the degradation of hydrogen peroxide in a competition assay with horse radish peroxidase (HRP) (Ogusucu *et al.*, 2007). Results from these studies have been contradictory, with NADPH oxidation occurring at an appreciably slower rate than the hydrogen peroxide degradation rate directly observed in the competition assay (Munhoz and Netto, 2004; Ogusucu *et al.*, 2007). Thus, and somewhat surprisingly, the reaction of peroxiredoxins and hydrogen peroxide may be proceeding faster than the system flux. While the competition assay is carried out in the absence of the peroxiredoxin recycling system (thioredoxin, thioredoxin reductase and NADH), this method is considered to yield a more accurate measure of Prx-dependent hydrogen peroxide reduction (Nelson and Parsonage, 2011). However, in the absence of the other peroxiredoxin system components, hyperoxidation of eukaryotic peroxiredoxins is inefficient (Cao *et al.*, 2014) and mutants of thioredoxin and thioredoxin reductase show great sensitivity to hydrogen peroxide (Ragu *et al.*, 2014), suggesting that peroxiredoxin activity is limited by its recycling system *in vivo*. Thus, although this competition assay shows the peroxidase potential of peroxiredoxins, monitoring NADPH oxidation may be more physiologically relevant.

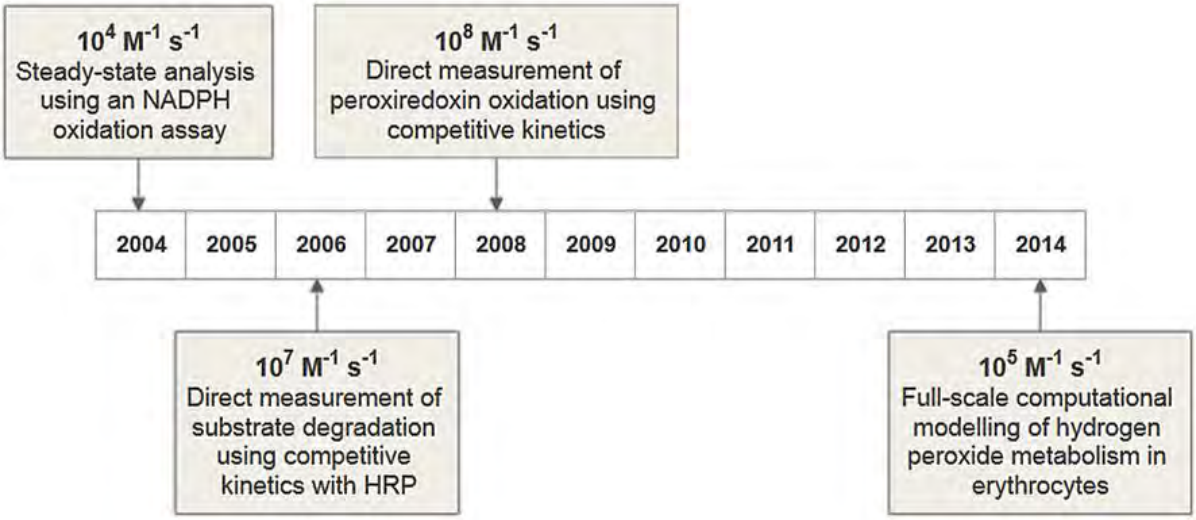

Figure 1.7 The peroxiredoxin rate constant for hydrogen peroxide reduction has varied depending on the method used to assay peroxiredoxin activity (Munhoz and Netto, 2004; Ogusucu *et al.*, 2007; Nelson *et al.*, 2008; Benfeitas *et al.*, 2014).

1.6 Aims of study

The first aim of this research was to determine the appropriate description of peroxiredoxins for systems biology studies. Computational models based on peroxiredoxin kinetics were simulated to determine if there were distinguishable quantitative and qualitative differences in their behaviour. The second aim was to use computational modelling and *in vitro* kinetics to determine the most appropriate method for analysing hydrogen peroxide reduction by peroxiredoxins in context of its cognate system. For clarity, the three kinetic descriptions of the peroxiredoxin system were referred to as the peroxiredoxin "kinetic models" (ping-pong enzyme, redox couple monomer and homodimer models), while an ODE model of the entire peroxiredoxin system (peroxiredoxin, thioredoxin, thioredoxin reductase and NAPDH) constituted a "computational model."

Chapter 2

Computational modelling of the peroxiredoxin system to distinguish its kinetic activity *in vitro*

2.1 Introduction

The basis for the discrepancies in the reported rate constants for peroxiredoxin activity has largely come from the methodologies used to characterise them. Peroxiredoxin activity has been studied using several *in vitro* assays since yeast peroxiredoxin TSA1 was first tested for its ability to protect glutamine synthetase from inactivation by the DTT/Fe^{3+}/O_2 oxidation system (Chae *et al.*, 1994b). Steady state system analysis with an NADPH-coupled assay yielded a second-order rate constant for hydrogen peroxide reduction (k_{cat}/K_m) of 10^4 M^{-1} s^{-1} (Munhoz and Netto, 2004). Assays were subsequently developed that omitted peroxiredoxin recycling in the steady state assay and directly measured hydrogen peroxide reduction using a competition assay with HRP. In these studies, peroxiredoxins were shown to rapidly react with peroxide substrates with second-order rate constants ranging from 10^5 to 10^8 M^{-1} s^{-1} (Ogusucu *et al.*, 2007; see for example Nagy *et al.*, 2011). Directly monitoring substrate degradation (see for example Trujillo *et al.*, 2006) or peroxiredoxin oxidation (see for example Nelson *et al.*, 2008) further refined this approach and fluorescence measurements at specific excitation wavelengths determined pseudo-first order rate constants (k_{obs}) for hydrogen peroxide reduction of between 10^6 to 10^8 M^{-1} s^{-1}. Peroxiredoxins were consequently proposed to be the primary cellular contributors to hydrogen peroxide degradation (Winterbourn and Hampton, 2008; Perkins *et al.*, 2015) which was confirmed by gene knockout studies in *Escherichia coli* (Seaver and Imlay, 2001), *S. cerevisiae* (Trotter *et al.*, 2008) and *S. pombe* (Paulo *et al.*, 2014).

Although peroxiredoxins may rapidly react with hydrogen peroxide, their activity like other peroxidases, may be limited by recycling with reductants such as thioredoxin (Mishra and Imlay, 2012), which may put their rate constants for hydrogen peroxide degradation in the range reported for steady state analysis of the system (Munhoz and Netto, 2004). While this steady state rate constant is lower than the rate constants determined with the direct assays described above, it is still greater than other peroxidases and, as peroxiredoxins are also more abundant in cells (Rabilloud *et al.*, 1995), they are still considered to be the

primary antioxidants during peroxide stress. Further support for the lower rate constant has come from a large scale computational model of the red blood cell peroxiredoxin system (Benfeitas *et al.*, 2014). In this model, peroxide reduction was indeed limited by the peroxiredoxin reduction suggesting that computational models that use rate constants of 10^6 - 10^8 M^{-1} s^{-1} without consideration of peroxiredoxin recycling are incorrect (Benfeitas *et al.*, 2014).

As described in Chapter 1, a further discrepancy noted in the literature is that three models for peroxiredoxin kinetic activity have been proposed although it could be argued that the ping-pong enzyme and redox couple monomer models are similar. The major difference between these two kinetic models is that the ping-pong kinetic mechanism explicitly includes the formation of the enzyme-substrate complex (*, Scheme 2.1 and 2.2, Cleland, 1963) which is implicit in the redox couple monomer model mechanism.

$$Prx_{SS} + Trx_{SH} \leftrightarrow \underbrace{Prx_{ss}Trx_{SH} \overset{k}{\leftrightarrow} Prx_{SH}Trx_{SS}}_{*} \overset{k_1}{\leftrightarrow} Prx_{SH} + Trx_{SS} \qquad 2.1$$

$$Prx_{SH} + H_2O_2 \leftrightarrow \underbrace{Prx_{SH}H_2O_2 \overset{k}{\leftrightarrow} Prx_{SS}2\ H_2O}_{*} \overset{k_1}{\leftrightarrow} Prx_{SS} + 2\ H_2O \qquad 2.2$$

To determine if these kinetic models do indeed make distinct predictions about the peroxiredoxin system, core computational models with hydrogen peroxide reduction were developed and compared. In addition, realistic computational models based on *in vitro* datasets were developed and their behaviour in response to parameter changes were compared. Flux control analysis was also performed to compare the predicted functional organisation of the peroxiredoxin system and the rate limiting steps in these systems were identified.

2.2 Methods

2.2.1 Core computational modelling of the peroxiredoxin system

Core computational modelling of the peroxiredoxin system was carried out with simplified kinetic parameters to determine if there were any differences between the model predicted behaviours of the system (Tables 2.1-2.2). To simplify analysis it was assumed that all reactions were irreversible given the large differences in the redox potentials of NADPH, thioredoxin, peroxiredoxin and hydrogen peroxide (Wood, 1988; Finn *et al.*, 2003; Watson *et*

al., 2003; Cox *et al.*, 2009; Garcia-Santamarina *et al.*, 2014). The Python Simulator for Cellular Systems (PySCeS) (Olivier *et al.*, 2005, http://pysces.sourceforge.net) was used for modelling analyses and the model and scripting files were written using Scintilla Text Editor (SciTE) (http://sourceforge.net/projects/scintilla/files/SciTE) and are available in the Appendix (1.1-1.2).

2.2.2 Realistic computational modelling of the peroxiredoxin system

Realistic models of the peroxiredoxin system were developed by modifying the core model scripts in SciTE with realistic reaction parameters and species concentrations obtained from BRENDA parameter database (http://www.brenda-enzymes.info) or from the literature (Tables 2.3-2.6, Results). Data fitting scripts (Appendix 2.1-2.2) were produced in the Python Notebook to fit all of the models to specific datasets using the Levenberg–Marquardt algorithm for non-linear least squares regression analysis which was available from SciPy (http://www.scipy.org). The data points in the *in vitro* datasets were obtained using PlotDigitizer 2.6.5 (http://sourceforge.net/projects/plotdigitizer/files/plotdigitizer/2.6.5/).

2.2.3 Flux control analysis of the peroxiredoxin system.

Flux control analysis of each kinetic model was completed in the Python Notebook (Appendix 2.14 and 2.2.4) using PySCeS.

2.3 Results

2.3.1 Core computational modelling revealed quantitative and qualitative differences between the peroxiredoxin kinetic models in response to changes in the system

The steady-state properties of the three proposed peroxiredoxin kinetic models (Figures 1.4 and 1.6) with core parameters (Tables 2.1-2.2) were compared by simulating the models at steady state using both linear (Figure 2.1A-D) and logarithmic plots (Figure 2.1E-F, Hofmeyr and Cornish-Bowden, 2000). The fluxes at different thioredoxin reductase and thioredoxin concentrations were analysed as peroxiredoxin reduction may be rate-limiting in the system. In all the models the flux increased similarly over all thioredoxin concentrations tested (Figure 2.1A and E), but different limiting rates were observed with increasing thioredoxin reductase concentrations (Figure 2.1B and F); system saturation occurred at a slightly lower thioredoxin reductase concentration in the ping-pong enzyme and redox couple monomer models as peroxiredoxin oxidation became the rate-limiting step in these systems.

Table 2.1 Reactions and reaction parameters for core computational modelling of the peroxiredoxin system.

Reaction	Parameter	Value
All Models		
R1: NADPH + Trx_{SS} → $NADP^+$ + Trx_{SH}	$k_{cat\ 1}$	1 s^{-1}
	K_{nadph}	1 μM
	K_{trxss}	1 μM
Ping-Pong Enzyme Model		
R2: Trx_{SH} + H_2O_2 → Trx_{SS} + H_2O	$k_{cat\ 2}$	1 s^{-1}
	K_{trxsh}	1 μM
	$K_{h_2O_2}$	1 μM
Redox Couple Monomer Model		
R2: H_2O_2 + Prx_{SH} → H_2O + Prx_{SS}	k_2	1 μM s^{-1}
R3: Prx_{SS} + Trx_{SH} → Prx_{SH} + Trx_{SS}	k_3	1 μM s^{-1}
Redox Couple Homodimer Model		
R2: $Prx_{SH}Prx_{SH}$ + H_2O_2 → $Prx_{SS}Prx_{SH}$ + H_2O	k_2	1 μM s^{-1}
R3: $Prx_{SS}Prx_{SH}$ + H_2O_2 → $Prx_{SS}Prx_{SS}$ + H_2O	k_2	1 μM s^{-1}
R4: $Prx_{SS}Prx_{SS}$ + Trx_{SH} → $Prx_{SS}Prx_{SH}$ + Trx_{SS}	k_3	1 μM s^{-1}
R5: $Prx_{SS}Prx_{SH}$ + Trx_{SH} → $Prx_{SH}Prx_{SH}$ + Trx_{SS}	k_3	1 μM s^{-1}

Table 2.2 Species concentrations of all system components for core computational modelling of the peroxiredoxin system.

Model	Species	Initial Concentration (µM)
All	NADPH	1
	$NADP^+$	1
	Trx_{SH}	0.5*
	Trx_{SS}	0.5
	TR	1
	H_2O_2	1
Ping-Pong Enzyme	Prx	1
Redox Couple Monomer	Prx_{SH}	0.5*
	Prx_{SS}	0.5
Redox Couple Homodimer	$Prx_{SH}Prx_{SH}$	0.33*
	$Prx_{SS}Prx_{SH}$	0.33
	$Prx_{SS}Prx_{SS}$	0.34

*Note that the total concentration (reduced and oxidised) of all moiety conserved species is 1.

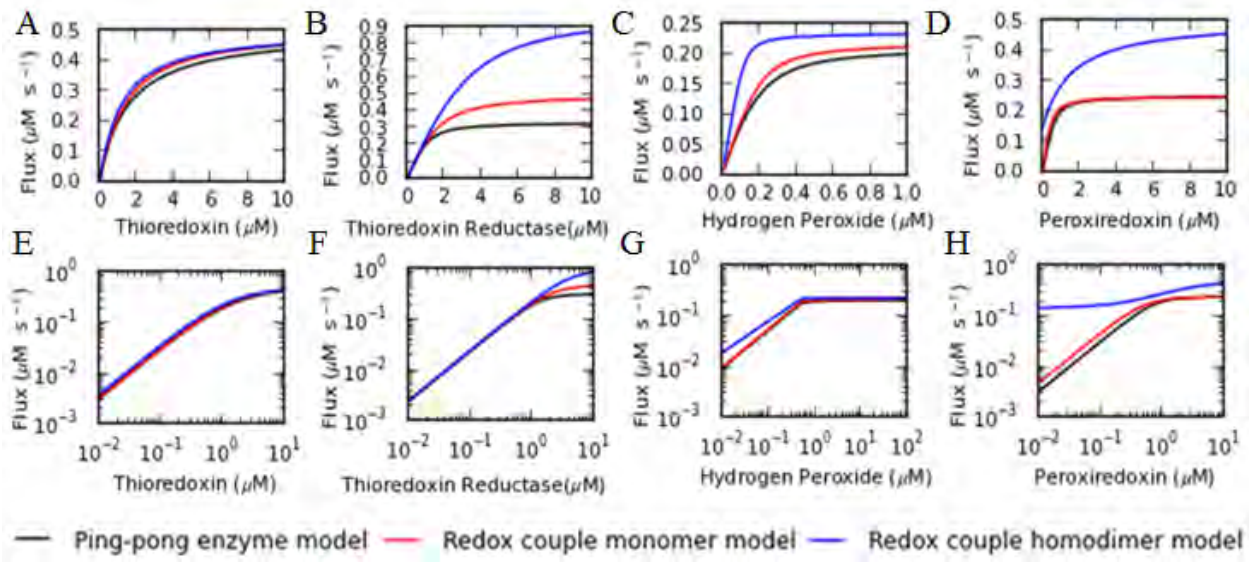

Figure 2.1 Flux-response analysis of the ping-pong enzyme, redox couple monomer and redox couple homodimer models for peroxiredoxin activity. Flux analysis was carried out to observe the sensitivity of each model to parameter changes in the system in linear (A-D) and double log space (E-H).

Compared to the perturbations in the thioredoxin system (Figure 2.1A-B), substrate saturation of the models was observed at relatively low hydrogen peroxide concentrations with the maximal flux slightly greater in the redox couple homodimer model (Figure 2.1C and G). The effect of changing peroxiredoxin concentrations in the system revealed that the maximal flux in the redox couple homodimer model was appreciably different to the ping-pong enzyme and redox couple monomer models (Figure 2.1D). Interestingly, flux analysis in double log space (Figure 2.1H) revealed a sigmoidal response to increasing peroxiredoxin concentrations in the redox couple homodimer model. In summary, the models showed similar kinetic profiles to some parameters changes but quantitative differences with varying thioredoxin reductase, hydrogen peroxide and peroxiredoxin concentrations were apparent in these core models.

In addition to the flux through the system, the reduced and oxidised thioredoxin concentrations also represent an important output of the peroxiredoxin system. At steady state, many thioredoxin-dependent reactions are affected by the reduced thioredoxin concentration (Pillay *et al.*, 2011). Consequently, the reduced and oxidised thioredoxin concentrations were also monitored in these models. With changes in peroxiredoxin and thioredoxin reductase concentrations, a switch in the proportion of the reduced to oxidised thioredoxin was observed at slightly different concentrations between the models (Figure

2.2). As peroxiredoxin concentrations increased, the demand for reduced thioredoxin to recycle peroxiredoxin increased, resulting in greater oxidised thioredoxin concentrations at steady state (Figure 2.2A). The flux in the redox couple homodimer model was much greater than the other models (Figure 2.1D and H) and therefore the thioredoxin oxidation rate was also greater and the crossover to a larger fraction of oxidised thioredoxin occurred at a much lower peroxiredoxin concentration relative to the other models. This crossover region was important as it can be experimentally detected in redox alkylation studies (Padayachee and Pillay, 2015) and may therefore be used to distinguish between the proposed peroxiredoxin kinetic models. As the thioredoxin reductase concentrations increased, the thioredoxin reduction rate increased and consequently the reduced thioredoxin fraction increased relative to the oxidised thioredoxin fraction (Figure 2.2B). The flux response to thioredoxin reductase was again greater in the redox couple homodimer model (Figure 2.1B and F) and therefore the thioredoxin reduction rate was greater than the other models causing the crossover to reduced thioredoxin to occur at a lower thioredoxin reductase concentration (Figure 2.2B).

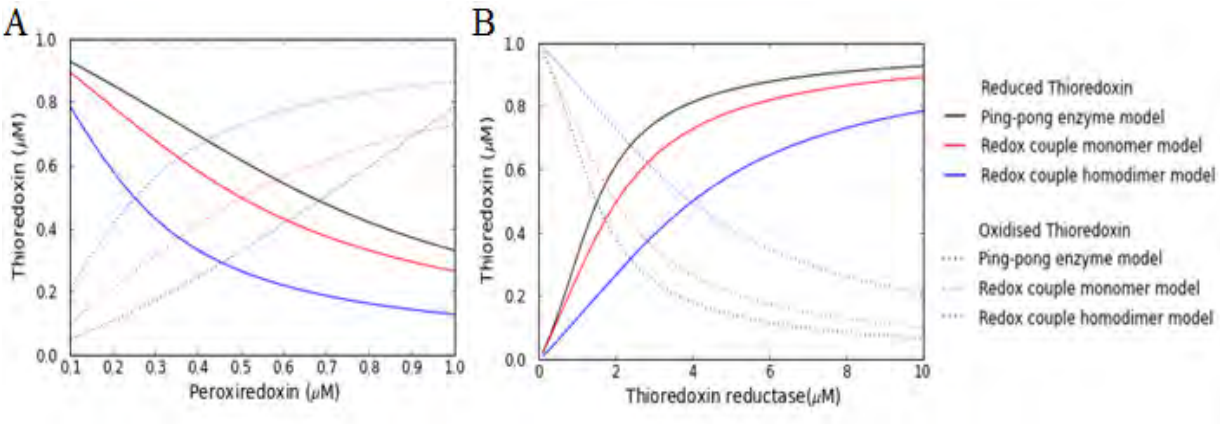

Figure 2.2 Core computational models for peroxiredoxin activity show quantitative differences in the steady state reduced and oxidised thioredoxin concentrations in response to increasing peroxiredoxin (A) and thioredoxin reductase (B) concentrations.

With increasing hydrogen peroxide concentrations, a crossover in the proportion of reduced to oxidised thioredoxin concentration occurred in the ping-pong enzyme and redox couple monomer models albeit at slightly different hydrogen peroxide concentrations (Figure 2.3). Notably, in the redox couple homodimer model, the oxidised thioredoxin concentration was greater than the reduced thioredoxin concentration over all concentrations of hydrogen peroxide supplied to the system. In this model, substrate saturation occurred at a lower hydrogen peroxide concentration than the ping-pong enzyme and redox couple models (Figure 2.3) causing complete thioredoxin oxidation at a low hydrogen peroxide

concentration (Figure 2.3). These differences suggested the dynamics of these kinetic models were different and offered a way to distinguish them.

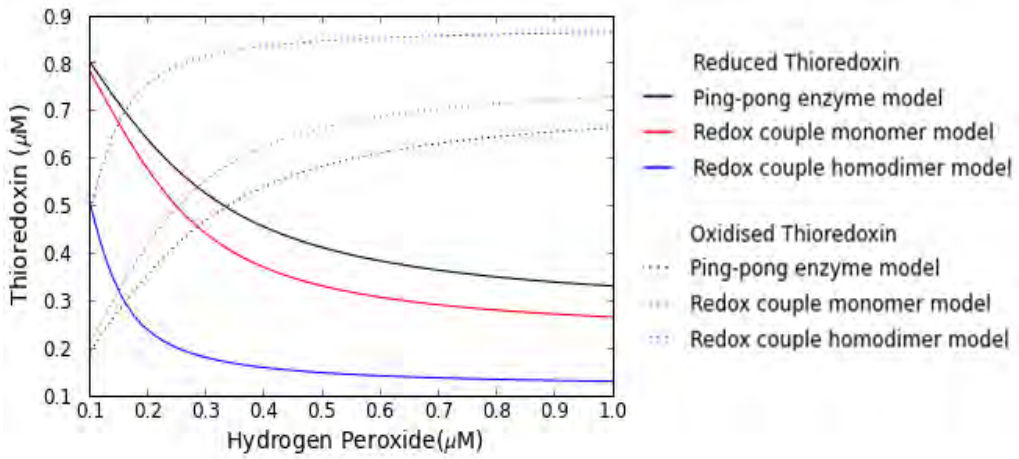

Figure 2.3 Core computational models for peroxiredoxin activity show differences in the redox state of thioredoxin in response to increasing hydrogen peroxide concentrations.

Differences in the thioredoxin redox state with changes to the NADPH concentration were also noted (Figure 2.4) with the reduced thioredoxin form dominating in the ping-pong enzyme model at high concentrations of NADPH as there was more NADPH available to reduce thioredoxin (Figure 2.4A). The reduced and oxidised thioredoxin concentrations were almost equal in the redox couple monomer model (Figure 2.4B). However in the redox couple homodimer model, the oxidised form was present in a greater concentration than the reduced form over all NADPH concentrations (Figure 2.4C). It is not clear why these results differed from the thioredoxin reductase parameter perturbations as both parameters should have increased the reducing equivalents available for peroxiredoxin reduction.

In conclusion, core modelling results suggested that the kinetic models proposed for peroxiredoxin activity are expected to show similar kinetic properties in some cases but in other cases, notable differences in their behaviour were observed and resulted in models with distinct properties especially with regard to the thioredoxin redox state. As thioredoxin is a control hub protein for many redox regulated processes (Tanaka *et al.*, 2000; Nishiyama *et al.*, 2001), this result suggests that computational models that have been built with these different kinetic models (Table 1.1) are expected to have different behaviours even if the same set of input parameters were used to develop them. To confirm these core modelling results, the peroxiredoxin kinetic models were fitted to *in vitro* datasets.

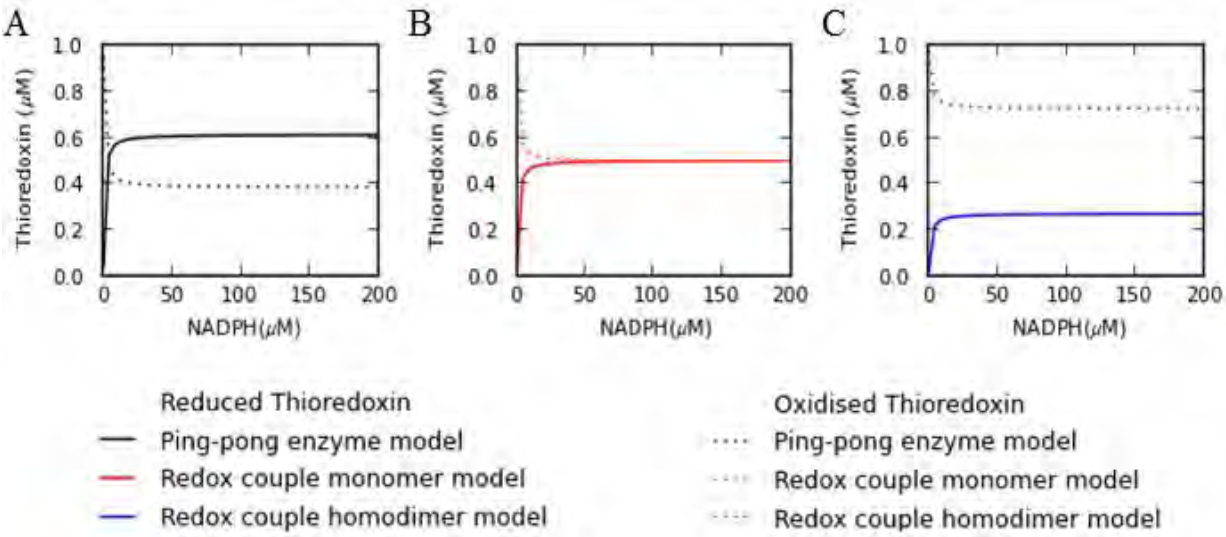

Figure 2.4 Changes in the NADPH concentration results in distinct changes to the thioredoxin redox couple in the ping-pong enzyme (A), redox couple monomer (B) and redox couple homodimer (C) peroxiredoxin models.

2.3.2 Kinetic modelling of an *in vitro* human peroxiredoxin dataset revealed deficiencies in our understanding of peroxiredoxin kinetics

The human erythrocyte peroxiredoxin system is among the most well studied peroxiredoxin systems because of its role in protecting red blood cells (RBC) against ROS whose production is catalysed by iron (O'neill and Reddy, 2011; Cho *et al.*, 2014; Bayer *et al.*, 2015). A steady-state substrate saturation dataset for human erythrocyte peroxiredoxin 2 activity was obtained by measuring the NADPH oxidation rate with increasing thioredoxin concentrations (Figure 2.5, Manta *et al.*, 2009). The species concentrations were carefully selected to ensure that hydrogen peroxide reduction was the purported rate-limiting step in this experiment and a rate constant for hydrogen peroxide reduction of 1.0×10^{8} M^{-1} s^{-1} was determined independently using a competition assay with HRP (Manta *et al.*, 2009). Kinetic parameters were taken from data in this paper, the BRENDA database and from the literature to develop computational models of the system based on the ping-pong enzyme, redox couple monomer and homodimer models (Tables 2.3-2.4). The resulting models therefore reflected our current understanding of human erythrocyte peroxiredoxin 2 kinetics.

Table 2.3 Realistic parameters for human peroxiredoxin 2 activity for modelling of an *in vitro* dataset (Manta *et al.*, 2009).

Reaction	Parameter	Value	Reference
	All Models		
R1: NADPH + Trx_{SS} → $NADP^+$ + Trx_{SH}	$k_{cat\ 1}$	25.78 s^{-1}	(Turanov *et al.*, 2006)
	K_{nadph}	6 μM	(Urig *et al.*, 2006)
	K_{trxss}	1.83 μM	(Turanov *et al.*, 2006)
	Ping-Pong Enzyme Model		
R2: Trx_{SH} + H_2O_2 → Trx_{SS} + H_2O	$k_{cat\ 2}$	13.2 s^{-1}	a
	K_{trxsh}	3.24 μM	(Manta *et al.*, 2009)
	K_{h2o2}	0.7 μM	(Manta *et al.*, 2009)
	Redox Couple Monomer Model		
R2: H_2O_2 + Prx_{SH} → H_2O + Prx_{SS}	k_2	100 $\mu M^{-1}\ s^{-1}$	(Manta *et al.*, 2009)
R3: Prx_{SS} + Trx_{SH} → Prx_{SH} + Trx_{SS}	k_3	0.074 $\mu M^{-1}\ s^{-1}$	(Manta *et al.*, 2009)
	Redox Couple Homodimer Model		
R2: $Prx_{SH}Prx_{SH}$ + H_2O_2 → $Prx_{SS}Prx_{SH}$ + H_2O	k_2	100 $\mu M^{-1}\ s^{-1}$	(Manta *et al.*, 2009)
R3: $Prx_{SS}Prx_{SH}$ + H_2O_2 → $Prx_{SS}Prx_{SS}$ + H_2O	k_2	100 $\mu M^{-1}\ s^{-1}$	(Manta *et al.*, 2009)
R4: $Prx_{SS}Prx_{SS}$ + Trx_{SH} → $Prx_{SS}Prx_{SH}$ + Trx_{SS}	k_3	0.074 $\mu M^{-1}\ s^{-1}$	(Manta *et al.*, 2009)
R5: $Prx_{SS}Prx_{SH}$ + Trx_{SH} →$Prx_{SH}Prx_{SH}$ + Trx_{SS}	k_3	0.074 $\mu M^{-1}\ s^{-1}$	(Manta *et al.*, 2009)

[a] estimated by data fitting De Franceschi *et al.* (2011)

Table 2.4 Species concentrations of the various system components used in each model for realistic modelling of human peroxiredoxin 2 activity obtained from Manta *et al.* (2009).

Model	Species	Initial Concentration (µM)
All	NADPH	200
	$NADP^+$	1
	Trx_{SH}	1*
	Trx_{SS}	1
	TR	1
	H_2O_2	30
Ping-Pong Enzyme	Prx	0.5
Redox Couple Monomer	Prx_{SH}	0.25*
	Prx_{SS}	0.25
Redox Couple Homodimer	$Prx_{SH}Prx_{SH}$	0.167*
	$Prx_{SS}Prx_{SH}$	0.167
	$Prx_{SS}Prx_{SS}$	0.167

*Note that the total concentration (reduced and oxidised) of all moiety conserved species is equal to the concentration used in the activity assay.

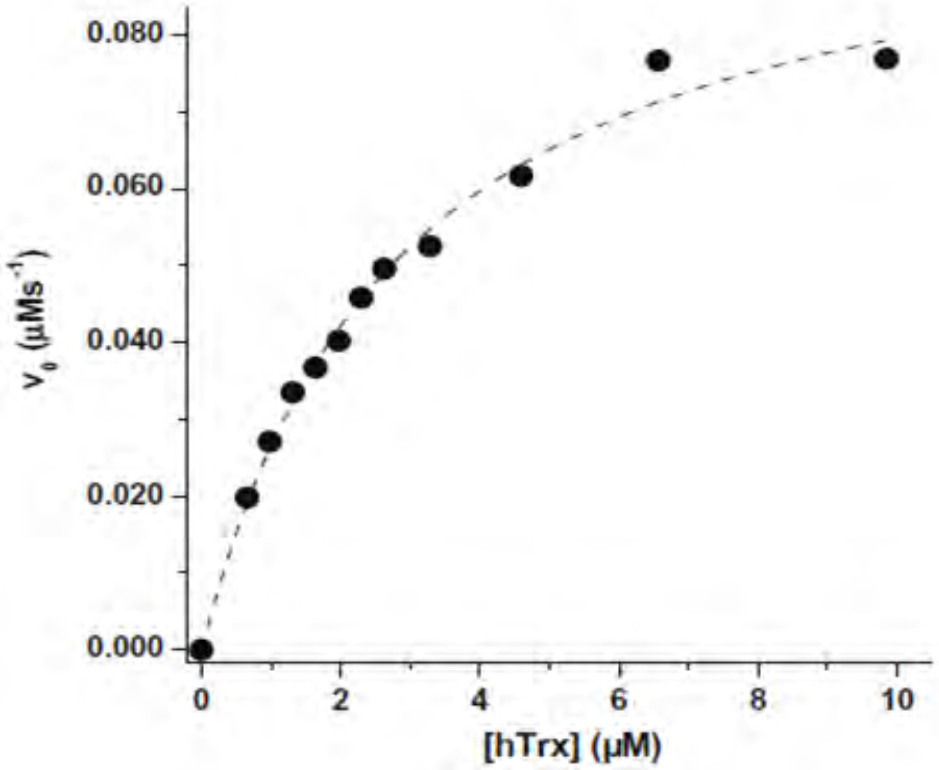

Figure 2.5 The effect of increasing human thioredoxin (hTrx) concentration on human peroxiredoxin 2 system activity was monitored in an NADPH-coupled assay. The assay consisted of 200 μM NADPH, 1 μM thioredoxin reductase, 0.5 μM peroxiredoxin and 30 μM H_2O_2 in 50 mM Tris–HCl buffer at pH 7.4 (Manta *et al.*, 2009).

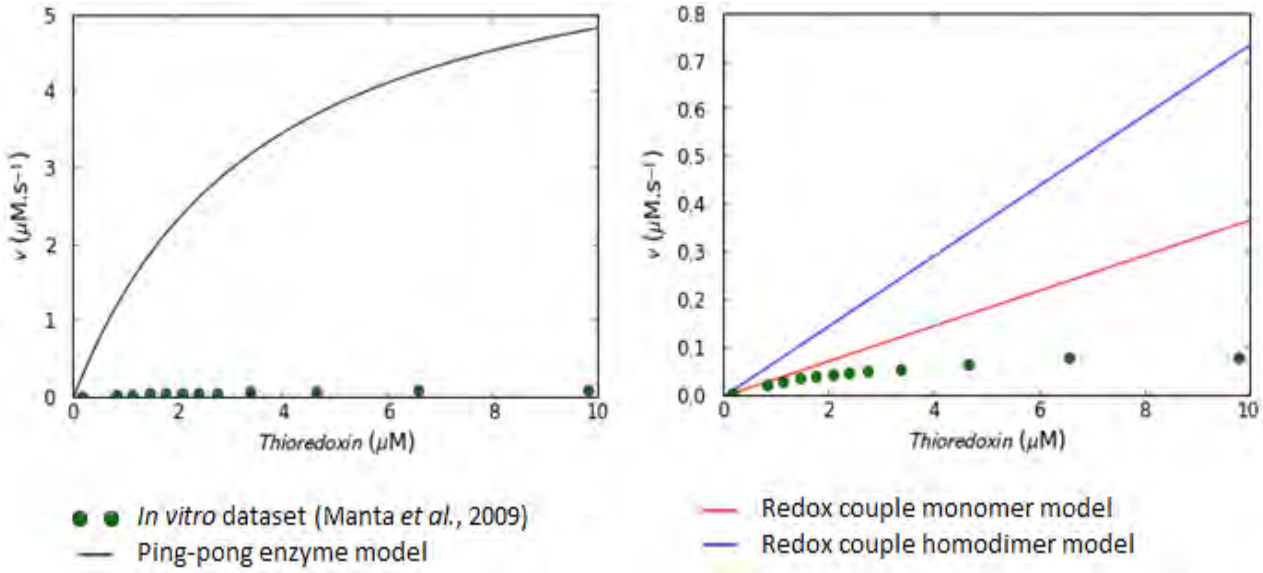

Figure 2.6 Kinetic models of a mammalian peroxiredoxin system failed to reproduce an *in vitro* dataset (Manta *et al.*, 2009) with increasing thioredoxin concentrations.

As a first step, the realistic peroxiredoxin computational models were simulated with increasing thioredoxin concentrations but all the models failed to reproduce this *in vitro* dataset and the responses also differed between the models (Figure 2.6). This discrepancy revealed a limitation in our current understanding of peroxiredoxin kinetics and showed that the kinetic models proposed for peroxiredoxin activity are indeed quantitatively distinct from each other (Figure 2.6). The models were then fit to this *in vitro* dataset using non-linear regression to estimate the parameters for hydrogen peroxide reduction (Table 2.5).

All the models were able to fit the *in vitro* dataset ($r^2 \geq 0.98$, Table 2.5), suggesting that kinetic experiments that utilise this set of experimental conditions only will not be able to distinguish between these models. The fitted rate constants for hydrogen peroxide reduction were 1.87×10^4 M^{-1} s^{-1} (k_{cat}/K_m) in the ping-pong enzyme model, 6.67×10^3 M^{-1} s^{-1} in the redox couple monomer model and 3.33×10^3 M^{-1} s^{-1} in the redox couple homodimer model (Table 2.5), which conflicted with the rate constant of 10^8 M^{-1} s^{-1} determined with the HRP competition assay (Manta *et al.*, 2009) but was closer to rate constants (~10^4 M^{-1} s^{-1}) obtained in assays that measure the steady state system rate (see for example Munhoz and Netto, 2004). These results suggests that the rate of hydrogen peroxide reduction by the peroxiredoxin system is not solely determined by the rate constant for hydrogen peroxide reduction and modelling results based on this assumption must be viewed with caution (see for example Winterbourn and Hampton, 2008). We then asked whether the fitted models were different to each other by simulating and comparing the responses between the models to parameter changes in the system (Figure 2.7).

With increasing thioredoxin reductase (Figure 2.7A and D) and peroxiredoxin concentrations (Figure 2.7B and E), the ping-pong enzyme and redox couple monomer models showed a similar flux response that was distinct from the redox couple homodimer model. Quantitative differences were also observed in the flux response to increasing hydrogen peroxide concentrations in all three models with the redox couple homodimer model saturating at a lower hydrogen peroxide concentration than the other models (Figure 2.7C and F).

Table 2.5 Parameters determined by fitting of the peroxiredoxin activity models to the human erythrocyte peroxiredoxin 2 *in vitro* dataset using non-linear regression analysis.

Parameter	Value	Fitted Curve
All Models		*In vitro* dataset (•) Ping-pong enzyme model (−) Redox couple monomer model (−) Redox couple homodimer model (−)
$k_{cat\,1}$ (TR)	0.179 s^{-1}	
Ping-Pong Enzyme Model		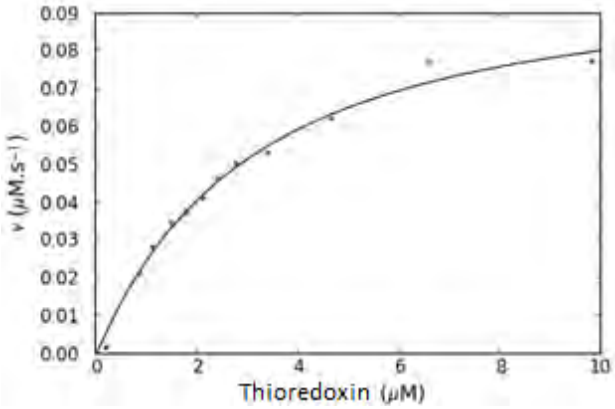
$k_{cat\,2}$ (Prx)	0.311 s^{-1}	
K_m (H_2O_2)	16.59 µM	
r^2	0.99	
Redox Couple Monomer Model		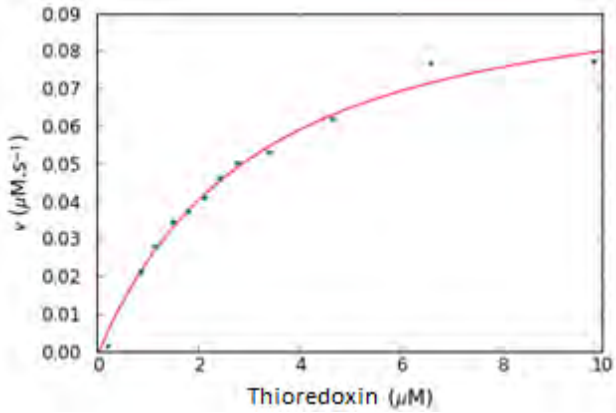
k_2	6.67×10^3 M^{-1} s^{-1}	
k_3	9.59×10^4 M^{-1} s^{-1}	
r^2	0.98	
Redox Couple Homodimer Model		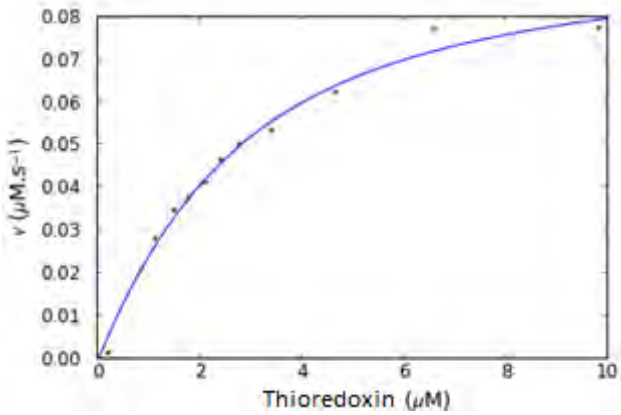
k_2	3.33×10^3 M^{-1} s^{-1}	
k_3	4.80×10^4 M^{-1} s^{-1}	
r^2	0.99	

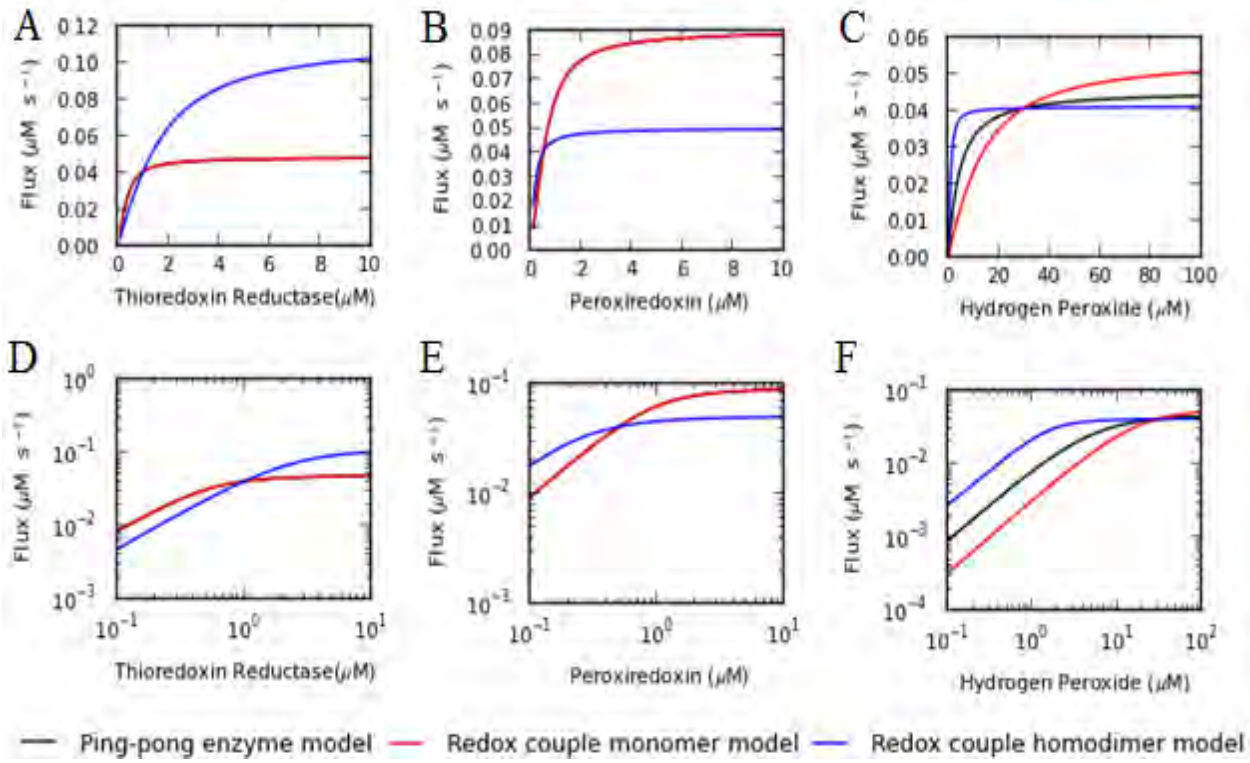

Figure 2.7 The responses of the fitted ping-pong enzyme, redox couple monomer and redox couple homodimer models for human erythrocyte peroxiredoxin 2 activity (Manta *et al.*, 2009) to parameter changes were compared in linear (A-C) and log scale (D-F). The responses of the ping-pong enzyme (black) and redox couple monomer (red) models overlap in A, B, D and E.

As with the core modelling (Figure 2.2-2.5), the thioredoxin redox state was then monitored to determine if there were also qualitative and quantitative differences in the response of the models. Firstly, the reduced thioredoxin concentration remained greater than the oxidised thioredoxin concentration over all hydrogen peroxide concentrations tested in the ping-pong enzyme and redox couple monomer model (Figure 2.8). However, in the redox coupler homodimer model, thioredoxin distributed into the oxidised form, consistent with the saturation of this model at a low hydrogen peroxide concentration (Figure 2.7C and F). The fitted redox couple homodimer model also showed a distinct quantitative response to increasing thioredoxin reductase and peroxiredoxin concentrations, while the ping-pong enzyme and redox couple monomer models had near identical responses to changes in these parameters (Figure 2.9). In summary, all three proposed kinetic models for peroxiredoxin activity can be fitted to the *in vitro* dataset described by Manta *et al.* (2009) and the parameters obtained by fitting the whole system of reactions did not agree with the parameters obtained when peroxiredoxin reduction of hydrogen peroxide was studied in

isolation of its cognate system using a competition assay. Finally, while the fitted ping-pong enzyme and redox couple monomer models showed similar responses in terms of flux and redox state of thioredoxin over most of the parameters tested, the redox couple homodimer model showed distinct responses to these parameters perturbations.

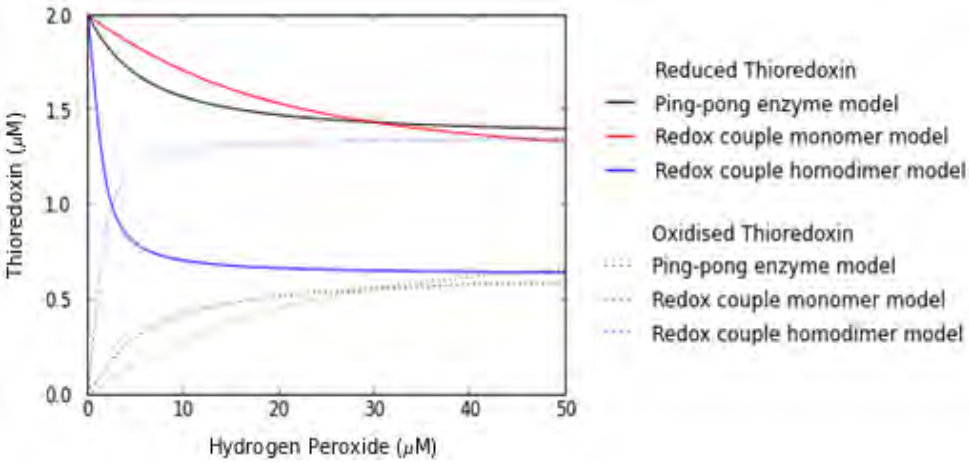

Figure 2.8 The fitted models for peroxiredoxin activity showed differences in the steady state reduced and oxidised thioredoxin concentrations in response to increasing hydrogen peroxide concentrations.

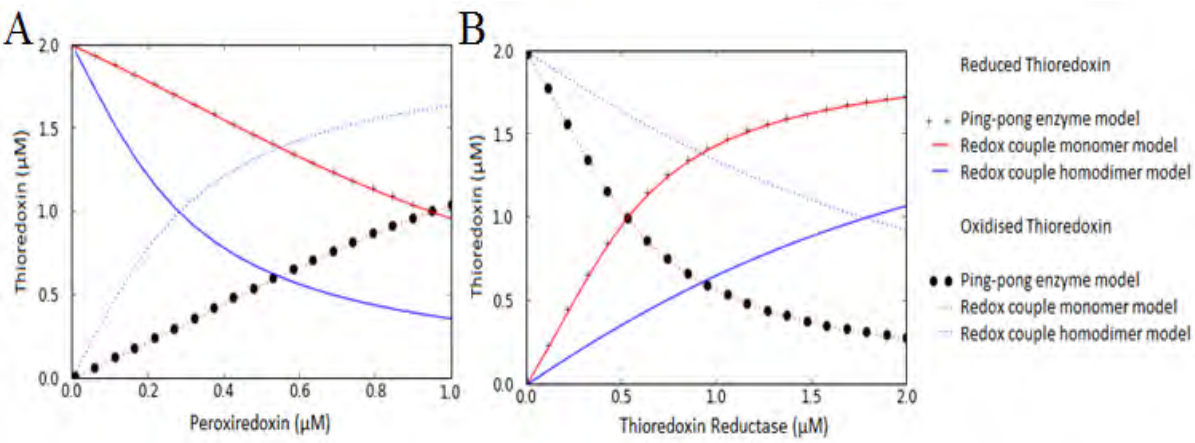

Figure 2.9 The redox couple homodimer fitted model for peroxiredoxin activity predicted different steady state reduced and oxidised thioredoxin concentrations to the ping-pong enzyme and redox couple monomer fitted models with increasing peroxiredoxin (A) and thioredoxin reductase (B) concentrations.

2.3.3 Flux control patterns of the fitted human peroxiredoxin 2 kinetic models

Operationally, flux control coefficients represent the percentage change, positive or negative, in the system flux caused by a one percent change in a single reaction. (Fell, 2005).

The flux control co-efficient can be precisely described using equation 2.3; where J represents the system flux and v_i represents the rate of reaction, i (Fell, 1997).

$$C_{v_i}^{J} = \frac{\partial J}{\partial v_i} \cdot \frac{v_i}{J} = \frac{\partial \text{In}\, J}{\partial \text{In}\, v_i} \qquad (2.3)$$

Using PySCeS, flux control coefficients were determined for the fitted peroxiredoxin activity models to understand the flux control in each of the fitted models (Table 2.5). No single reaction (flux control coefficient ~ 1) held complete flux control in both the fitted ping-pong enzyme and redox couple monomer models, suggesting that hydrogen peroxide reduction was not the sole rate-limiting step despite the experimental conditions chosen for this purpose (Manta *et al.*, 2009). Interestingly, in both models, the flux control coefficient for thioredoxin reduction (Reaction 1, Table 2.6) were a similar value (0.232) and the peroxiredoxin redox cycle held the remaining flux control (0.768), emphasizing the similarity of these two models. In the fitted redox couple homodimer model, flux control was mostly distributed across the thioredoxin reduction and hydrogen peroxide reduction reactions and again no single reaction could be described as rate-limiting in this system. The redox couple homodimer model therefore had a complex flux control pattern suggesting that assigning a rate-limiting step in the system would be difficult under these experimental conditions. These flux control patterns suggest that fitting of an entire computational model to *in vitro* kinetic datasets may be the best method to determine kinetic parameters for this system (see for example Pillay *et al.*, 2009; Mashamaite *et al.*, 2015; Padayachee and Pillay, 2015).

Table 2.6 Comparison of flux control coefficients for each reaction in the peroxiredoxin kinetic activity models fitted to the human peroxiredoxin 2 dataset *

Reactions	Flux Control Coefficients
Ping-Pong Enzyme Model	
1	$C_{R1}^{JR1} = 0.232$
$NADPH + Trx_{SS} \rightarrow NADP^{+} + Trx_{SH}$	$C_{R2}^{JR1} = 0.768$
2	$C_{R1}^{JR2} = 0.232$
$Trx_{SH} + H_2O_2 \rightarrow TrxSS + H_2O$	$C_{R2}^{JR2} = 0.768$

Redox Couple Monomer Model	
1 $NAD_{PH} + Trx_{SS} \rightarrow NADP^{+} + Trx_{SH}$	$C_{R1}^{JR1} = 0.232$ $C_{R2}^{JR1} = 0.313$ $C_{R3}^{JR1} = 0.455$
2 $H_2O_2 + Prx_{SH} \rightarrow H_2O + Prx_{SS}$	$C_{R1}^{JR2} = 0.232$ $C_{R2}^{JR2} = 0.313$ $C_{R3}^{JR2} = 0.455$
3 $Prx_{SS} + Trx_{SH} \rightarrow Prx_{SH} + Trx_{SS}$	$C_{R1}^{JR3} = 0.232$ $C_{R2}^{JR3} = 0.313$ $C_{R3}^{JR3} = 0.455$
Redox Couple Homodimer Model*	
1 $NADPH + Trx_{SS} \rightarrow NADP^{+} + Trx_{SH}$	$C_{R1}^{JR1} = 0.771$ $C_{R4}^{JR1} = 0.207$
2 $Prx_{SH}Prx_{SH} + H_2O_2 \rightarrow PrxS_{S}Prx_{SH} + H_2O$	$C_{R3}^{JR2} = -0.977$ $C_{R5}^{JR2} = 0.928$
3 $Prx_{SS}Prx_{SH} + H_2O_2 \rightarrow Prx_{SS}Prx_{SS} + H_2O$	$C_{R1}^{JR3} = 0.733$ $C_{R4}^{JR3} = 0.242$
4 $Prx_{SS}Prx_{SS} + Trx_{SH} \rightarrow Prx_{SS}Prx_{SH} + Trx_{SS}$	$C_{R1}^{JR4} = 0.733$ $C_{R4}^{JR4} = 0.242$
5 $Prx_{SS}Prx_{SH} + Trx_{SH} \rightarrow Prx_{SH}Prx_{SH} + Trx_{SS}$	$C_{R3}^{JR5} = -0.977$ $C_{R5}^{JR5} = 0.928$

*Table has been truncated to exclude reactions with low flux control, for the full table of reactions refer to the appendix (Table S1, Appendix 2.14). The reaction with the highest flux control is shown in column three for clarity.

2.3.4 Kinetic modelling of an *in vitro* bacterial peroxiredoxin dataset confirms a deficiency in our understanding of peroxiredoxin kinetics

The regulation and activity of mammalian peroxiredoxins is considered to be more complex than bacterial peroxiredoxins as they are considerably more susceptible to hyperoxidation by hydrogen peroxide (Section 1.3.2). The peroxiredoxin kinetic models were also fitted to a bacterial substrate saturation dataset to see if the differences observed in the mammalian dataset were present in a 'simpler' bacterial system.

Caulobacter crescentus peroxiredoxin activity was determined by measuring NADPH oxidation at 340 nm with increasing hydrogen peroxide concentrations (Figure 2.10, Cho *et al.*, 2012). For realistic system modelling, kinetic parameters were obtained from the BRENDA parameter database for the *E. coli* thioredoxin and thioredoxin reductase which were used in this assay. Simulation of the peroxiredoxin activity models with these parameters (Table 2.7) and the species concentrations used in this assay (Table 2.8, Cho *et al.*, 2012) failed to reproduce the *in vitro* dataset and the responses also differed between the models (Figure 2.11) as was seen with the human peroxiredoxin dataset (Figure 2.6).

Table 2.7 Realistic parameters used for modelling of a *C. crescentus* peroxiredoxin *in vitro* dataset (Cho *et al.*, 2012).

Reaction	Parameter	Value	Reference
	All Models		
R1: NADPH + Trx_{SS} → $NADP^+$ + Trx_{SH}	$k_{cat\ 1}$	22.75 s^{-1}	(Gleason *et al.*, 1990)
	K_{nadph}	1.2 μM	(Williams Jr, 1976)
	K_{trxss}	2.8 μM	(Williams Jr, 1976)
	Ping-Pong Enzyme Model		
R2: Trx_{SH} + H_2O_2 → Trx_{SS} + H_2O	$k_{cat\ 2}$	73 s^{-1}	(Baker and Poole, 2003)
	K_{trxsh}	24 μM	(Baker and Poole, 2003)
	K_{h2o2}	106 μM	(Cho *et al.*, 2012)
	Redox Couple Monomer Model		
R2: H_2O_2 + Prx_{SH} → H_2O + Prx_{SS}	k_2	0.74 μM^{-1} s^{-1}	(Cho *et al.*, 2012)
R3: Prx_{SS} + Trx_{SH} → Prx_{SH} + Trx_{SS}	k_3	2.98 μM^{-1} s^{-1}	a

Redox Couple Homodimer Model			
R2: $Prx_{SH}Prx_{SH} + H_2O_2 \rightarrow Prx_{SS}Prx_{SH} + H_2O$	k_2	0.74 μM^{-1} s^{-1}	(Cho *et al.*, 2012)
R3: $Prx_{SS}Prx_{SH} + H_2O_2 \rightarrow Prx_{SS}Prx_{SS} + H_2O$	k_2	0.74 μM^{-1} s^{-1}	(Cho *et al.*, 2012)
R4: $Prx_{SS}Prx_{SS} + Trx_{SH} \rightarrow Prx_{SS}Prx_{SH} + Trx_{SS}$	k_3	2.98 μM^{-1} s^{-1}	a
R5: $Prx_{SS}Prx_{SH} + Trx_{SH} \rightarrow Prx_{SH}Prx_{SH} + Trx_{SS}$	k_3	2.98 μM^{-1} s^{-1}	a

[a] estimated from k_{cat}/K_m ratio by Baker and Poole (2003).

Table 2.8 Species concentrations of the various system components used in each model for realistic modelling of the periplasmic peroxiredoxin from *C. crescentus* obtained from Cho *et al.* (2012).

Model	Species	Initial Concentration (µM)
All	NADPH	100
	NADP	1
	Trx_{SH}	4*
	Trx_{SS}	4
	TR	0.5
	H_2O_2	5-500
Ping-Pong Enzyme	Prx	0.5
Redox Couple Monomer	Prx_{SH}	0.25*
	Prx_{SS}	0.25
Redox Couple Homodimer	$Prx_{SH}Prx_{SH}$	0.167*
	$Prx_{SS}Prx_{SH}$	0.167
	$Prx_{SS}Prx_{SS}$	0.166

*Note that the total concentration (reduced and oxidised) of all moiety conserved species is equal to the final concentration used in the activity assay.

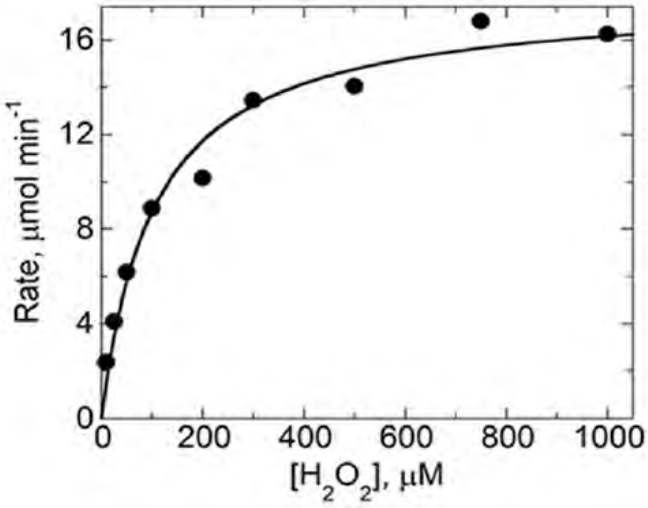

Figure 2.10 The activity of a periplasmic peroxiredoxin from *C. crescentus* was determined in a NADPH-coupled activity assay (Cho *et al.*, 2012). The assay consisted of 100 µM NADPH, 8 µM *E.coli* thioredoxin, 0.5 µM *E.coli* thioredoxin reductase and 0.5 µM peroxiredoxin.

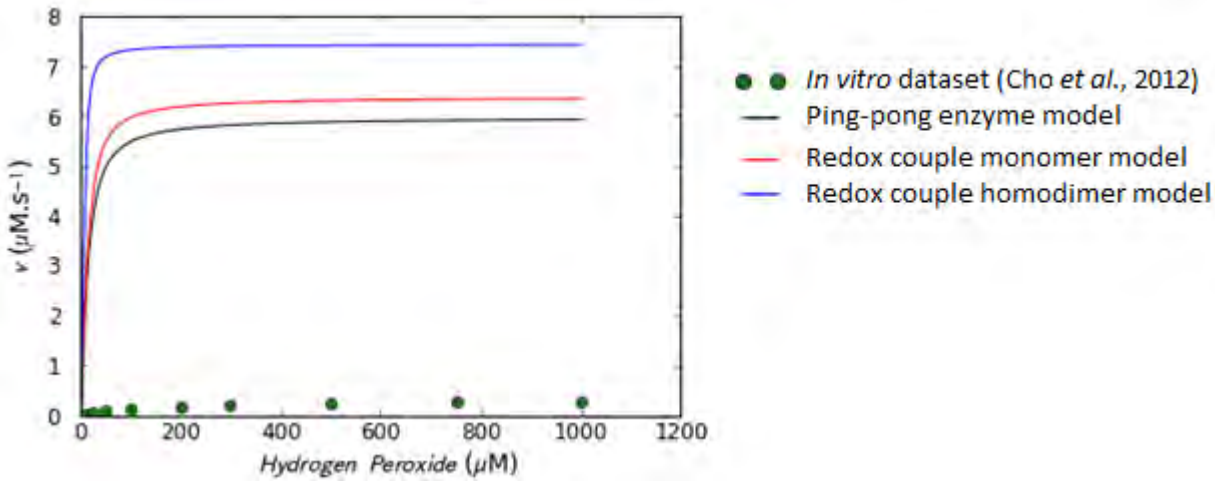

Figure 2.11 Kinetic models of a bacterial peroxiredoxin system failed to reproduce an *in vitro* dataset (Cho *et al.*, 2012) with increasing hydrogen peroxide concentrations.

The rate constants used in the computational models for the thioredoxin-dependent reduction of peroxiredoxin (k_3) were estimated from the *E. coli* peroxiredoxin system (Baker and Poole, 2003). These constants could therefore be different for the *C. crescentus* peroxiredoxin, which could account for discrepancies between the models and the *in vitro* dataset (Figure 2.11). However, these rate constants were in a similar range to rate constants reported for other peroxiredoxins and the models were then fitted to this dataset to determine parameters for the *C. crescentus* peroxiredoxin system (Table 2.9).

Table 2.9 Kinetic parameters determined by data fitting of the models to the *in vitro* *C. crescentus* periplasmic peroxiredoxin dataset.

Parameter	Value	Fitted Curve
		In vitro dataset (•) Ping-pong enzyme model (−) Redox couple monomer (−) Redox couple monomer model (−)
Ping-Pong Enzyme Model		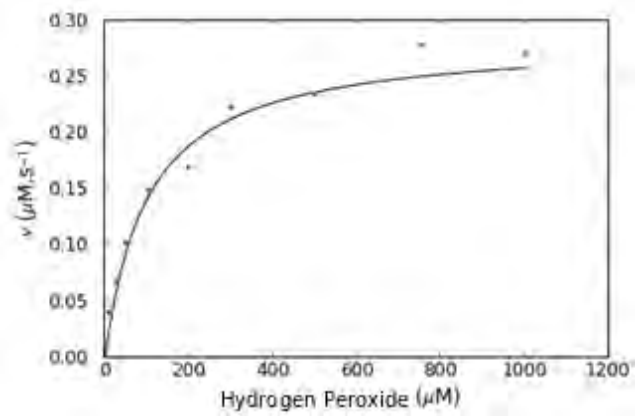
$k_{cat\,2}$ (Prx)	0.592 s^{-1}	
K_{trxsh}	0.347 μM	
r^2	0.98	
Redox Couple Monomer Model		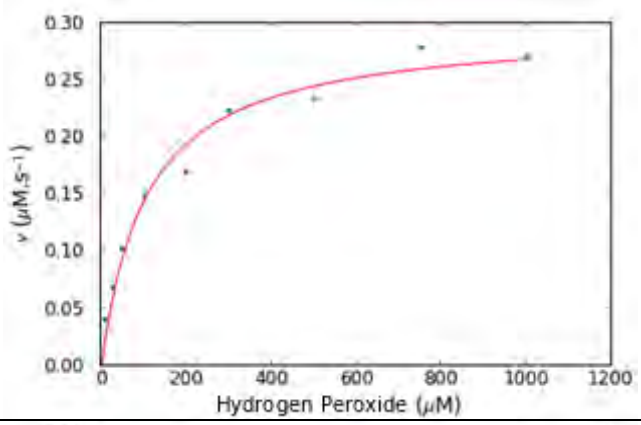
k_2	5.61×10^3 M^{-1} s^{-1}	
k_3	7.47×10^4 M^{-1} s^{-1}	
r^2	0.98	
Redox Couple Homodimer Model		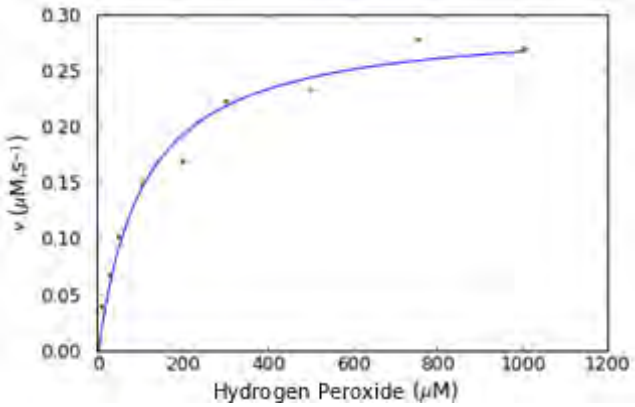
k_2	2.80×10^3 M^{-1} s^{-1}	
k_3	3.73×10^4 M^{-1} s^{-1}	
r^2	0.98	

As with the human peroxiredoxin 2 fitted models (Table 2.5), the rate constants for hydrogen peroxide reduction differed from the range of rate constants (10^6-10^8 M^{-1} s^{-1})

usually determined by competition assay for other peroxiredoxins (Table 2.9). The fitted rate constant for hydrogen peroxide reduction was 5.58 × 10^3 M^{-1} s^{-1} in the ping-pong enzyme model, 5.61 × 10^3 M^{-1} s^{-1} in the redox couple monomer model and 2.80 × 10^3 M^{-1} s^{-1} in the redox couple homodimer model (r^2= 0.98, Table 2.9). Using these fitted parameters, the peroxiredoxin kinetic models were then simulated to determine if there were differences in their response to parameter changes. Flux analysis of the models showed that when compared to the redox couple monomer and homodimer models, the ping-pong enzyme model had a distinct response to increasing thioredoxin reductase (Figure 2.12A and D), thioredoxin (Figure 2.12B and E), and peroxiredoxin concentrations (Figure 2.12C and F). The greatest difference was observed with increasing thioredoxin concentrations, where the ping-pong enzyme model showed substrate saturation at a lower thioredoxin concentrations and the maximal flux obtained was also much lower than the other models. The redox couple monomer and homodimer models gave near identical response to all parameters changes tested in the system (Figure 2.12A-F).

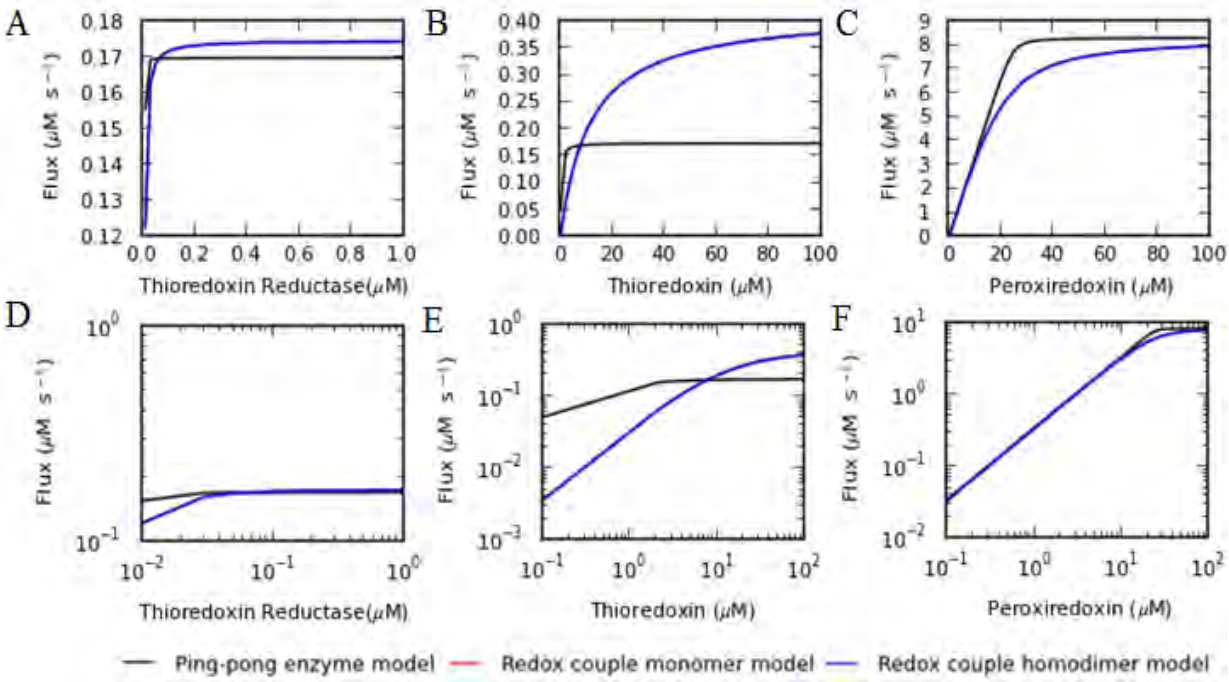

Figure 2.12 The ping-pong enzyme, redox couple monomer and redox couple homodimer models for peroxiredoxin activity were fitted to an *in vitro C. crescentus* peroxiredoxin dataset. Changes to the system were monitored in linear and double log space with 150 µM of hydrogen peroxide chosen as this concentration is non-saturating in the system (Table 2.9). The response of the redox couple monomer (red) and homodimer (blue) models overlap in A-F.

The thioredoxin redox state showed similar response in all the models to most parameter changes made to the system (data not shown). However with increasing peroxiredoxin concentrations, differences between the ping-pong enzyme model and the redox couple monomer and homodimer models were revealed (Figure 2.13). In summary and in contrast to the human erythrocyte peroxiredoxin 2 models (Section 2.3.2), the fitted *C. crescentus* redox couple monomer and homodimer models showed similar responses to parameter changes that were distinct to some responses of the ping-pong model. These results emphasised the complex kinetic relationships between these models and flux control analysis was then performed to determine the flux control pattern in these models (Table 2.10)

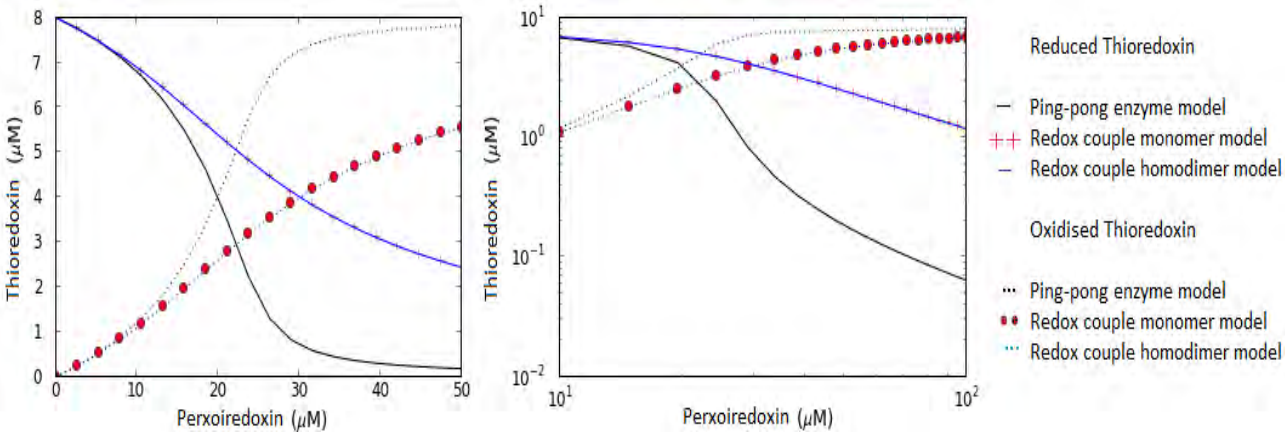

Figure 2.13 The fitted models for peroxiredoxin activity show differences in the steady state reduced and oxidised thioredoxin concentrations in response to increasing peroxiredoxin concentrations and a non-saturating hydrogen peroxide concentration of 150 μM.

2.3.5 Flux control patterns of the fitted periplasmic peroxiredoxin kinetic models

Flux control in the fitted ping-pong enzyme model was determined to be primarily in the hydrogen peroxide reduction reaction and split between the peroxiredoxin redox cycle reactions in redox couple monomer model (Table 2.10). In the fitted redox couple homodimer model, a complex flux control pattern was observed with flux control split among several reactions including hydrogen peroxide reduction and the two peroxiredoxin reduction reactions.

Table 2.10 Comparison of flux control coefficients for each reaction in the peroxiredoxin activity models fitted to the *C. crescentus* periplasmic peroxiredoxin dataset. *

Reaction	Flux Control Co-efficient
Ping-Pong Enzyme Model	
1 $NADPH + Trx_{SS} \rightarrow NADP^{+} + Trx_{SH}$	$C_{R2}^{JR1} = 0.9999$
2 $Trx_{SH} + H_2O_2 \rightarrow Trx_{SS} + H_2O$	$C_{R2}^{JR2} = 0.9999$
Redox Couple Monomer Model	
`1 $NADPH + Trx_{SS} \rightarrow NADP^{+} + Trx_{SH}$	$C_{R1}^{JR1} = 0.00329$ $C_{R2}^{JR1} = 0.413$ $C_{R3}^{JR1} = 0.584$
2e $H_2O_2 + Prx_{SH} \rightarrow H_2O + Prx_{SS}$	$C_{R1}^{JR2} = 0.00329$ $C_{R2}^{JR2} = 0.413$ $C_{R3}^{JR2} = 0.584$
3 $Prx_{SS} + Trx_{SH} \rightarrow Prx_{SH} + Trx_{SS}$	$C_{R1}^{JR3} = 0.00329$ $C_{R2}^{JR3} = 0.413$ $C_{R3}^{JR3} = 0.584$
Redox Couple Homodimer Model*	
1 $NADPH + Trx_{SS} \rightarrow NADP^{+} + Trx_{SH}$	$C_{R3}^{JR1} = 0.242$ $C_{R4}^{JR1} = 0.342$ $C_{R5}^{JR1} = 0.242$
2	$C_{R3}^{JR2} = -0.345$

$Prx_{SH}Prx_{SH} + H_2O_2 \rightarrow Prx_{SS}Prx_{SH} + H_2O$	$C_{R4}^{JR2} = 0.341$ $C_{R5}^{JR2} = 0.827$
3 $Prx_{SS}Prx_{SH} + H_2O_2 \rightarrow Prx_{SS}Prx_{SS} + H_2O$	$C_{R3}^{JR3} = 0.656$ $C_{R4}^{JR3} = 0.343$
4 $Prx_{SS}Prx_{SS} + Trx_{SH} \rightarrow Prx_{SS}Prx_{SH} + Trx_{SS}$	$C_{R3}^{JR4} = 0.656$ $C_{R4}^{JR4} = 0.343$
5 $Prx_{SS}Prx_{SH} + Trx_{SH} \rightarrow PrxS_{H}Prx_{SH} + Trx_{SS}$	$C_{R3}^{JR5} = -0.345$ $C_{R4}^{JR5} = 0.341$ $C_{R5}^{JR5} = 0.827$

*Table has been truncated to exclude the reactions with low flux control, for full table of reactions refer to appendix (Table S2, 2.12). The reaction with the highest flux control is shown in column three for clarity.

2.4 Discussion

Computational modelling of the peroxiredoxin system aimed to analyse the three kinetic descriptions of the system in the literature. Peroxiredoxins have been described with both ping-pong and mass action kinetics and the functional unit of their activity has been modelled as both a monomer and a homodimer (Figure 1.6). To determine if these descriptions were equivalent, peroxiredoxin kinetic models were analysed with core parameters which revealed quantitative differences in their responses to increasing thioredoxin reductase, hydrogen peroxide and peroxiredoxin concentrations (Figure 2.1). Although these kinetic descriptions have been used interchangeably in published literature on the system, these results revealed that the computational models based on these peroxiredoxin kinetic models are expected to have distinct behaviours and some of the published computational models (Table 1.1) are likely to be inaccurate.

Simulation of the peroxiredoxin activity models with realistic parameters for human peroxiredoxin 2 failed to reproduce an *in vitro* dataset for this peroxiredoxin (Figure 2.6), showing a disconnect between the proposed models for peroxiredoxin activity and the kinetic parameters that have been generated for their activity (Manta *et al.*, 2009). The models were then fitted to the *in vitro* dataset to determine the parameters necessary to reproduce the

dataset and all the models showed excellent fits, highlighting the complexity of kinetic analysis of this system (Table 2.5). Parameter changes made to the fitted models showed similar responses in the fitted ping-pong enzyme and redox couple monomer models, while the redox couple homodimer model had distinct responses (Figure 2.7 and 2.10). The models were also fitted to an *in vitro* dataset for *C. crescentus* peroxiredoxin after again failing to reproduce the dataset (Figure 2.11). Simulation of the fitted models revealed a similar response between the redox couple monomer and homodimer models which was different to the response of the ping-pong enzyme model (Figure 2.12 and 2.14) and confirmed that the peroxiredoxin kinetic models cannot be used interchangeably. Data fitting of the models generated parameters that set the rate constants for hydrogen peroxide reduction in the range of 10^3-10^4 M^{-1} s^{-1} (Table 2.5 and 2.9) which contrasts with rate constants (k_{obs}) of 10^6-10^8 M^{-1} s^{-1} that have been reported for peroxiredoxins in absence of their cognate system (see for example Nelson *et al.*, 2008; Manta *et al.*, 2009). Recently, a large scale realistic model of hydrogen peroxide reduction in erythrocytes (Benfeitas *et al.*, 2014) also reported that the rate constant for hydrogen peroxide reduction by peroxiredoxins was in the range of 10^5 M^{-1} s^{-1}. In summary, studying the peroxiredoxin system as a whole and system-wide data fitting may be a more accurate method for parameter estimation *in vitro*.

Using core modelling, the thioredoxin redox state was monitored with increasing thioredoxin reductase, peroxiredoxin, hydrogen peroxide and NADPH concentrations (Figure 2.2 – 2.5). Qualitative and quantitative differences between the models were observed and further support that the proposed peroxiredoxin kinetic models were not interchangeable. Analysis of the models with realistic parameters was then carried out which also revealed thioredoxin redox state differences with the fitted human peroxiredoxin 2 (Figure 2.8-2.10) and *C. crescentus* models (Figure 2.13). These redox states, which have largely been ignored in previous *in vitro* studies, could be useful outputs for analysing peroxiredoxin activity and distinguishing the peroxiredoxin kinetic models.

Flux control analysis of the peroxiredoxin kinetic models with parameters from both the fitted models for human peroxiredoxin 2 (Table 2.6) and *C. crescentus* peroxiredoxin (Table 2.10) revealed that in some kinetic models complete flux control was not in any single step. Further, the redox couple monomer and homodimer kinetic models had very complex flux control patterns, suggesting that assigning a rate limiting step for this system *in vitro* is not trivial. Collectively, these results argue that it is critical that the correct kinetic model be used for peroxiredoxin activity and that whole system fitting may be the most appropriate

method for determining the rate constants for hydrogen peroxide reduction. The difference in flux control pattern between the models and the quantitative and qualitative differences observed between the peroxiredoxin activity models could potentially be used to distinguish the models *in vitro* and determine which model should be used in system biology studies of the peroxiredoxin system.

Chapter 3

The cloning of yeast peroxiredoxin *TSA1* and the purification of the peroxiredoxin system proteins.

3.1 Introduction

The *S. cerevisiae* cytosolic TSA1 peroxiredoxin system was chosen for this project to resolve the conflicting descriptions of peroxiredoxin activity. The system consisted of a peroxiredoxin, thioredoxin, thioredoxin reductase and NADPH and the steady state system rate for hydrogen peroxide degradation could be determined by measuring NADPH oxidation at 340 nm (Munhoz and Netto, 2004; Nelson and Parsonage, 2011). Expression plasmids for *S. cerevisiae* thioredoxin (*TRX1*) and thioredoxin reductase (*TRR1*) were already present in the laboratory for expression and purification of these proteins. The cloning of *TSA1* and the purification of the TSA1, TRX1 and TRR1 proteins will be described below.

3.2 Materials and Methods

3.2.1 Materials

Polymerases and all other PCR reagents, including PCR primers for the yeast peroxiredoxin *TSA1*, were obtained from Inqaba Biotech (Johannesburg, South Africa). The Thermo Scientific (Massachusetts, United States) InsTAclone PCR, Rapid Ligation and GeneJET Gel Purification Kits were also purchased from Inqaba Biotech (Johannesburg, South Africa). The NEB restriction enzymes (NEB, Massachusetts, United States), NdeI and HindIII, were obtained from The Scientific Group (Midrand, South Africa). Dithiothreitol (DTT), Coomassie G-250 and R-250 powder, TEMED and ammonium persulfate were obtained from Sigma (Capital Labs, Johannesburg, South Africa). Agarose for gel electrophoresis and the Qiagen (Hilden, Germany) Ni-NTA agarose resin for protein purification were obtained from Whitehead Scientific (Pty) Ltd (Cape Town, South Africa). Acrylamide: Bis (37:5:1) ready to use solution was obtained from Merck (South Africa) and the non-denaturing PAGE kit for molecular weights 14 kDa – 272 kDa was obtained from Sigma (Kawasaki, Japan and distributed by Capital Labs, Johannesburg, South Africa). All

other common chemicals such as Tris-HCl and EDTA were of the highest purity available and were obtained from Saarchem/Merck (Johannesburg, South Africa).

3.2.1. *Saccharomyces cerevisiae* genomic DNA isolation

Genomic DNA was isolated from *Saccharomyces cerevisiae* BY4743 (*MATa/MATα his3Δ0/his3Δ0 leu2Δ0/leu2Δ0 MET15/met15Δ0 LYS2/lys2Δ0 ura3Δ0 /ura3Δ0*) using Bust n' Grab protocol (Harju *et al.*, 2004). An overnight culture of yeast cells grown in YPD media was centrifuged to pellet the cells (20 000 × *g*, 5 minutes, RT). The pellet was resuspended in lysis buffer (200 µl, 2% (v/v) Triton X-100, 1% (w/v) SDS, 10 mM Tris-HCl, 1 mM EDTA, and 100 mM NaCl, pH 8.0) and the cells were freeze-thawed twice by incubation at -75°C (5 minutes) and then at 95°C (1 minute). Chloroform (200 µl) was added to the cell suspension, which was then centrifuged (20 000 × *g*, 3 minutes, RT). Three distinct layers were formed and the upper aqueous phase was transferred into a fresh micro-centrifuge tube containing 100% (v/v) ice-cold ethanol (400 µl) to precipitate the DNA. The precipitated DNA was pelleted by centrifugation (20 000 × *g*, 5 minutes, RT), the pellet was washed with 70% (v/v) ethanol (500 µl) and centrifuged (13 000 × *g*, 1 minute, RT). The pellet was air-dried and resuspended in TE buffer (100 µl, 10 mM Tris-HCl and 1 mM EDTA, pH 8.0). The genomic DNA was analysed by agarose gel electrophoresis and using a NanoDrop™ 2000 UV-Vis Spectrophotometer to estimate the concentration and purity.

3.2.2 *TSA1* Primer Design

PCR primers for *TSA1* were designed using Primer3 (bioinfo.ut.ee/primer3-0.4.0/) and their specificity was confirmed using Primer Blast (NCBI) to ensure that *E. coli* peroxiredoxins were not inadvertently amplified by PCR. The *TSA1* gene was amplified from yeast genomic DNA using the forward primer 5'-agc<u>catATG</u>GTCGCTCAAGTTCAAAAGC-3' containing an NdeI restriction site and the reverse primer 5'-acg<u>aagcTT</u>ATTTGTTGGCAGCTTCGAAG-3' containing a HindIII restriction site (underlined). Extra bases were added to the 5' end of the restriction site to aid with cutting of the PCR product by restriction enzymes.

3.2.3 PCR amplification of *TSA1*

PCR was used to clone the yeast peroxiredoxin gene *TSA1* and to confirm the presence of the gene in plasmids. The PCR reaction contained DreamTaq buffer (1X, containing $MgCl_2$), dNTP mix (200 µM), forward and reverse primer (500 nM each),

additional $MgCl_2$ was added to give a final reaction concentration of 2.5 mM, template DNA (0.2-1 ng), DreamTaq DNA polymerase (0.5 U/25 µl) and sterile nuclease-free water. The PCR reaction conditions were as follows: initial denaturation at 94ºC (3 minutes), denaturation at 94ºC (30 seconds), annealing 55ºC (30 seconds), extension at 72ºC (1 minute) and a final extension at 72ºC (7 minutes or 20 minutes for TA cloning). The PCR reactions were run for 25 cycles and the amplicons were visualized by agarose gel electrophoresis to estimate the concentration and purity of the product.

3.2.4 Ligation

For all ligation reactions, a molar insert to vector ratio of 3:1 was used. For ligation of *TSA1* into pTZ57R/T, the Thermo Scientific InsTAclone PCR kit was used while the Thermo Scientific Rapid Ligation Kit was used for ligation of *TSA1* into pET28a. Ligations were performed at room temperature (1 hour) then transferred to 4°C (overnight).

3.2.5 TA cloning of *TSA1* into *Escherichia coli* JM109

To make *E. coli* JM109 cells competent, C-media (2 ml, Thermo Scientific InsTAclone PCR cloning kit) was inoculated with *E. coli* JM109 cells and grown at 37°C (overnight). The *E. coli* JM109 cell culture (150 µl) was added to fresh pre-warmed C-medium (1.5 ml) and incubated at 37ºC (20 minutes, 150 rpm). The cells were then pelleted by centrifugation in a desktop centrifuge (maximum speed, 1 minute, RT) and then treated with T-solution (300 µl, Thermo Scientific InsTAclone PCR cloning kit) to make the cells competent. The ligation mix (2.5 µl) was added to the competent cells and incubated on ice (30 minutes). The cells were then plated onto LB agar plates containing ampicillin (50 µg/ml), X-gal (80 µg/ml) and IPTG (0.1 mM) for blue/white colony selection. Several control plates were also prepared including competent cells on LB media to check the viability of the cells, a negative control of competent cells on LB media containing ampicillin to check that the ampicillin was not denatured during plate preparation, a negative control of competent cells transformed with uncut pTZ57R/T vector and a positive control of competent cells transformed with pTZ57R/T vectors that have been ligated with a fragment insert to ensure that the cells were competent and that the X-gal and IPTG had not been denatured. This final control plate was also used to determine the transformation efficiency. The plates were left to grow in an incubator overnight at 37°C, white colonies were then randomly chosen from the LB media plates containing ampicillin, X-gal and IPTG and inoculated into

LB broth containing ampicillin (100 µg/ml) and grown overnight at 37°C. The plasmids were isolated by plasmid mini-prep and the presence of the *TSA1* gene insert was confirmed by PCR and restriction digestion.

3.2.6 Plasmid Mini-Prep

An alkaline lysis plasmid mini-prep (Sambrook and Russell, 2006) was performed to isolate plasmids from an overnight culture (10 ml, 150 rpm). The overnight culture was centrifuged (7250 x *g*, 5 minutes, RT) and the cells were resuspended in GTE solution (200 µl, 50 mM glucose, 25 mM Tris-HCl, 10 mM EDTA, pH 8.0), RNase A solution (2 µl, 20 mg/ml stock) was added and the tube was incubated at room temperature for 5 minutes. The cell suspension was transferred to a fresh 1.5 ml Eppendorf tube, NaOH/SDS (400 µl, 0.2 M NaOH, 1% SDS) was added and the tube was gently inverted six times, then incubated at room temperature (5 minutes). Potassium acetate (300 µl, 3 M) was added to the tube, which was again gently inverted six times, then incubated at room temperature (5 minutes). The tube was centrifuged in a desktop centrifuge (maximum speed, 5 minutes, RT) and the supernatant (800 µl) was transferred to a fresh 1.5 ml Eppendorf tube. Ice-cold isopropanol (600 µl) was added to the tube, which was then incubated at -20ºC (30 minutes) to precipitate the DNA. The tube was then centrifuged in a desktop centrifuge (maximum speed, 5 minutes), the supernatant discarded and 70% ice-cold ethanol (0.5 ml) was used to wash the pellet. The tube was then centrifuged in a desktop centrifuge (maximum speed, 1 minute, RT), the supernatant removed and the pellet air-dried for 10 minutes. The pellet was resuspended in TE buffer (50 µl, 10 mM Tris-HCl and 1 mM EDTA, pH 8.0).

3.2.7 Restriction digestion of plasmids

Plasmid DNA (1 µg) was digested overnight at 37°C with restriction enzymes NdeI (2 U) and HindIII (1 U) in NEB Buffer 2. NdeI cuts both pTZ57R/T and pET28a once while HindIII cuts pTZ57R/T once and pET28a twice. For all reactions an uncut control and single digest with NdeI or HindIII was performed as controls to check DNA quality prior to digestion and to ensure that both enzymes were active.

3.2.8 Transformation of pET28 with TSA1 into *Escherichia coli* BL21

Competent *E. coli* BL21 cells were made by calcium chloride treatment (Dagert and Ehrlich, 1979). In this method, an overnight *E. coli* BL21 culture (2 ml) was transferred to

LB broth (50 ml) and grown until the OD_{600} reading was between 0.3-0.4. The cell culture was chilled on ice (10 minutes) and then centrifuged (4500 x *g*, 10 minutes, 4ºC). The pellet was resuspended in ice-cold $CaCl_2$ (40 ml, 0.1 M) and the cells were then pelleted by centrifugation (4500 x *g*, 10 minutes, 4ºC). The pellet was resuspended in ice-cold $CaCl_2$ (2 ml, 0.1 M, 30 minutes). Competent cells (20 µl) were then incubated with the ligation mix (2.5 µl, 30 minutes, 4ºC), heat shocked (42ºC for 90 seconds) and cooled (4ºC for 2 minutes). Pre-warmed SOC media (80 µl at 37°C, 2% (w/v) tryptone, 0.5% (w/v) yeast extract, 10 mM $MgCl_2$, 10 mM NaCl, 2.5 mM KCl and 20 mM filter sterilized glucose was added after autoclaving) was added to the cells, which were then incubated at 37ºC in a shaking water bath (1 hour). The transformation mix (50 µl) was spread on LB agar plates containing kanamycin (30 µg/ml) and the cells were grown overnight at 37°C.

Controls were set up to check viability of the cells after the competent cell treatment, to determine transformation efficiency and to ensure that the kanamycin antibiotic in the plates was still active. Recombinant colonies were randomly selected from the LB agar plates and inoculated into LB broth containing kanamycin (10 ml, 30 µg/ml) which were grown shaking overnight at 37°C. The plasmids were isolated by plasmid mini-prep (3.2.2.6) and the presence of the *TSA1* gene insert was confirmed by PCR and restriction digestion.

3.2.9 Gel Purification

Gel purification of double digested PCR and plasmid products was performed using the GeneJET Gel Purification Kit (Fermentas). The purified product was then run on agarose gel electrophoresis to estimate the concentration and to confirm the purity obtained.

3.2.10 Agarose gel electrophoresis

Agarose gel electrophoresis was used for visualisation of all DNA products. A 1.0% (w/v) agarose gel for genomic DNA samples, 1.2% (w/v) gel for plasmid DNA and a 1.5% (w/v) gel for PCR products. Ethidium bromide (2 µl, 10 mg/ml stock) was added to agarose dissolved in 1 X TAE (40 ml, 40 mM Tris-HCl, 20 mM acetic acid, 1 mM EDTA, pH 8.0) and the gel was allowed to polymerize (30 minutes) in a casting tray. Gels were run at 80 V until the tracking dye had run ¾ of the length of the gel (90-120 minutes) and the DNA bands were visualised under ultraviolet light and photographed using a DNR MiniBIS Pro Versadoc.

3.2.11 Plasmid sequencing

Two isolated plasmid clone samples, pBETSA1a and pBETSA1b, were sequenced in both directions (Central Analytical Facility, Stellenbosch University) and an alignment was performed using ClustalX on the resulting sequence data with the *TSA1* gene sequence (NCBI accession number NC_001145.3).

3.2.12 Protein expression

A high cell density culture method (Sivashanmugam *et al.*, 2009) was used for high yield protein expression of TSA1 for purification. *E. coli* BL21 cells transformed with the TSA1 expression plasmid were grown at 37ºC (overnight, A_{600} ~ 5-7, 150 rpm) in 2 × YT media (250 ml, 1.6% (w/v) tryptone, 1% (w/v) yeast extract, 0.5% (w/v) NaCl, pH 7.0), then centrifuged (1 500 × *g*, 10 minutes) and resuspended in high cell density media (2 × YT, 50 mM Na_2HPO_4, 25 mM KH_2PO_4, 5 mM $MgSO_4$, 0.2 mM $CaCl_2$, 0.1% (w/v) NH_4Cl, 1% (v/v) glucose, pH 8.2). The cells were grown at 37ºC until the A_{600} had increased by one unit (1-1.5 hours, 150 rpm), IPTG (0.5 mM) was then added to the cultures and induction of the recombinant protein expression proceeded at 30ºC (1-6 hours, 150 rpm). Cells were centrifuged at room temperature (12 000 × *g*, 10 minutes), the supernatant discarded and the weight of the cells recorded. Plasmid clones of *TRX1* and *TRR1* were kindly supplied by Miss L. Padayachee (UKZN) and Miss M. Photolo (UKZN) respectively and these recombinant proteins were similarly induced.

3.2.13 Tris-Tricine Gel Electrophoresis

Protein samples were visualised on a 15% Tris-Tricine gel (Table 3.1). Tris-Tricine gels were made up with acrylamide: bis (37:5:1) ready to use solution, Gel Buffer (3 M Tris-HCl, 0.3% (m/v) SDS, pH 8.4), distilled water and polymerisation was initiated with TEMED and freshly made 10% (w/v) ammonium persulfate. The resolving gel solution was allowed to polymerise for 30 minutes in the gel casting tray before the stacking gel was added and polymerised for a further 30 minutes. Protein samples were prepared in reducing or non-reducing treatment buffer (125 mM Tris-HCl, 0.01% (m/v) bromophenol blue, 4% (m/v) SDS, 20% (v/v) glycerol, 10% (v/v) β-mercaptoethanol (reducing buffer only), 0.01% (m/v) bromophenol blue, pH 6.8, stored at 4°C) and boiled for 5 minutes before loading onto the gel.

Gels were run at 50 mA using cathode (0.1 M Tris-HCl, 0.1 M Tricine, 0.1% (m/v) SDS, pH 8.25) and anode buffer (0.2 M Tris-HCl, pH 8.9) until the dye front had reached the bottom of the gel (~120 minutes). Gels were stained with Coomassie blue gel stain (0.125% (m/v) Coomassie brilliant blue R-250, 50% (v/v) methanol and 10% (v/v) acetic acid) overnight on a shaker, de-stained with de-stain solution I (45% (v/v) methanol, 9% (v/v) glacial acetic acid) until the background was clear and finally placed in de-stain solution II (5% (v/v) methanol, 7% (v/v) acetic acid) to rehydrate the gel. Gels were photographed under white light using a DNR MiniBIS Pro Versadoc.

Table 3.1 Tris-Tricine stacking and resolving gel mixture for visualising small proteins.

	4% Stacking Gel	**15% Resolving Gel**
	Volume (ml)	
Water	3	3.71
Acrylamide: Bisacrylamide Solution	0.67	8
Gel Buffer	1.3	4
TEMED	0.005	0.008
10% Ammonium persulfate	0.025	0.282
Total Volume	5	16

3.2.14 Preparation of Crude Protein Extract

Cell pellets were resuspended in a volume of ice-cold extraction buffer (20 mM Tris-HCl, 1 mM EDTA, 0.5 mM AEBSF protease inhibitor, 5 mM DTT, 10 mM NaCl, pH 7.5) equal to ten times the weight of the cells and sonicated using the Virsonic 60 Ultrasonic Cell Disrupter (5 W) for 20 seconds sonication followed by 20 seconds on ice. This procedure was repeated three times. The cell suspension was then centrifuged (12 000 × *g*, 30 minutes at 4°C) and the supernatant stored at -20°C.

3.2.15 Nickel Affinity Protein Purification

Protein purification columns (15 ml total volume) were packed with Ni-NTA agarose beads (2 ml) suspended in 20% ethanol. The columns were washed with two volumes of equilibration buffer (0.5 M NaCl, 0.02 M imidazole, 0.02 M Tris-HCl, 0.001 M β-mercaptoethanol, pH 8.0) before the addition of crude protein extract (6 ml). Columns were then rotated on a Labnet Revolver 360° sample mixer overnight at 4°C. The unbound crude

protein extract was eluted from the column and the column was washed with two volumes of wash buffer (0.02 M Tris-HCl, 0.5 M NaCl, 30 mM imidazole, pH 8.0). Elution buffer (3 ml, 0.02 M Tris-HCl, 0.5 M NaCl, 250 mM imidazole, pH 8.0) was added to the columns, which were then rotated for 30 minutes at 4°C. Protein factions were then collected and the columns were washed with one volume of 0.5 M NaOH and two volumes of distilled water. The Ni-NTA resin was stored in the column in 20% ethanol and regenerated once the resin had lost its blue colour (~ 5 purifications). The purity of the protein was determined by visualising the collected fractions on a 15% Tris-Tricine gel along with samples of the crude protein extract, the unbound protein and flow-through from each wash step.

3.3 Results

3.3.1 Cloning and sequence confirmation of the *TSA1* expression plasmid

Genomic DNA was isolated from two cultures of *S. cerevisiae* BY4743 using Bust n' Grab protocol (Figure 3.1A). A restriction map of the *TSA1* gene, generated using NEBcutter (tools.neb.com/NEBcutter.com) showed that it did not contain the restriction sites for the restriction enzymes NdeI and HindIII. Therefore these restriction sites were incorporated into the 5' ends of the *TSA1* PCR primers for cloning. The use of NdeI restriction enzyme also had an advantage in that its recognition site, CATATG, already contained the ATG start codon and thus overlapped the first 5' codon in the *TSA1* gene coding sequence which allowed the design of primers that could target more of the downstream gene sequence, increasing the accuracy of primer binding. The yeast peroxiredoxin *TSA1* gene was subsequently PCR amplified from the genomic DNA and was determined to be the expected size of 601bp (Figure 3.1B). No contamination was present in the no template control reaction.

The PCR product was gel purified, ligated into pTZ57R/T using a molar insert to vector ratio of 3:1 and transformed into *E. coli* JM109 cells using the Thermo Scientific InsTAclone PCR cloning kit. The transformed cells were plated onto LB agar plates containing ampicillin, X-gal and IPTG for blue/white colony selection. The control plates showed that the *E. coli* JM109 cells had not been previously transformed with pTZ57R/T, had not acquired ampicillin antibiotic resistance and also confirmed that the ampicillin, X-gal and IPTG and were still active after preparation of the LB agar plates. The transformation efficiency was calculated as 3.78×10^4 CFU/µg of plasmid DNA.

Using blue/white colony selection, six recombinant clones were selected and their plasmids were isolated to confirm that they contained the *TSA1* gene insert by PCR (Figure 3.1C). All six samples had a positive PCR result and no contamination was present in the no template control. Three of the confirmed plasmids (pTTSA1a, pTTSA1b, pTTSA1c) were again tested for the presence of the *TSA1* gene insert by restriction digestion. Double digestion of the plasmids with NdeI and HindIII liberated the *TSA1* insert from the plasmids (Figure 3.2). As a control, the plasmids were also digested with either NdeI or HindIII, to ensure that the enzymes were active and the restriction sites were successfully incorporated into the *TSA1* sequence.

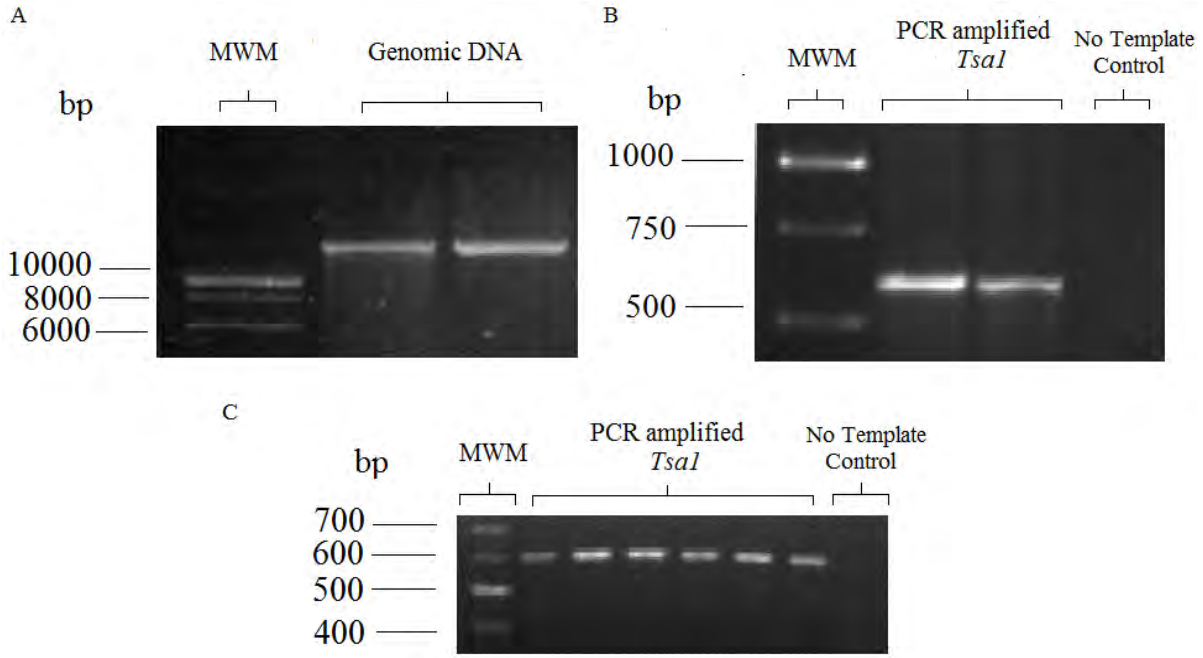

Figure 3.1 Genomic DNA was isolated from *S. cerevisiae* (A). *TSA1* was PCR amplified from the genomic DNA (B), gel purified and ligated into pTZ57R/T and transformed into *E. coli* JM109 cells. The recombinant plasmids were then isolated from the cells and *TSA1* was PCR amplified from the plasmids to confirm the presence of the gene insert (C).

For sub-cloning into pET28a, the restriction liberated *TSA1* fragments together with double digested pET28a were gel purified. The purified *TSA1* and pET28a fragments were then ligated using the Thermo Scientific Rapid Ligation Kit and transformed into *E. coli* BL21 cells which were made competent by calcium chloride treatment (Dagert and Ehrlich, 1979). The transformation efficiency was calculated as 2.81 x 10^3 CFU/µg of plasmid DNA. Plasmids were then isolated from two of the recombinant colonies and PCR confirmed that the *TSA1* gene insert indeed was present in the plasmids (Figure 3.3). The two plasmid samples, named pBETSA1a and pBETSA1b were then sent for sequencing (Central

Analytical Facility, Stellenbosch University) and the inserts in both plasmids were determined to have 100% identity with the *TSA1* sequence (NCBI, accession number NC_001145.3) by alignment with ClustalX2 (Figure 3.4). Thus *TSA1* was successfully sub-cloned into pET28a. The plasmid clones could now be used for the expression and purification of TSA1 for *in vitro* analysis.

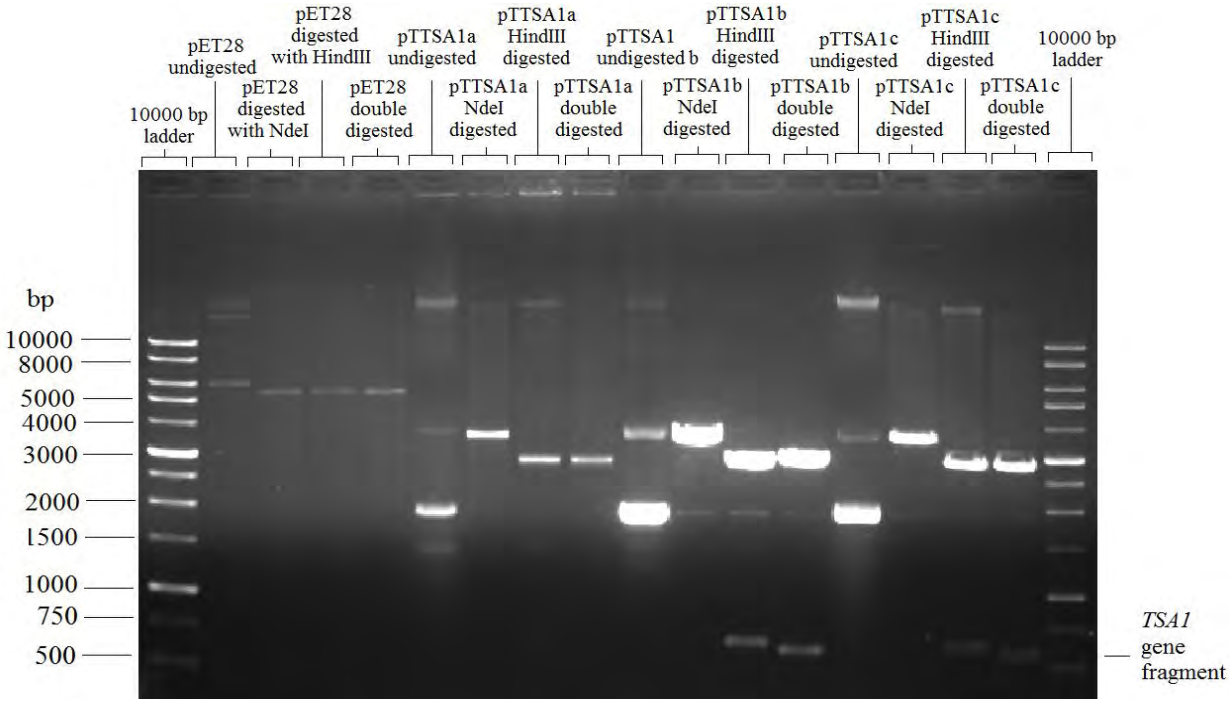

Figure 3.2 Restriction digestion of the isolated plasmids (pTTSA1a, pTTSA1b, pTTSA1c) for cloning of *TSA1* into pTZ57R/T. Upon double digestion with NdeI and HindIII, the restriction liberated *TSA1* gene insert could be visualised and sized. The size of insert was found to be 601bp. HindIII and NdeI double digested pET28a and *TSA1* fragments were then gel extracted for sub-cloning of *TSA1* into pET28a.

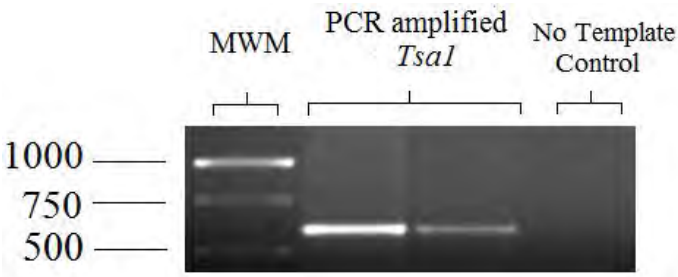

Figure 3.3 PCR amplification of *TSA1* from the isolated plasmids (pBETSA1a and pBETSA1b) to confirm the presence of the gene in the plasmids.

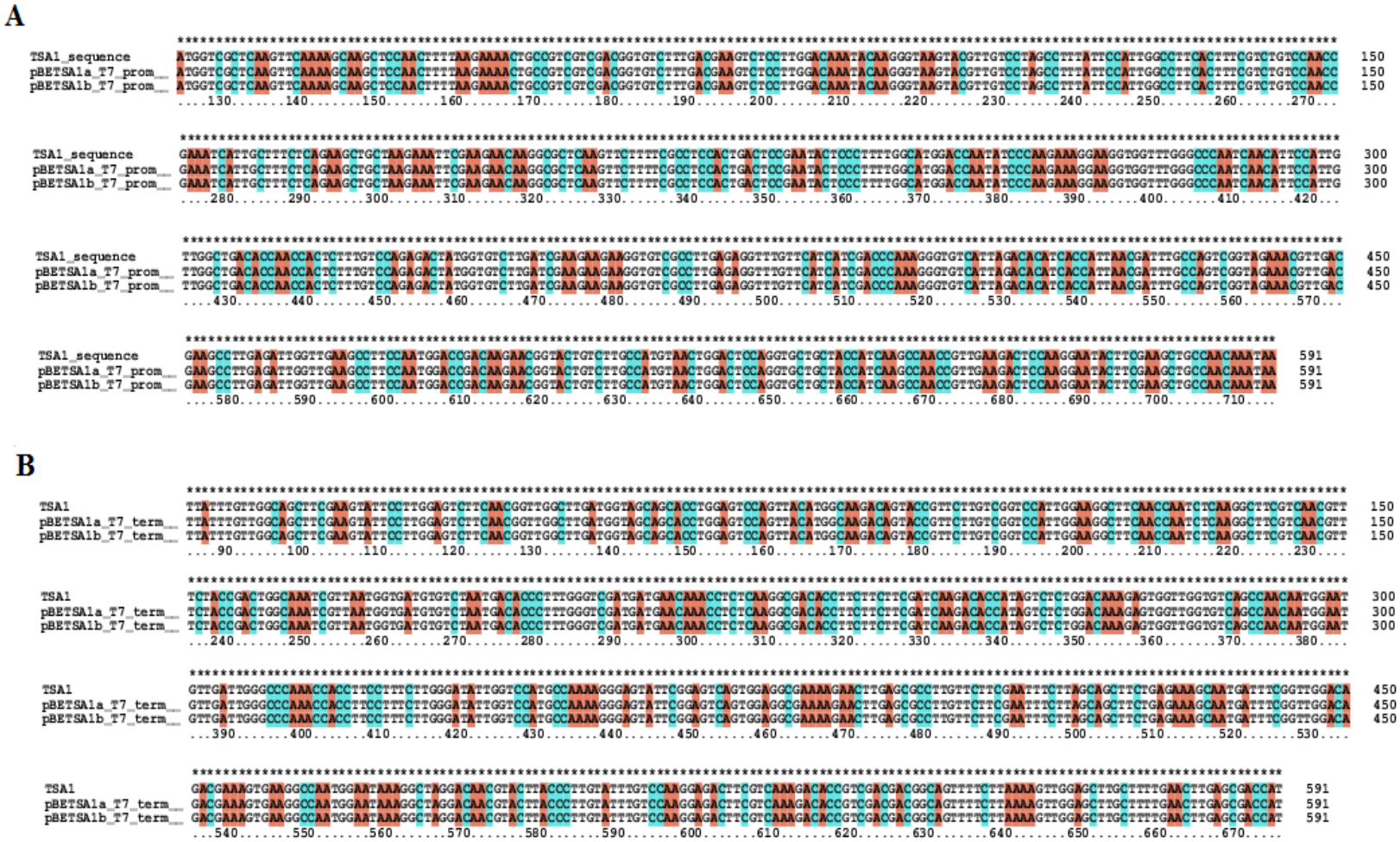

Figure 3.4 Alignment of pBETSA1a and pBETSA1b plasmid clones with the *TSA1* sequence (NCBI) to confirm the identity of the insert. (A) Promoter sequences were aligned with the *TSA1* sequence and (B) terminator sequences were aligned with the *TSA1* reverse compliment sequence (Blue highlight-alignment of cytosine and red highlight-alignment of adenine).

3.3.2 Expression of TSA1 and purification of the peroxiredoxin system proteins

E. coli BL21 cells containing the plasmid clone pBETSA1a were induced with IPTG to express TSA1 using a high cell density method to maximise protein yield (Sivashanmugam *et al.*, 2009). Samples of the cell culture were taken before addition of IPTG and after addition of IPTG, the protein concentration normalized against the culture optical density and analysed by SDS-PAGE to determine if the induced expression of TSA1 was successful (Figure 3.5). The resulting expressed protein was about the expected size of 23 kDa in a reducing SDS-PAGE gel. Sizing of the proteins was done using a standard curve generated by measuring the distance migrated from the well by each protein in the molecular weight marker. Stock cultures of the recombinant cells were made and frozen at -70ºC, available for use throughout the remainder of the project.

After protein induction, the recombinant *E. coli* BL21 cells were pelleted and sonicated in ice-cold extraction buffer to produce crude protein extract. Nickel affinity purification columns were used to purify His-tagged TSA1 protein from the crude protein extract and samples of the purified protein were run on a 13% Tris-Tricine acrylamide gel to confirm the purity of the protein samples (Figure 3.6). Contaminating bands were not observed on the SDS gel and therefore the proteins were sufficiently pure for the kinetic assays. Approximately 75 mg of TSA1 protein was purified from a 250 ml culture of recombinant *E. coli* BL21 cells. Thioredoxin reductase and thioredoxin were similarly expressed and purified with 65 mg (Figure 3.7) and 20 mg (Figure 3.8) of protein isolated per 250 ml culture respectively.

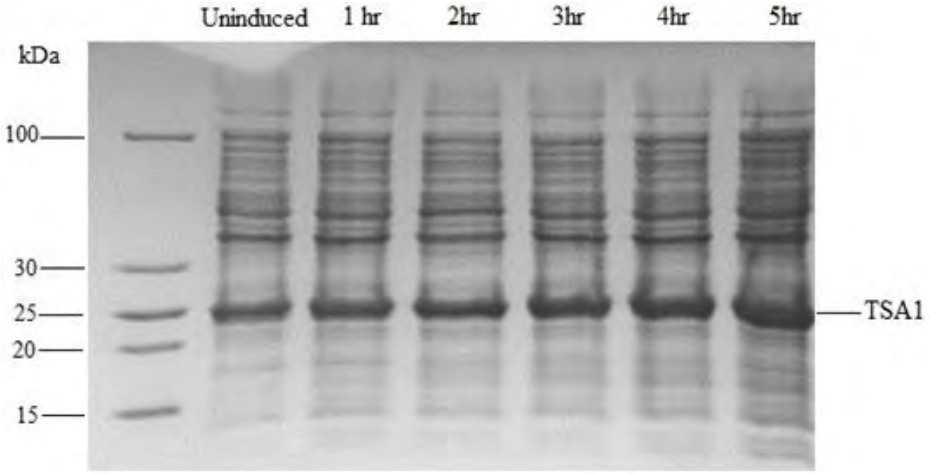

Figure 3.5 IPTG induced expression of TSA1 in recombinant *E. coli* BL21 cells. Samples were taken from the culture every hour for 5 hours after induction. The induced protein was sized at about 23 kDa.

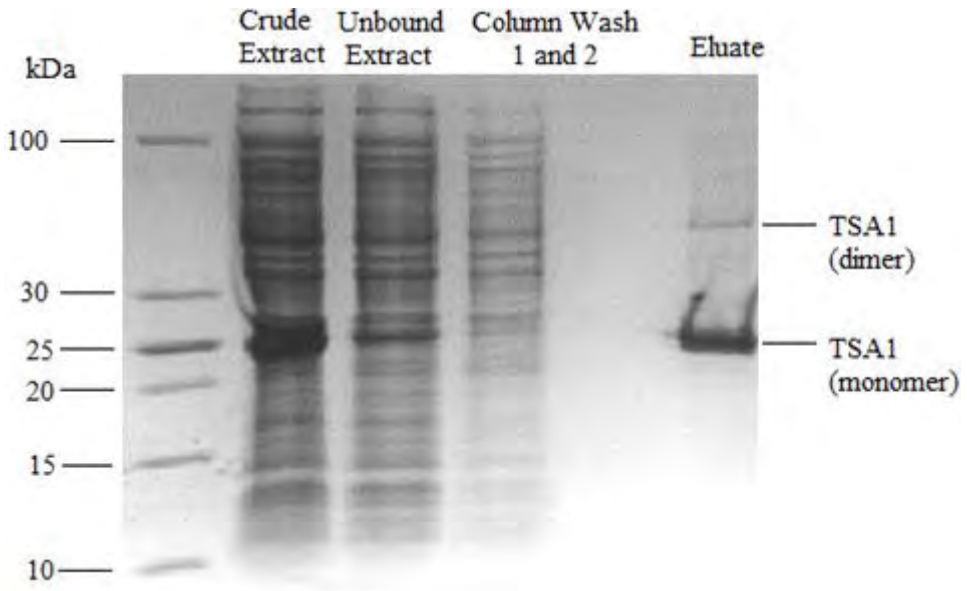

Figure 3.6 Purification of His-tagged TSA1 protein from crude extract of IPTG-induced recombinant *E.coli* BL21 using Ni-NTA agarose bead resin. The beads were washed with buffer to remove contaminating proteins prior to elution with an imidazole containing buffer.

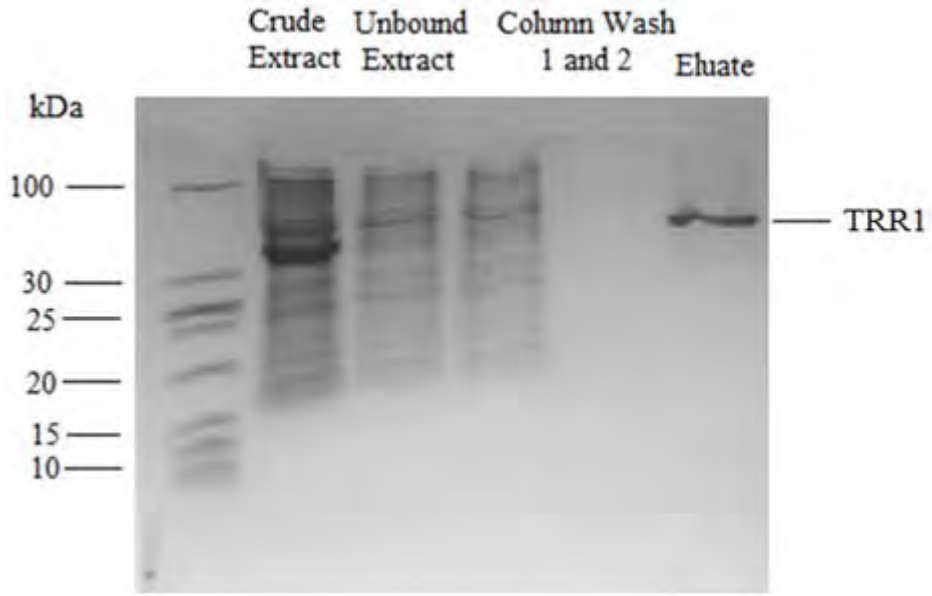

Figure 3.7 Purification of his-tagged TRR1 protein from crude extract of IPTG-induced recombinant *E.coli* BL21 using Ni-NTA agarose bead resin. The protein was sized at 35 kDa. The beads were washed with buffer to remove contaminating proteins prior to elution with an imidazole containing buffer.

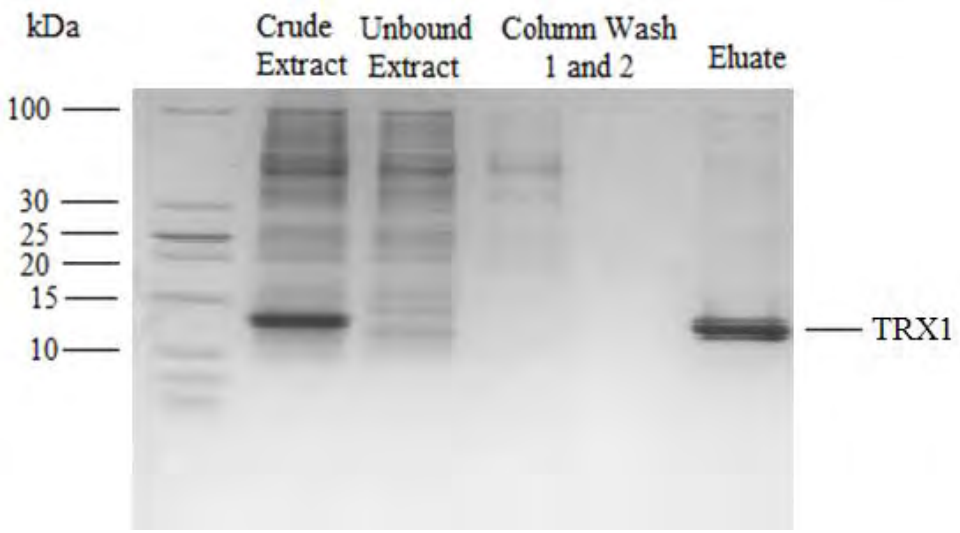

Figure 3.8 Purification of his-tagged TRX1 protein from crude extract of IPTG-induced recombinant *E.coli* BL21 using Ni-NTA agarose bead resin. The protein was sized at 12 kDa. The beads were washed with buffer to remove contaminating proteins prior to elution with an imidazole containing buffer.

3.4 Discussion

As previously discussed (Chapter 2.1), a number of assays have been established to determine peroxiredoxin activity (Nelson and Parsonage, 2011). The steady state system rate can be measured by monitoring NADPH oxidation as 340 nm, an assay requiring pure thioredoxin, thioredoxin reductase and peroxiredoxin proteins. Purchasing of these proteins would have been costly and expression plasmid clones for *S. cerevisiae* thioredoxin and thioredoxin reductase had previously been developed in our laboratory and were available for expression and purification of these proteins. The *TSA1* gene was successfully cloned into pET28a (Figure 3.1-3.3) and its sequence was confirmed by DNA sequencing (Figure 3.4). TSA1 was then expressed (Figure 3.5) and purified (Figure 3.6) from recombinant *E.coli* BL21 cells. As peroxiredoxin, thioredoxin and thioredoxin reductase were required at high concentrations for the kinetic assays, a high density cell culture method (Sivashanmugam *et al.*, 2009) was employed for overexpression of the proteins. Nickel affinity purification was then successfully used to purify the proteins from crude protein extract (Figure 3.6-3.7) with high yields determined for each protein (20-75 mg/250 ml culture) and these proteins were used for *in vitro* kinetic studies.

Chapter 4

In vitro analysis of the peroxiredoxin system for validation of fitted kinetic parameters.

4.1 Introduction

Computational modelling generated hypotheses about the different peroxiredoxin kinetic models and the necessity of whole system fitting for parameter determination due to the complexity of the peroxiredoxin system (Chapter 2). *In vitro* kinetic and computational analysis of the cytosolic TSA1 peroxiredoxin system from *S. cerevisiae* was then carried out to further verify these results. Initial modelling of the TSA1 peroxiredoxin system used parameters from the literature, for example a K_m of 12 μM for hydrogen peroxide (Munhoz and Netto, 2004) and a second-order rate constant for hydrogen peroxide reduction of 2.2 $\times 10^7$ M^{-1} s^{-1} (Ogusucu *et al.*, 2007). Modelling studies were complimented by *in vitro* kinetic studies in which the NADPH oxidation rate was monitored spectrophotometrically to generate datasets and the entire peroxiredoxin system were fitted to these datasets for parameter determination.

A limitation of the NADPH-dependent assay is a lack of sensitivity in measuring the flux with low hydrogen peroxide concentrations (<20 μM) (Nelson and Parsonage, 2011) and therefore accurate hydrogen peroxide saturation datasets could not be reliably produced and instead thioredoxin and peroxiredoxin saturation datasets were determined. An additional consideration was that a decrease in the activity of His-tagged recombinant bovine peroxiredoxin due to a change in its native structure because of the presence of the His-tag had previously been reported (Cao *et al.*, 2007; Barranco-Medina *et al.*, 2009). Therefore, the activity of our recombinant TSA1 protein with and without the His-tag was tested and its conformation determined using Blue Native PAGE.

4.2 Materials and Methods

4.2.1 Materials

Bovine serum albumin (BSA), dithiothreitol (DTT), 5,5′-dithio-bis (2-nitrobenzoic acid) (DTNB), NADPH, insulin from bovine pancreas, dialysis tubing (average flat width of 9 mm and 25 mm) and the Thrombin CleanCleave™ Kit were obtained from Sigma (Kawasaki, Japan and

distributed by Capital Labs, South Africa). 30% Hydrogen peroxide was obtained from Laboratory and Analytical Supplies (Durban, South Africa) and stored at 4°C. All other common reagents such as EDTA were obtained from Saarchem (Merck, South Africa). TSA1, thioredoxin reductase and thioredoxin were purified as described in Chapter 3 and their extinction coefficients were determined using ProtParam (http://web.expasy.org/protparam/) as 24 075 M^{-1} cm^{-1}, 24 660 M^{-1} cm^{-1} and 10 095 M^{-1} cm^{-1}, respectively.

4.2.2 Computational modelling of the peroxiredoxin system from *Saccharomyces cerevisiae*

Realistic modelling of peroxiredoxin activity and flux control analyses were undertaken as previously described (Chapter 2) using PySCeS with reaction parameters obtained from the literature and the species concentrations from our kinetic assays (Appendix 2.3). Model fitting to our *in vitro* datasets used non-linear regression analysis (Chapter 2).

4.2.3 Protein activity assays

The activity of purified peroxiredoxin was determined using a DTT peroxidase assay whereby the oxidation of DTT was monitored at 310 nm (Tairum *et al.*, 2012) in a UV-1800 Shimadzu spectrophotometer. Varying concentrations of purified TSA1 (1 µM, 2 µM and 5 µM) were incubated with freshly prepared solutions of 10 mM DTT and 30 µM hydrogen peroxide in reaction buffer (25 mM potassium phosphate, 1 mM EDTA, 100 mM ammonium sulfate, pH 7.0) at 30°C in a 1 ml reaction volume for 10 minutes. A control sample was also measured that excluded TSA1 from the reaction and reactions were performed in triplicate. The absorbance at 310 nm was monitored and activity expressed as µM of DTT/min/mg of protein

The activity of thioredoxin reductase was determined by measuring the reduction of DNTB at 412 nm in an NADPH-dependent assay (Arner and Holmgren, 2001). Varying amounts of purified thioredoxin reductase (0.5 µM, 1 µM and 3 µM) were incubated with 2.5 mM DTNB (50 mM stock solution was made up in absolute ethanol), 0.24 mM NADPH (from a 15 mM stock solution was made up in 0.01 M NaOH), 50 mM KCl, 10 mM EDTA, 0.2 mg/ml BSA, and 500 mM NaCl in 500 mM potassium phosphate (pH 7.0) in a 1 ml reaction volume and was followed for 10 minutes. A control sample was also measured that excluded thioredoxin reductase from the reaction and reactions were performed in triplicate. The absorbance at 412 nm was monitored and activity expressed as µM of TNB/min/mg of protein.

The activity of thioredoxin was determined using an insulin reduction assay measured by monitoring the change in absorbance at 650 nm (Arner and Holmgren, 2001). The reaction mixture was made up to a final volume of 1 ml containing 0.01 mM insulin from bovine pancreas, 2 mM EDTA, 1 mM DTT and 63 mM potassium phosphate buffer (pH 7.0) and purified thioredoxin protein (1 μM, 2 μM and 5 μM) and followed for 10 minutes. Insulin was prepared by suspending 50 mg of the peptide in 100 mM potassium phosphate buffer (pH 6.5) and adjusting the pH to 2-3 using concentrated HCl to dissolve the insulin. The pH was then readjusted to 6.5 using NaOH, made up to a final volume of 5 ml with ultrapure water to yield a 1.6 mM solution that was stored at -20°C. A control sample was also measured that excluded thioredoxin from the reaction and the reactions were performed in triplicate and the activity was expressed as ΔA_{650}/min.

4.2.4 Peroxiredoxin activity assay

Substrate saturation datasets with increasing thioredoxin concentrations were generated using fresh aliquots of purified protein and hydrogen peroxide and NADPH were prepared fresh daily. The concentration of diluted hydrogen peroxide solutions were verified using the extinction co-efficient of 43.6 M^{-1} cm^{-1} (Hildebraunt and Roots, 1975). The assays contained 150 μM NADPH, 5 μM thioredoxin, 0.5 μM thioredoxin reductase and 1 μM peroxiredoxin and reaction buffer (25 mM potassium phosphate, 1 mM EDTA, 100 mM ammonium sulfate, pH 7.0) in a 1 ml UV cuvette which was equilibrated at 25°C for 5 minutes before the assay was initiated with the addition of 30 μM of hydrogen peroxide and followed for 5 minutes. In these assays, the thioredoxin concentration was ten times greater than thioredoxin reductase and five times greater than peroxiredoxin as recommended by Nelson and Parsonage (2011) to ensure that hydrogen peroxide reduction and not thioredoxin recycling was the rate-limiting step in the system.

A series of assays were performed with varied thioredoxin (0-15 μM) and peroxiredoxin concentrations (0.5, 1 and 2 μM) and control reactions were run simultaneously omitting the variable species in the reaction series. A minimum of eight concentrations were analysed per series and readings at each level were replicated at least three times. The reaction rate was determined from the initial linear portion of the curve using the extinction co-efficient for NADPH oxidation (ε_{340} = 6 220 M^{-1} cm^{-1}). The activity of the control reaction was subtracted from each reaction in the series, final activity was determined

from an average of the replicates and standard errors are shown in the resulting figures unless otherwise stated.

4.2.5 His-tag cleavage of TSA1

The Thrombin CleanCleave™ Kit from Sigma was used for cleavage of TSA1 His-tags. TSA1 was initially dialysed with buffer (50 mM Tris-HCl, 10 mM $CaCl_2$, pH 8.0) to remove any residual salts from purification which could inhibit cleavage. Thrombin resin (100 µl) was prepared by gentle centrifugation (500 × *g*, 2 minutes, RT) and removal of the supernatant. The resin was twice washed with 500 µl of 1 × Cleavage Buffer (50 mM Tris-HCl, 10 mM $CaCl_2$, pH 8.0) and finally resuspended in 10 × Cleavage Buffer (100µl, 500 mM Tris-HCl, 100 mM $CaCl_2$, pH 8.0). About 1 mg of protein was added to the reaction and topped up to a volume of 1 ml with distilled water. The reaction was incubated overnight while rotating (room temperature). A sample was then analysed on SDS-PAGE and at least 95% was estimated to have been cleaved successful (data not shown, estimated from SDS gel). The remaining thrombin resin was removed from the sample by centrifugation (500 × *g*, 2 minutes, RT) and the cleaved His-tags were removed by dialysis. The activity of the protein was then tested and compared to His-tagged protein.

4.2.6 Blue native (BN) PAGE

In order to visualise the native form of TSA1, recombinant protein samples were run on a 4 to 13% native acrylamide gradient gel (Table 4.1, Wittig *et al.*, 2006). Native gels were made up of acrylamide: bisacrylamide solution (48% (w/v) acrylamide, 1.5% (w/v) bisacrylamide, stored at 7°C), gel buffer (75 mM imidazole, pH 7.0), 100% (v/v) glycerol, distilled water and polymerisation was initiated with TEMED and freshly made 10% (w/v) ammonium persulfate for 30 minutes in the gel casting tray. The gel was poured in a gradient from a 13% to 4% acrylamide solution. The gradient gel was mixed and poured manually without the use of a peristaltic pump. Protein samples were prepared in loading buffer (5% (m/v) Coomassie blue G-250, 20% (v/v) glycerol, pH 7.0, stored at room temperature) immediately before loading of samples.

Gels were run at constant 100 V until the samples entered the gel (~10 minutes) and then then switched to constant 15 mA until the blue dye front reached the bottom of the gel (~90 minutes at 4°C) using a cathode (50 mM Tricine, 7.5 mM imidazole, 0.02% (m/v) Coomassie blue G-250, pH 7.0) and anode buffer (25 mM imidazole, pH 7.0). Gels were

stained with Coomassie blue gel stain (0.125% (m/v) Coomassie brilliant blue R-250, 50% (v/v) methanol and 10% (v/v) acetic acid) overnight on a shaker, de-stained with de-stain solution I (45% (v/v) methanol, 9% (v/v) glacial acetic acid) until the background was clear and finally placed in de-stain solution II (5% (v/v) methanol, 7% (v/v) acetic acid) to rehydrate and store the gel. Gels were photographed under white light using a DNR MiniBIS Pro Versadoc.

Table 4.1 BN-PAGE gradient gel mixtures for visualising native proteins.

	4% Acrylamide Gel	**13% Acrylamide Gel**
	Volume (ml)	
Water	10.4	3
Acrylamide: Bisacrylamide Solution	1.5	3.9
Gel Buffer	6	5
Glycerol	-	3
TEMED	0.010	0.0075
10% Ammonium persulfate	0.1	0.075
Total Volume	18	15

4.3 Results

4.3.1 Comparison of the activity of His-tagged and His-tag cleaved TSA1 protein

Previous analysis of bovine peroxiredoxin 3 found that the presence of His-tags could negatively affect recombinant C-terminus tagged protein activity (Cao *et al.*, 2007; Barranco-Medina *et al.*, 2009) and therefore His-tags were subsequently cleaved from our recombinant N-terminal tagged TSA1 in this study and compared to the activity of His-tagged protein (Figure 4.1). His-tagged and His-tag cleaved protein activities were measured at similar rates of 2.1×10^5 $M.s^{-1}$ and 2.0×10^5 $M.s^{-1}$ respectively showing that the N-terminal tag did not dramatically affect peroxiredoxin activity.

TSA1 predominantly forms monomers at 23 kDa on a reducing SDS gel and homodimers at 46 kDa on a non-reducing SDS gel but is present as a decamer *in vivo* (De Oliveira *et al.*, 2007; Tairum *et al.*, 2012). Purified TSA1 was run on one-dimensional BN-PAGE gels to visualise the native form of this protein (Figure 4.2, Wittig *et al.*, 2006). BN-

PAGE omits detergents such as SDS that dissociate proteins in typical protein electrophoresis and instead Coomassie blue dye is used to resolve the proteins by suppling a charge to allow them to separate according to size in their native form. A decameric form of peroxiredoxin was sized at about 210 kDa (Standard curve, Appendix 2.3.3) close to an expected size of 220 kDa, while no lower molecular weight forms were observed. A second multimeric structure was also observed at a higher molecular weight than the decamer but was outside the range of the molecular weight marker and this is presumably a high molecular weight isoform that has been reported to have chaperone activity (Barranco-Medina *et al.*, 2009; Cao *et al.*, 2015; Radjainia *et al.*, 2015). The native form of the recombinant peroxiredoxin was therefore determined to be primarily a decameric structure, in agreement with published studies of other peroxiredoxins (De Oliveira *et al.*, 2007; Tairum *et al.*, 2012) and was not affected by the presence of an N-terminal His-tag.

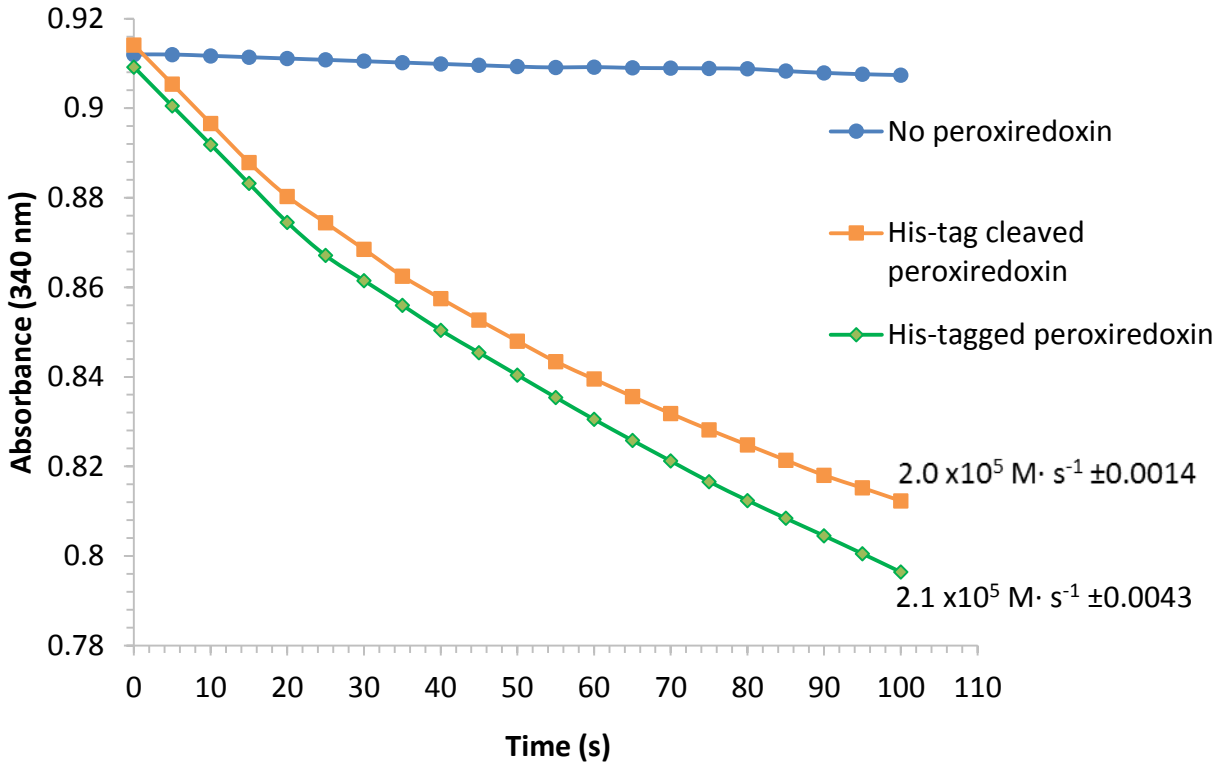

Figure 4.1 Comparison of the activity of His-tagged (—◆—) and His-tag cleaved (—■—) TSA1 protein in an NADPH-dependent assay. The assay was carried out with 150 µM NADPH, 5 µM thioredoxin, 0.5 µM thioredoxin reductase, 2 µM peroxiredoxin and 30 µM hydrogen peroxide in reaction buffer pH 7.0. The results are representative of three replicate experiments and the standard errors are shown.

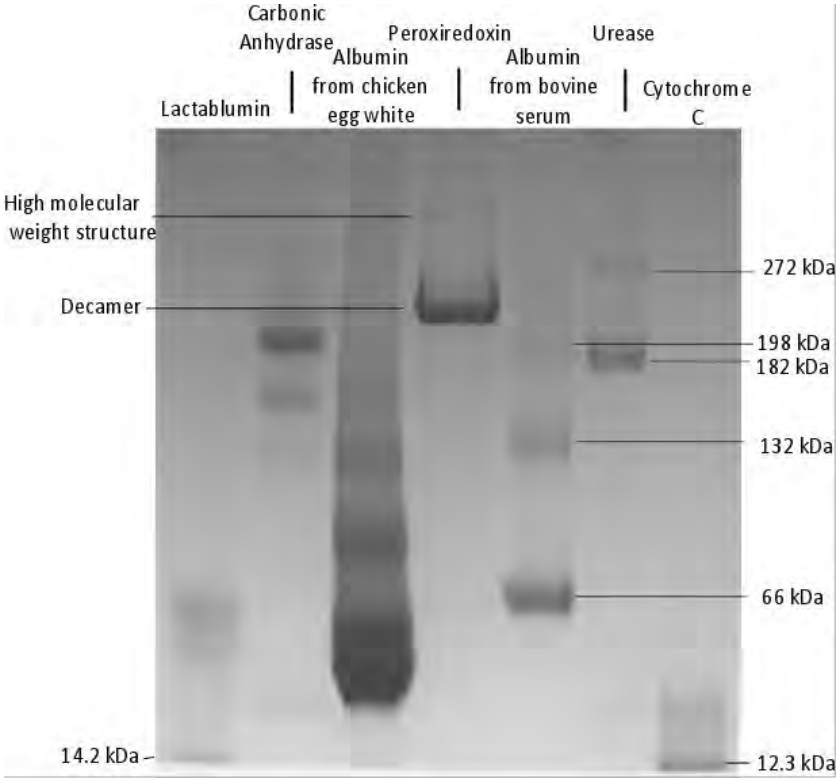

Figure 4.2 BN-PAGE of TSA1 protein revealed two high molecular weight structures of the protein. A non-denaturing PAGE kit (Sigma) for molecular weights 14 kDa – 272 kDa and cytochrome C (12.3 kDa) were used to generate a standard curve for sizing of TSA1.

4.3.2 Data fitting of the models to a thioredoxin substrate saturation dataset for parameter determination

The proposed peroxiredoxin models were simulated with increasing thioredoxin concentrations, using kinetic parameters from the literature (Table 4.2) and compared to an *in vitro* dataset generated using a peroxiredoxin concentration of 1 μM (Table 4.3). While one parameter used in the modelling experiment was obtained from recycling of the *E.coli* Tpx system, the rate constant for peroxiredoxin reduction is in a similar range for all peroxiredoxins and the reaction conditions of our experiment were developed so that hydrogen peroxide reduction should have been rate-limiting (Nelson and Parsonage, 2011). As with previous analyses (Chapter 2), all the models revealed distinct responses and failed to reproduce the *in vitro* dataset (Figure 4.3) confirming that some parameters reported in the literature should be used with caution when developing models of the peroxiredoxin system. The peroxiredoxin kinetic models were then fitted to the *in vitro* dataset to estimate parameters for the system, the ping-pong enzyme and redox couple monomer models were able to fit the *in vitro* dataset (r^2 value = 0.98, Table 4.4) but attempts at fitting the redox

couple homodimer model were unsuccessful and therefore this model was excluded from further analysis.

Table 4.2 Reactions and reaction parameters for computational modelling of the TSA1 peroxiredoxin system from *S. cerevisiae.*

Reaction	Parameter	Value	Reference
	All Models		
R1: NADPH + Trx_{SS} → $NADP^+$ + Trx_{SH}	$k_{cat\ 1}$	66 s^{-1}	(Speranza *et al.*, 1973)
	K_{nadph}	1.2 μM	(Williams Jr, 1976)
	K_{trxss}	4.4 μM	(Williams Jr, 1976)
	Ping-Pong Enzyme Model		
R2: Trx_{SH} + H_2O_2 → Trx_{SS} + H_2O	$k_{cat\ 2}$	0.31 s^{-1}	(Munhoz and Netto, 2004)
	K_{trxsh}	22.5 μM	[a]
	K_{h2o2}	12 μM	(Munhoz and Netto, 2004)
	Redox Couple Monomer Model		
R2: H_2O_2 + Prx_{SH} → H2O + Prx_{SS}	k_2	22 μM^{-1} s^{-1}	(Ogusucu *et al.*, 2007)
R3: Prx_{SS} + Trx_{SH} → Prx_{SH} + Trx_{SS}	k_3	3 μM^{-1} s^{-1}	[a]
	Redox Couple Homodimer Model		
R2: $Prx_{SH}Prx_{SH}$ + H_2O_2 → $Prx_{SS}Prx_{SH}$ + H_2O	k_2	22 μM^{-1} s^{-1}	(Ogusucu *et al.*, 2007)
R3: $Prx_{SS}Prx_{SH}$ + H_2O_2 → $Prx_{SS}Prx_{SS}$ + H_2O	k_2	22 μM^{-1} s^{-1}	(Ogusucu *et al.*, 2007)
R4: $Prx_{SS}Prx_{SS}$ + Trx_{SH} → $Prx_{SS}Prx_{SH}$ + Trx_{SS}	k_3	3 μM^{-1} s^{-1}	[a]
R5: $Prx_{SS}Prx_{SH}$ + Trx_{SH} →$Prx_{SH}Prx_{SH}$ + Trx_{SS}	k_3	3 μM^{-1} s^{-1}	[a]

[a] parameters obtained for *E.coli* Tpx system (Baker and Poole, 2003).

Table 4.3 Species concentrations of the various system components used in each model for realistic modelling of the TSA1 peroxiredoxin system from *S. cerevisiae*.

Model	Species	Initial Concentration (µM)
All	NADPH	150
	$NADP^+$	1
	Trx_{SH}	2.5*
	Trx_{SS}	2.5
	TR	0.5
	H_2O_2	30
Ping-Pong Enzyme	Prx	1
Redox Couple Monomer	Prx_{SH}	0.5*
	Prx_{SS}	0.5
Redox Couple Homodimer	$Prx_{SH}Prx_{SH}$	0.33*
	$Prx_{SS}Prx_{SH}$	0.33
	$Prx_{SS}Prx_{SS}$	0.34

*Note that the total concentration (reduced and oxidised) of all moiety conserved species is equal to the final concentration used in the activity assay

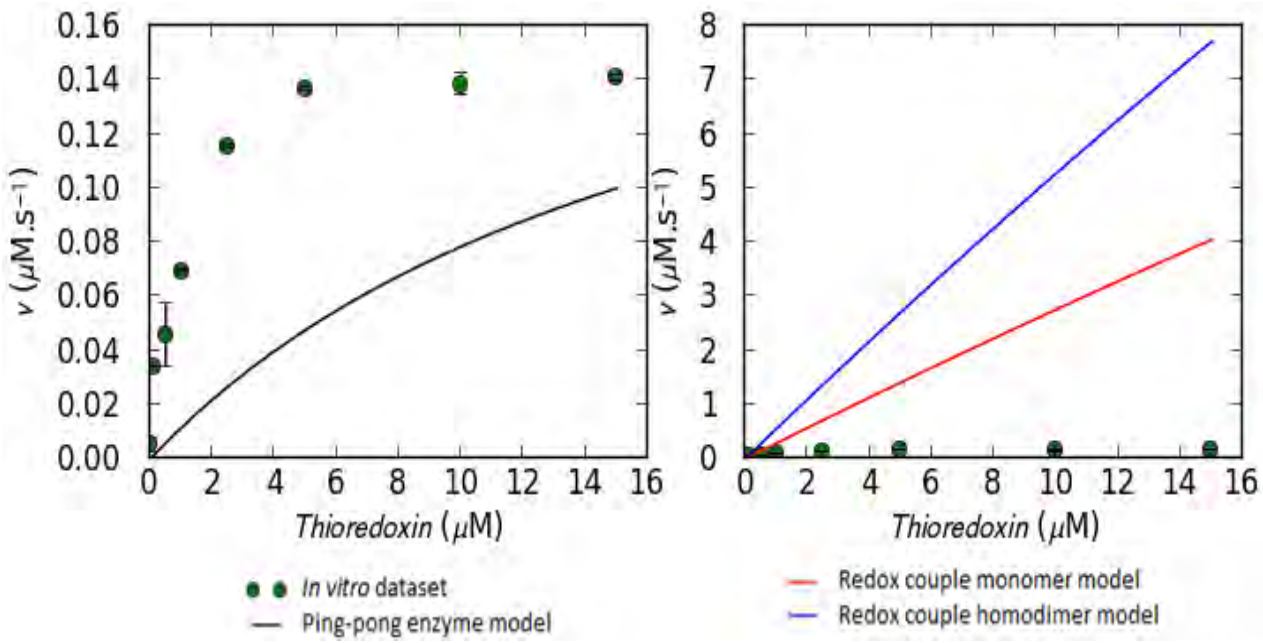

Figure 4.3 The three peroxiredoxin activity models produced a different response with parameters from the literature to the *in vitro* dataset generated with increasing thioredoxin concentrations. The assays were carried out with 150 µM NADPH, 5 µM thioredoxin, 0.5 µM thioredoxin reductase and 1 µM peroxiredoxin and 30 µM hydrogen peroxide in a reaction buffer (pH 7.0). The results are representative of three replicate experiments and where standard errors are not visible they are smaller than the symbol (n=3).

Second order rate constants for hydrogen peroxide reduction of 4.4×10^5 M^{-1} s^{-1} and 5.1×10^3 M^{-1} s^{-1} were determined for the ping-pong enzyme (k_{cat}/K_m) and redox couple monomer models respectively. As with the earlier fitting experiments (Chapter 2), these parameters were smaller than the rate constant of 10^7 M^{-1} s^{-1} determined by a competition assay with horse radish peroxidase (Ogusucu *et al.*, 2007). The rate constant of 10^3 M^{-1} s^{-1} fitted for the redox couple monomer model was also consistent with the fitted rate constants determined with the fitted human erythrocyte peroxiredoxin 2 and *C. crescentus* periplasmic peroxiredoxin models (Chapter 2). To test the accuracy of the resulting fitted models, two independent *in vitro* datasets were generated with varying thioredoxin concentrations and peroxiredoxin concentrations of 0.5 µM and 2 µM and compared to simulations of the fitted models (Figure 4.4). The ping-pong enzyme and redox couple monomer models were able to reasonably predict the datasets and showed near identical responses to changes in the thioredoxin and peroxiredoxin concentrations (Figure 4.4).

To differentiate these kinetic models, the fitted models were then used to simulate additional datasets with increasing thioredoxin reductase and peroxiredoxin concentrations (Figure 4.5) and the redox state of thioredoxin was monitored (Figure 4.6). Similarities were observed between the models suggesting these *in vitro* datasets could be reasonably described by either the ping-pong enzyme or redox couple monomer models.

Table 4.4 Parameters determined by fitting of the peroxiredoxin activity models to an *in vitro* dataset with increasing thioredoxin concentrations using non-linear regression analysis.

Parameter	Value	Fitted Curve
Ping-Pong Enzyme Model		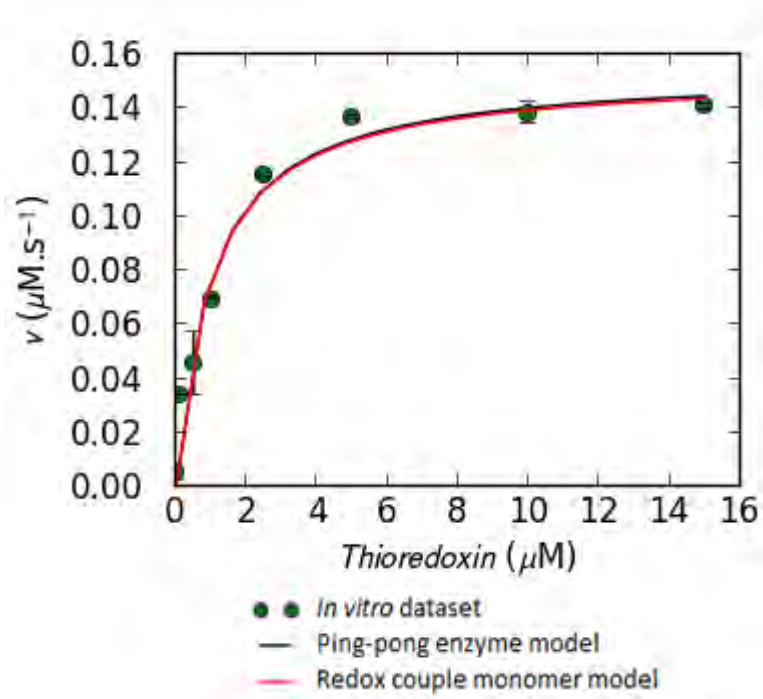
$k_{cat\,2}$ (Prx)	0.156 s^{-1}	
$K_{H_2O_2}$	0.358 μM	
$K_{Trx^{SH}}$	0.996 μM	
r^2	0.98	
Redox Couple Monomer Model		
k_2	5.1×10^3 M^{-1} s^{-1}	
k_3	1.57×10^4 M^{-1} s^{-1}	Note: ping-pong enzyme and redox couple monomer fitted models datasets overlap)
r^2	0.98	

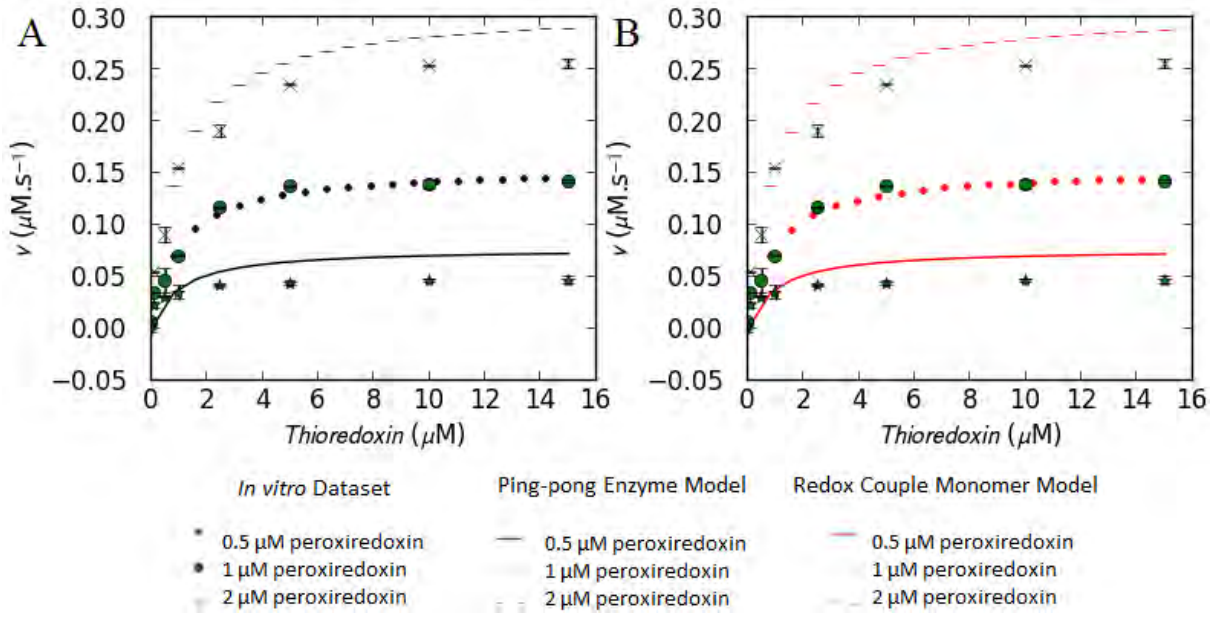

Figure 4.4 Fitted peroxiredoxin kinetic models based on the ping-pong (A) and redox couple mechanisms (B) can predict independent *in vitro* datasets. Steady state assays were carried out with 150 μM NADPH, 0.5 μM thioredoxin reductase, 30 μM hydrogen peroxide in a reaction buffer pH 7.0 at varying thioredoxin (0-15 μM) and peroxiredoxin (0.5, 1 and 2 μM) concentrations. The standard errors for the datasets are shown (*n*=3).

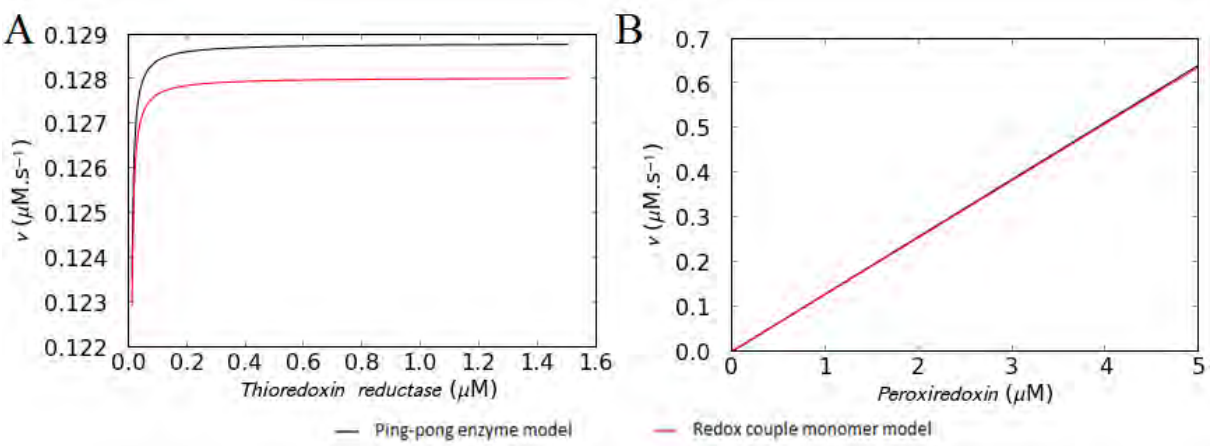

Figure 4.5 The fitted ping-pong enzyme and redox couple monomer models show similar responses to increasing thioredoxin reductase (A) and peroxiredoxin concentrations (B). The ping-pong enzyme and redox couple monomer model datasets overlap in (B).

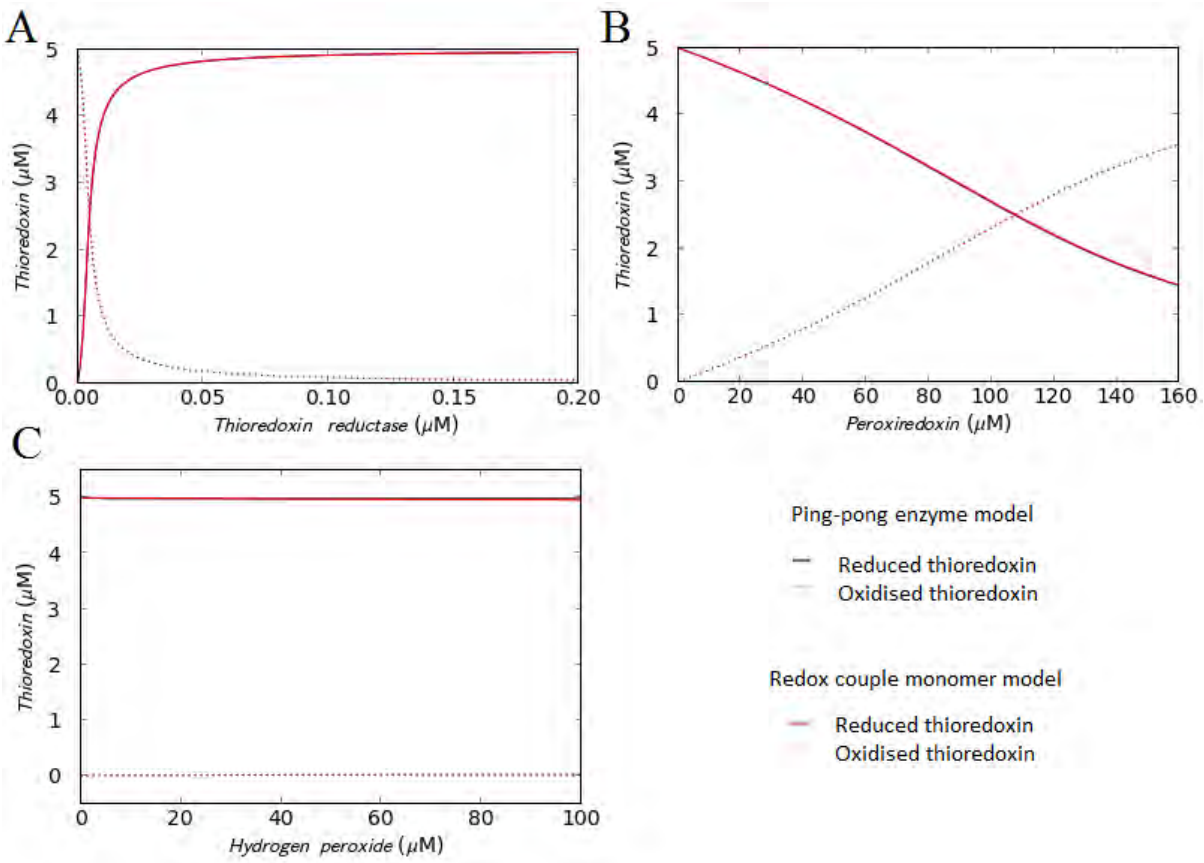

Figure 4.6 Simulation of the fitted ping-pong enzyme and redox couple monomer models yielded similar predictions on the redox state of thioredoxin with increasing thioredoxin reductase (A), peroxiredoxin (B) and hydrogen peroxide concentrations (C). The ping-pong enzyme and redox couple monomer model datasets overlap in (A), (B) and (C).

Despite their similar properties, the ping-pong enzyme and redox couple monomer models had a 100-fold difference in the fitted rate constants for hydrogen peroxide reduction (Table 4.4). The models were simulated with increasing hydrogen peroxide and saturated the system at very low hydrogen peroxide concentrations in the ping-pong enzyme model, while the rate continued to gradually increase throughout this range of concentrations in the redox couple monomer model (Figure 4.7). This result showed that these kinetic models do indeed yield distinct predictions but this could not be confirmed *in vitro* due to the rapid depletion of hydrogen peroxide in the steady state NADPH oxidation assay. Modification of the assay at low hydrogen peroxide concentrations or use of a more sensitive spectrophotometer is needed to carry out this analysis in the future.

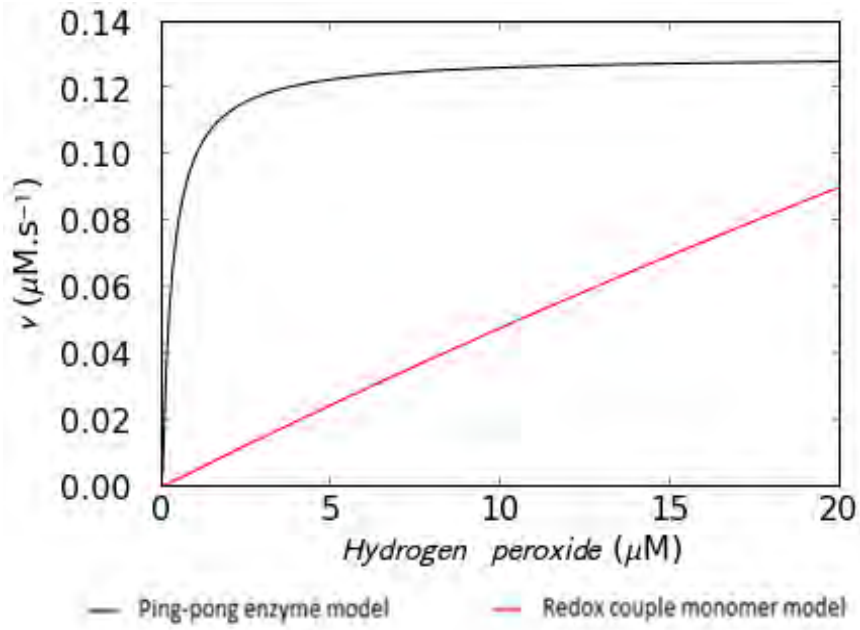

Figure 4.7 The fitted ping-pong enzyme and redox couple monomer models showed distinct responses to increasing hydrogen peroxide concentrations.

4.3.3 Flux control patterns of the fitted *Saccharomyces cerevisiae* peroxiredoxin kinetic models.

Flux control for both models lay primarily with the hydrogen peroxide reduction step (Table 4.5) suggesting that this reaction was indeed rate-limiting in the system. The flux control pattern in the fitted ping-pong enzyme model was consistent with the human erythrocyte peroxiredoxin 2, *C. crescentus* peroxiredoxin and *S. cerevisiae* TSA1 systems (Tables 2.8, 2.10 and 4.5). In the fitted redox couple monomer models, the peroxiredoxin recycling reaction had primary flux control for the human erythrocyte peroxiredoxin 2 and *C. crescentus* peroxiredoxin systems although the species concentrations used in these experiments were not necessarily chosen so that hydrogen peroxide recycling was rate-limiting (Manta *et al.*, 2009; Cho *et al.*, 2012). Determining the flux control coefficient in the fitted redox couple monomer models with varying thioredoxin concentrations showed that the thioredoxin concentration used to produce the human erythrocyte peroxiredoxin 2 and *C. crescentus* periplasmic peroxiredoxin *in vitro* datasets was too low for the hydrogen reduction reaction to have primary flux control (Figure 4.8) but was sufficient in our *S. cerevisiae in vitro* datasets. Determining the relative concentrations of reactants needed to ensure a given reaction is rate-limiting in a peroxiredoxin steady state assay is therefore complex and

suggests that fitting all reactions in a computational model is necessary for analysing such complex systems.

Table 4.5 Comparison of flux control coefficients for each reaction in the peroxiredoxin activity models fitted to the *S. cerevisiae* peroxiredoxin *in vitro* dataset.

Reaction	**Flux Control Co-efficient**
Ping-Pong Enzyme Model	
1 $NADPH + Trx_{SS} \rightarrow NADP_{+} + Trx_{SH}$	$C_{R1}^{JR1} = 0.0006$ $C_{R2}^{JR1} = 0.9994$
2 $Trx_{SH} + H_2O_2 \rightarrow Trx_{SS} + H_2O$	$C_{R1}^{JR1} = 0.0006$ $C_{R2}^{JR1} = 0.9994$
Redox Couple Monomer Model	
1 $NADPH + Trx_{SS} \rightarrow NADP^{+} + Trx_{SH}$	$C_{R1}^{JR1} = 0.001$ $C_{R2}^{JR1} = 0.836$ $C_{R3}^{JR1} = 0.163$
2 $H_2O_2 + Prx_{SH} \rightarrow H_2O + Prx_{SS}$	$C_{R1}^{JR1} = 0.0006$ $C_{R2}^{JR1} = 0.836$ $C_{R3}^{JR1} = 0.163$
3 $Prx_{SS} + Trx_{SH} \rightarrow Prx_{SH} + Trx_{SS}$	$C_{R1}^{JR1} = 0.001$ $C_{R2}^{JR1} = 0.836$ $C_{R3}^{JR1} = 0.163$

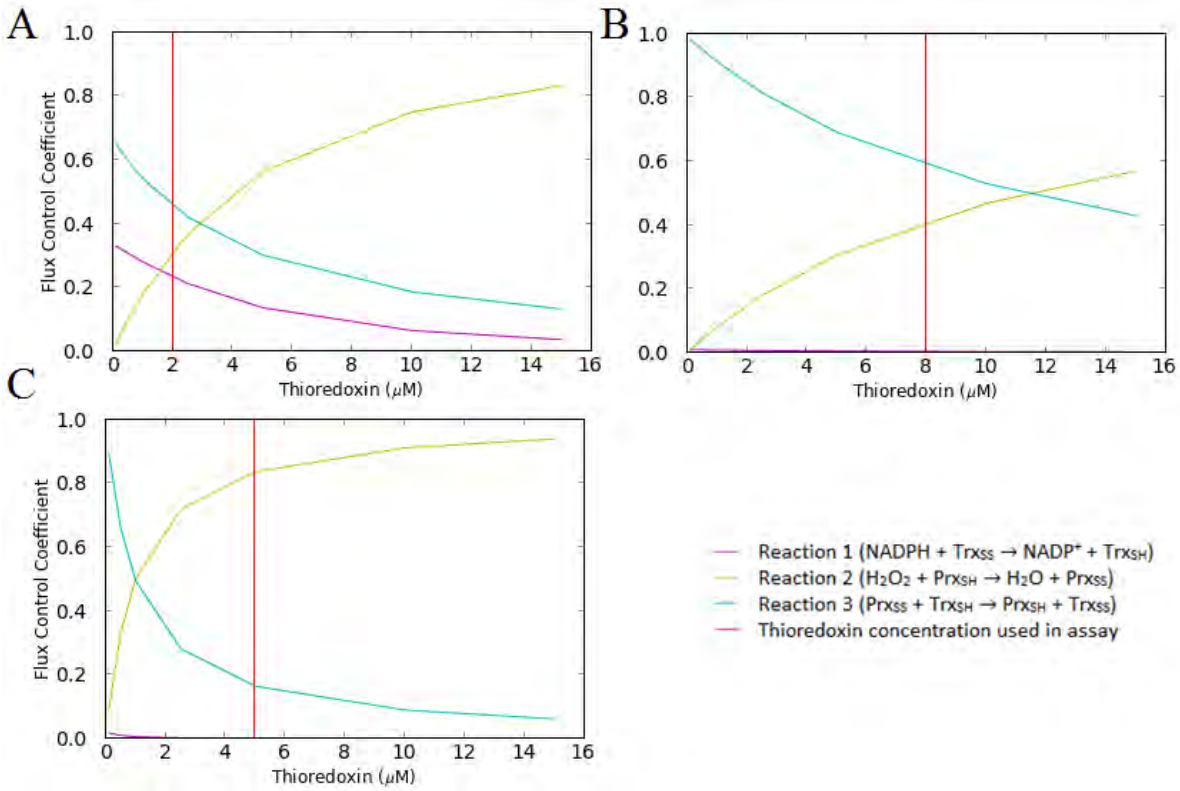

Figure 4.8 Flux control in the fitted redox couple monomer models was determined with varying thioredoxin concentrations for the human erythrocyte peroxiredoxin 2 (A), *C. crescentus* peroxiredoxin (B) and *S. cerevisiae* TSA1 (C) peroxiredoxin systems. At lower thioredoxin concentrations, peroxiredoxin reduction (reaction 3) was rate-limiting but as its concentration increased hydrogen peroxide reduction (reaction 2) became rate-limiting.

4.4 Discussion

In most kinetic studies of the peroxiredoxin system, the kinetic parameters for hydrogen peroxide reduction were obtained with either an *in vitro* steady state, competition or direct peroxiredoxin oxidation assay. Initial modelling studies using all three peroxiredoxin models with parameters from the literature failed to reproduce an *in vitro* dataset generated during this study (Figure 4.3) and therefore a different experimental strategy was pursued in which the entire peroxiredoxin system was fitted to steady state *in vitro* datasets (Table 4.4). The parameters obtained from these fitting experiments were then verified for accuracy by comparing the fitted models to independent *in vitro* datasets with varying thioredoxin and peroxiredoxin concentrations. Attempts at fitting of the redox couple homodimer model failed while the ping-pong enzyme and redox couple monomer models determined fitted rate constants for hydrogen peroxide reduction in the range of 10^5 (k_{cat}/K_m ratio) and 10^3 M^{-1} s^{-1}

respectively and not the rate of 10^7 M^{-1} s^{-1} previously measured for TSA1 in a competition assay (Ogusucu *et al.*, 2007). This rate constant is consistent with range determined through fitting for human erythrocyte peroxiredoxin 2 and *C. crescentus* peroxiredoxin dataset (Chapter 2). Using the parameters determined by data fitting, the ping-pong enzyme and redox couple monomer models were successfully able to reproduce two independent *in vitro* datasets (Figure 4.4). The fitted models (Figure 4.5 and 4.6) also showed similar flux and thioredoxin redox state responses to increasing thioredoxin reductase and peroxiredoxin concentrations, suggesting that these fitted kinetic models could be used interchangeably for this set of experimental conditions. The ability of these fitted models to reproduce independent datasets validated the fitting strategy used to determine these parameters. Core computational modelling suggested that changes to the thioredoxin reductase and peroxiredoxin concentrations should have been able to distinguish the models (Chapter 2) but our experiments yielded similar responses with the fitted models (Figure 4.5 and 4.6). Unfortunately, the 100-fold difference in the hydrogen peroxide reduction rate constant between the ping-pong enzyme and redox couple monomer models (Figure 4.7) could not be investigated in this study due to the difficulty measuring rates with low hydrogen peroxide concentrations that quickly depleted. Further analysis could use stopped-flow spectrophotometry or the flux in the assay could be reduced by lower thioredoxin reductase or NADPH concentrations. Fitting of the redox couple homodimer could also be re-attempted on this dataset or possibly other datasets that are generated.

Flux control analysis showed that even with careful selection of reactant concentrations, assigning a rate-limiting step in the peroxiredoxin kinetic models is difficult (Table 4.5 and Figure 4.8). For example, in the redox couple monomer model, the ratio of thioredoxin to thioredoxin reductase in the assay appears to determine if hydrogen peroxide reduction will be the rate-limiting reaction in the system but the ratio required varied between the different peroxiredoxin systems tested which can be challenging for setting up *in vitro* assays. This result also argued that using whole system data fitting may be the most accurate method for parameter determination in the peroxiredoxin system.

An argument for the redox couple monomer model compared to the ping-pong enzyme model is that data about the oxidised and reduced peroxiredoxin concentrations can be obtained from this model. These concentrations can be quantified using redox Western blotting analysis with anti-peroxiredoxin antibodies which already have been generated in the

laboratory and will be purified in future studies so that this experiment can be undertaken (Brown *et al.*, 2013; Soethoudt *et al.*, 2014).

Chapter 5

General discussion

Hydrogen peroxide is a metabolic by-product associated with oxidative stress but has also recently been found to initiate redox signalling processes at physiological concentrations (Veal *et al.*, 2007; Finkel, 2011; Veal and Day, 2011). Peroxiredoxins appear to mediate the balance between hydrogen peroxide detoxification and signal transduction (Jarvis *et al.*, 2012; Randall *et al.*, 2013; Perkins *et al.*, 2015; Sobotta *et al.*, 2015). Understanding the precise role of peroxiredoxins in these processes is difficult as these processes are complex and therefore the use of systems biology tools is necessary. Unfortunately three different peroxiredoxin kinetic models have proposed and used interchangeably in computational analyses of peroxiredoxin activity (Table 1.1, Figure 1.6). The rate constants for hydrogen peroxide reduction have also varied depending on the method used to measure this parameter and it is unclear which constants should be used in computational models (Section 2.1). Collectively, these discrepancies have limited the use of systems biology tools to further our understanding of peroxiredoxin activity.

Core computational modelling of the peroxiredoxin kinetic models determined different behaviours in terms of the flux and steady state thioredoxin concentrations in response to parameter changes and therefore these models were distinct and should not be used interchangeably (Section 2.3.1). These results were confirmed using *in vitro* computational analyses of the human erythrocyte peroxiredoxin 2 and *C. crescentus* peroxiredoxin systems (Section 2.3.2 and 2.3.4) and therefore a precise description of the peroxiredoxin system is needed for systems biology studies. Further, the effect of parameter changes on the steady state thioredoxin concentrations could be as an important system output to distinguish the peroxiredoxin kinetic models. The modelling also revealed the difficulty in determining the rate-limiting step for *in vitro* assays due to the complex flux control pattern of the peroxiredoxin system (Section 2.3.3 and 2.3.5). Determining the rate-limiting step was not necessary in this study however, as the rate constants for hydrogen peroxide reduction (10^3-10^5 M^{-1} s^{-1}) were determined by whole system fitting to *in vitro* datasets and these constants were much lower than those determined by competition assay.

To confirm these results, the *S. cerevisiae* TSA1 system was cloned, expressed and purified in large amounts using a high yield expression protocol (Sivashanmugam *et al.*,

2009) for *in vitro* analysis of this system (Chapter 3). In our hands, the recombinant His-tagged TSA1 activity was similar to the His-tag cleaved TSA1 and the protein conformation was predominantly decameric (Section 4.3.1, De Oliveira *et al.*, 2007; Tairum *et al.*, 2012). An *in vitro* dataset was generated and whole system data fitting was again used to determine kinetic parameters, which unlike other studies, were then verified by predicting independent datasets with varying thioredoxin and peroxiredoxin concentrations (Chapter 4). While the ping-pong enzyme and redox couple monomer models could fit and predict these datasets, the redox couple homodimer model failed to fit all datasets produced in this study. Interestingly the redox couple homodimer kinetic model has been used in a comprehensive model of hydrogen peroxide metabolism in red blood cells (Benfeitas *et al.*, 2014). We speculate that the failure of this kinetic model for the TSA1 peroxiredoxin system is due to conformational changes occurring during peroxiredoxin catalysis. In some peroxiredoxins, oxidation of the peroxidatic cysteine triggers structural changes in the peroxiredoxin dimer interface which obscures the second active site causing decamer dissociation (Parsonage *et al.*, 2005; Hall *et al.*, 2010). Thus, the stoichiometry of this reaction involves the reduction of a single hydrogen peroxide per catalytic cycle. The redox couple homodimer model was therefore excluded from further analysis while the fitted ping-pong enzyme and redox couple monomer models produced similar responses to almost all parameter changes and therefore both appear to be applicable to the TSA1 peroxiredoxin system. The flux response with increasing hydrogen peroxide concentrations was the only difference between these two fitted kinetic models and a modification of the *in vitro* assay in future studies could distinguish these models.

As with the human erythrocyte peroxiredoxin 2 and *C. crescentus* peroxiredoxin systems, the hydrogen peroxide reduction rate constants for the fitted TSA1 kinetic models was also in the range of 10^3-10^5 M^{-1} s^{-1} which suggests that peroxiredoxin recycling is important for hydrogen peroxide reduction and the thioredoxin redox couple can affect peroxiredoxin activity. In addition, this lower estimate for hydrogen peroxide reduction rate constant is in agreement with the kinetics of hydrogen peroxide signalling. For example, glutathione peroxidase-like protein 3 (Gpx3), must compete with TSA1 for hydrogen peroxide in order to oxidise the transcription factor YAP1 (Ghaemmaghami *et al.*, 2003; Tachibana *et al.*, 2009). The concentrations of Gpx3 and Yap1 are several orders lower than TSA1 and TSA1 with a purported rate constant of 10^7 M^{-1} s^{-1} (Ogusucu *et al.*, 2007) should easily outcompete Gpx3 for hydrogen peroxide. However, YAP1 is still activated at 0.1 mM

hydrogen peroxide *in vivo* (Delaunay *et al.*, 2002) suggesting that the peroxiredoxin rate constants of 10^6-10^8 M^{-1} s^{-1} obtained by the competition assay may be a severe overestimate.

In summary, the work in this thesis has confirmed that the kinetic models used to describe peroxiredoxin activity can yield computational models with distinct properties. In future studies, we plan to use redox Western blotting and a modified kinetic assay to distinguish the ping-pong enzyme and redox couple monomer models. The second major outcome is that the rate constants for hydrogen peroxide reduction by peroxiredoxins may need to be reviewed. This work emphasises how the kinetic linkages within the peroxiredoxin system are as important as the reaction of hydrogen peroxide and peroxiredoxin. With revised peroxiredoxin kinetic models, insight may be found into the multitude of diseases associated with hydrogen peroxide dysregulation using systems biology tools.

References

Adimora, N.J., Jones, D.P., and Kemp, M.L. (2010). A Model of Redox Kinetics Implicates the Thiol Proteome in Cellular Hydrogen Peroxide Responses. Antioxidant & Redox Signalling *13*, 731-743.

Adolfsen, K.J., and Brynildsen, M.P. (2015). A Kinetic Platform to Determine the Fate of Hydrogen Peroxide in Escherichia Coli. PLoS Computational Biology *11*, e1004562.

Aon, M.A., Stanley, B.A., Sivakumaran, V., Kembro, J.M., O'rourke, B., Paolocci, N., and Cortassa, S. (2012). Glutathione/Thioredoxin Systems Modulate Mitochondrial H2o2 Emission: An Experimental-Computational Study. The Journal of General Physiology *139*, 479-491.

Apel, K., and Hirt, H. (2004). Reactive Oxygen Species: Metabolism, Oxidative Stress, and Signal Transduction. Annual Review of Plant Biology *55*, 373-399.

Arner, E.S., and Holmgren, A. (2000). Physiological Functions of Thioredoxin and Thioredoxin Reductase. European Journal of Biochemistry/FEBS *267*, 6102-6109.

Arner, E.S., and Holmgren, A. (2001). Measurement of Thioredoxin and Thioredoxin Reductase. Current Protocols in Toxicology *Chapter 7*, Unit 7.4.

Baker, L.M., and Poole, L.B. (2003). Catalytic Mechanism of Thiol Peroxidase from Escherichia Coli. Sulfenic Acid Formation and Overoxidation of Essential Cys61. The Journal of Biological Chemistry *278*, 9203-9211.

Barranco-Medina, S., Lázaro, J.-J., and Dietz, K.-J. (2009). The Oligomeric Conformation of Peroxiredoxins Links Redox State to Function. FEBS Letters *583*, 1809-1816.

Bayer, S.B., Hampton, M.B., and Winterbourn, C.C. (2015). Accumulation of Oxidized Peroxiredoxin 2 in Red Blood Cells and Its Prevention. Transfusion *55*, 1909-1918.

Benfeitas, R., Selvaggio, G., Antunes, F., Coelho, P.M., and Salvador, A. (2014). Hydrogen Peroxide Metabolism and Sensing in Human Erythrocytes: A Validated Kinetic Model and Reappraisal of the Role of Peroxiredoxin Ii. Free Radical Biology & Medicine *74*, 35-49.

Bhat, N.R., and Zhang, P. (1999). Hydrogen Peroxide Activation of Multiple Mitogen-Activated Protein Kinases in an Oligodendrocyte Cell Line. Journal of Neurochemistry *72*, 112-119.

Bienert, G.P., Schjoerring, J.K., and Jahn, T.P. (2006). Membrane Transport of Hydrogen Peroxide. Biochimica et Biophysica Acta *1758*, 994-1003.

Biteau, B., Labarre, J., and Toledano, M.B. (2003). Atp-Dependent Reduction of Cysteine-Sulphinic Acid by S. Cerevisiae Sulphiredoxin. Nature *425*, 980-984.

Boronat, S., Domenech, A., Paulo, E., Calvo, I.A., Garcia-Santamarina, S., Garcia, P., Encinar Del Dedo, J., Barcons, A., Serrano, E., Carmona, M.*, et al.* (2014). Thiol-Based H2o2 Signalling in Microbial Systems. Redox Biology *2*, 395-399.

Brown, J.D., Day, A., Taylor, S., Tomalin, L., Morgan, B., and Veal, E. (2013). A Peroxiredoxin Promotes H2o2 Signaling and Oxidative Stress Resistance by Oxidizing a Thioredoxin Family Protein. Cell Reports *5*, 1425-1435.

Cabiscol, E., Piulats, E., Echave, P., Herrero, E., and Ros, J. (2000). Oxidative Stress Promotes Specific Protein Damage in Saccharomyces Cerevisiae. The Journal of Biological Chemistry *275*, 27393-27398.

Cao, Z., Bhella, D., and Lindsay, J.G. (2007). Reconstitution of the Mitochondrial Prxiii Antioxidant Defence Pathway: General Properties and Factors Affecting Prxiii Activity and Oligomeric State. The Journal of Molecular Biology *372*, 1022-1033.

Cao, Z., Mcgow, D.P., Shepherd, C., and Lindsay, J.G. (2015). Improved Catenated Structures of Bovine Peroxiredoxin Iii F190l Reveal Details of Ring-Ring Interactions and a Novel Conformational State. PLoS ONE *10*, e0123303.

Cao, Z., Subramaniam, S., and Bulleid, N.J. (2014). Lack of an Efficient Endoplasmic Reticulum-Localized Recycling System Protects Peroxiredoxin Iv from Hyperoxidation. The Journal of Biological Chemistry *289*, 5490-5498.

Cao, Z., Tavender, T.J., Roszak, A.W., Cogdell, R.J., and Bulleid, N.J. (2011). Crystal Structure of Reduced and of Oxidized Peroxiredoxin Iv Enzyme Reveals a Stable Oxidized

Decamer and a Non-Disulfide-Bonded Intermediate in the Catalytic Cycle. The Journal of Biological Chemistry *286*, 42257-42266.

Chabes, A., Georgieva, B., Domkin, V., Zhao, X., Rothstein, R., and Thelander, L. (2003). Survival of DNA Damage in Yeast Directly Depends on Increased Dntp Levels Allowed by Relaxed Feedback Inhibition of Ribonucleotide Reductase. Cell *112*, 391-401.

Chae, H.Z., Chung, S.J., and Rhee, S.G. (1994a). Thioredoxin-Dependent Peroxide Reductase from Yeast. The Journal of Biological Chemistry *269*, 27670-27678.

Chae, H.Z., and Rhee, S.G. (1994). A Thiol-Specific Antioxidant and Sequence Homology to Various Proteins of Unknown Function. Biofactors *4*, 177-180.

Chae, H.Z., Uhm, T.B., and Rhee, S.G. (1994b). Dimerization of Thiol-Specific Antioxidant and the Essential Role of Cysteine 47. Proceedings of the National Academy of Sciences of the United States of America *91*, 7022-7026.

Chelikani, P., Fita, I., and Loewen, P.C. (2004). Diversity of Structures and Properties among Catalases. Cellular and molecular life sciences : CMLS *61*, 192-208.

Chiang, A.W., Liu, W.C., Charusanti, P., and Hwang, M.J. (2014). Understanding System Dynamics of an Adaptive Enzyme Network from Globally Profiled Kinetic Parameters. Cancer Cell *8*, 4.

Cho, C.S., Yoon, H.J., Kim, J.Y., Woo, H.A., and Rhee, S.G. (2014). Circadian Rhythm of Hyperoxidized Peroxiredoxin Ii Is Determined by Hemoglobin Autoxidation and the 20s Proteasome in Red Blood Cells. Proceedings of the National Academy of Sciences of the United States of America *111*, 12043-12048.

Cho, S.H., Parsonage, D., Thurston, C., Dutton, R.J., Poole, L.B., Collet, J.F., and Beckwith, J. (2012). A New Family of Membrane Electron Transporters and Its Substrates, Including a New Cell Envelope Peroxiredoxin, Reveal a Broadened Reductive Capacity of the Oxidative Bacterial Cell Envelope. mBio *3*, e00291-00211.

Cleland, W.W. (1963). The Kinetics of Enzyme-Catalyzed Reactions with Two or More Substrates or Products. I. Nomenclature and Rate Equations. Biochimica et Biophysica Acta *67*, 104-137.

Cox, A.G., Peskin, A.V., Paton, L.N., Winterbourn, C.C., and Hampton, M.B. (2009). Redox Potential and Peroxide Reactivity of Human Peroxiredoxin 3. Biochemistry *48*, 6495-6501.

D'autreaux, B., and Toledano, M.B. (2007). Ros as Signalling Molecules: Mechanisms That Generate Specificity in Ros Homeostasis. Nature Reviews. Molecular Cell Biology *8*, 813-824.

Dagert, M., and Ehrlich, S.D. (1979). Prolonged Incubation in Calcium Chloride Improves the Competence of Escherichia Coli Cells. Gene *6*, 23-28.

Day, A.M., Brown, J.D., Taylor, S.R., Rand, J.D., Morgan, B.A., and Veal, E.A. (2012). Inactivation of a Peroxiredoxin by Hydrogen Peroxide Is Critical for Thioredoxin-Mediated Repair of Oxidized Proteins and Cell Survival. Molecular Cell *45*, 398-408.

De Franceschi, L., Bertoldi, M., De Falco, L., Santos Franco, S., Ronzoni, L., Turrini, F., Colancecco, A., Camaschella, C., Cappellini, M.D., and Iolascon, A. (2011). Oxidative Stress Modulates Heme Synthesis and Induces Peroxiredoxin-2 as a Novel Cytoprotective Response in Beta-Thalassemic Erythropoiesis. Haematologica *96*, 1595-1604.

De Oliveira, M.A., Genu, V., Discola, K.F., Alves, S.V., Netto, L.E., and Guimaraes, B.G. (2007). Crystallization and Preliminary X-Ray Analysis of a Decameric Form of Cytosolic Thioredoxin Peroxidase 1 (Tsa1), C47s Mutant, from Saccharomyces Cerevisiae. Acta Crystallographica. Section F, Structural Biology and Crystallization Communications *63*, 665-668.

Delaunay, A., Pflieger, D., Barrault, M.B., Vinh, J., and Toledano, M.B. (2002). A Thiol Peroxidase Is an H2o2 Receptor and Redox-Transducer in Gene Activation. Cell *111*, 471-481.

Driessens, N., Versteyhe, S., Ghaddhab, C., Burniat, A., De Deken, X., Van Sande, J., Dumont, J.E., Miot, F., and Corvilain, B. (2009). Hydrogen Peroxide Induces DNA Single- and Double-Strand Breaks in Thyroid Cells and Is Therefore a Potential Mutagen for This Organ. Endocrine-related Cancer *16*, 845-856.

Fell, D. (1997). Understanding the Control of Metabolism (London: Portland Press).

Fell, D.A. (2005). Enzymes, Metabolites and Fluxes. Journal of Experimental Botany *56*, 267-272.

Finkel, T. (2011). Signal Transduction by Reactive Oxygen Species. The Journal of Cell Biology *194*, 7-15.

Finn, R.D., Basran, J., Roitel, O., Wolf, C.R., Munro, A.W., Paine, M.J., and Scrutton, N.S. (2003). Determination of the Redox Potentials and Electron Transfer Properties of the Fad- and Fmn-Binding Domains of the Human Oxidoreductase Nr1. European Journal of Biochemistry / FEBS *270*, 1164-1175.

Firuzi, O., Miri, R., Tavakkoli, M., and Saso, L. (2011). Antioxidant Therapy: Current Status and Future Prospects. Current Medicinal Chemistry *18*, 3871-3888.

Garcia-Santamarina, S., Boronat, S., and Hidalgo, E. (2014). Reversible Cysteine Oxidation in Hydrogen Peroxide Sensing and Signal Transduction. Biochemistry *53*, 2560-2580.

Ghaemmaghami, S., Huh, W.-K., Bower, K., Howson, R.W., Belle, A., Dephoure, N., O'shea, E.K., and Weissman, J.S. (2003). Global Analysis of Protein Expression in Yeast. Nature *425*, 737-741.

Gleason, F.K., Lim, C.J., Gerami-Nejad, M., and Fuchs, J.A. (1990). Characterization of Escherichia Coli Thioredoxins with Altered Active Site Residues. Biochemistry *29*, 3701-3709.

Grek, C.L., Zhang, J., Manevich, Y., Townsend, D.M., and Tew, K.D. (2013). Causes and Consequences of Cysteine S-Glutathionylation. The Journal of Biological Chemistry *288*, 26497-26504.

Hall, A., Karplus, P.A., and Poole, L.B. (2009). Typical 2-Cys Peroxiredoxins: Structures, Mechanisms and Functions. The FEBS Journal *276*, 2469-2477.

Hall, A., Parsonage, D., Poole, L.B., and Karplus, P.A. (2010). Structural Evidence That Peroxiredoxin Catalytic Power Is Based on Transition State Stabilization. Journal of Molecular Biology *402*, 194-209.

Halliwell, B. (2006). Reactive Species and Antioxidants. Redox Biology Is a Fundamental Theme of Aerobic Life. Plant Physiology *141*, 312-322.

Hanschmann, E.M., Godoy, J.R., Berndt, C., Hudemann, C., and Lillig, C.H. (2013). Thioredoxins, Glutaredoxins, and Peroxiredoxins--Molecular Mechanisms and Health Significance: From Cofactors to Antioxidants to Redox Signaling. Antioxidants & Redox Signaling *19*, 1539-1605.

Harju, S., Fedosyuk, H., and Peterson, K.R. (2004). Rapid Isolation of Yeast Genomic DNA: Bust N' Grab. BMC Biotechnology *4*, 8.

Hildebraunt, A.G., and Roots, I. (1975). Reduced Nicotinamide Adenine Dinucleotide Phosphate (Nadph)-Dependent Formation and Breakdown of Hydrogen Peroxide During Mixed Function Oxidation Reactions in Liver Microsomes. Archives of Biochemistry and Biophysics *171*, 385-397.

Hofmeyr, J.S., and Cornish-Bowden, A. (2000). Regulating the Cellular Economy of Supply and Demand. FEBS Letters *476*, 47-51.

Holmgren, A. (1988). Thioredoxin and Glutaredoxin: Small Multi-Functional Redox Proteins with Active-Site Disulphide Bonds. Biochemical Society Transactions *16*, 95-96.

Huang, B.K., and Sikes, H.D. (2014). Quantifying Intracellular Hydrogen Peroxide Perturbations in Terms of Concentration. Redox Biology *2*, 955-962.

Ideker, T., Galitski, T., and Hood, L. (2001). A New Approach to Decoding Life: Systems Biology. Annual Review of Genomics and Human Genetics *2*, 343-372.

Iraqui, I., Kienda, G., Soeur, J., Faye, G., Baldacci, G., Kolodner, R.D., and Huang, M.E. (2009). Peroxiredoxin Tsa1 Is the Key Peroxidase Suppressing Genome Instability and Protecting against Cell Death in Saccharomyces Cerevisiae. PLoS Genetics *5*, e1000524.

Jang, H.H., Lee, K.O., Chi, Y.H., Jung, B.G., Park, S.K., Park, J.H., Lee, J.R., Lee, S.S., Moon, J.C., Yun, J.W.*, et al.* (2004). Two Enzymes in One; Two Yeast Peroxiredoxins Display Oxidative Stress-Dependent Switching from a Peroxidase to a Molecular Chaperone Function. Cell *117*, 625-635.

Jara, M., Vivancos, A.P., Calvo, I.A., Moldon, A., Sanso, M., and Hidalgo, E. (2007). The Peroxiredoxin Tpx1 Is Essential as a H2o2 Scavenger During Aerobic Growth in Fission Yeast. Molecular Biology of the Cell *18*, 2288-2295.

Jarvis, R.M., Hughes, S.M., and Ledgerwood, E.C. (2012). Peroxiredoxin 1 Functions as a Signal Peroxidase to Receive, Transduce, and Transmit Peroxide Signals in Mammalian Cells. Free Radical Biology & Medicine *53*, 1522-1530.

Johnson, R.M., Goyette, G., Jr., Ravindranath, Y., and Ho, Y.S. (2005). Hemoglobin Autoxidation and Regulation of Endogenous H2o2 Levels in Erythrocytes. Free Radical Biology & Medicine *39*, 1407-1417.

Karplus, P.A., and Poole, L.B. (2012). Peroxiredoxins as Molecular Triage Agents, Sacrificing Themselves to Enhance Cell Survival During a Peroxide Attack. Molecular Cell *45*, 275-278.

Kawazu, S., Komaki-Yasuda, K., Oku, H., and Kano, S. (2008). Peroxiredoxins in Malaria Parasites: Parasitologic Aspects. Parasitology International *57*, 1-7.

König, J., Galliardt, H., Jütte, P., Schäper, S., Dittmann, L., and Dietz, K.-J. (2013). The Conformational Bases for the Two Functionalities of 2-Cysteine Peroxiredoxins as Peroxidase and Chaperone. Journal of Experimental Botany *64*, 3483-3497.

Koshkin, A., Zhou, X.T., Kraus, C.N., Brenner, J.M., Bandyopadhyay, P., Kuntz, I.D., Barry, C.E., 3rd, and Ortiz De Montellano, P.R. (2004). Inhibition of Mycobacterium Tuberculosis Ahpd, an Element of the Peroxiredoxin Defense against Oxidative Stress. Antimicrobial Agents and Chemotherapy *48*, 2424-2430.

Laurent, T.C., Moore, E.C., and Reichard, P. (1964). Enzymatic Synthesis of Deoxyribonucleotides. Iv. Isolation and Characterization of Thioredoxin, the Hydrogen Donor from Escherichia Coli B. The Journal of Biological Chemistry *239*, 3436-3444.

Lillig, C.H., Berndt, C., and Holmgren, A. (2008). Glutaredoxin Systems. Biochimica et Biophysica Acta *1780*, 1304-1317.

Lim, J.B., Huang, B.K., Deen, W.M., and Sikes, H.D. (2015). Analysis of the Lifetime and Spatial Localization of Hydrogen Peroxide Generated in the Cytosol Using a Reduced Kinetic Model. Free Radical Biology and Medicine *89*, 47-53.

Lim, J.C., Choi, H.I., Park, Y.S., Nam, H.W., Woo, H.A., Kwon, K.S., Kim, Y.S., Rhee, S.G., Kim, K., and Chae, H.Z. (2008). Irreversible Oxidation of the Active-Site Cysteine of

Peroxiredoxin to Cysteine Sulfonic Acid for Enhanced Molecular Chaperone Activity. The Journal of Biological Chemistry *283*, 28873-28880.

Liochev, S.I. (2013). Reactive Oxygen Species and the Free Radical Theory of Aging. Free Radical Biology & Medicine *60*, 1-4.

Liou, G.-Y., and Storz, P. (2010). Reactive Oxygen Species in Cancer. Free Radical Research *44*, 479-496.

Liu, H., Zhang, H., Iles, K.E., Rinna, A., Merrill, G., Yodoi, J., Torres, M., and Forman, H.J. (2006). The Adp-Stimulated Nadph Oxidase Activates the Ask-1/Mkk4/Jnk Pathway in Alveolar Macrophages. Free Radical Research *40*, 865-874.

Manta, B., Hugo, M., Ortiz, C., Ferrer-Sueta, G., Trujillo, M., and Denicola, A. (2009). The Peroxidase and Peroxynitrite Reductase Activity of Human Erythrocyte Peroxiredoxin 2. Archives of Biochemistry and Biophysics *484*, 146-154.

Martin, J.L. (1995). Thioredoxin--a Fold for All Reasons. Structure *3*, 245-250.

Mashamaite, Lefentse n., Rohwer, Johann m., and Pillay, Ché s. (2015). The Glutaredoxin Mono- and Di-Thiol Mechanisms for Deglutathionylation Are Functionally Equivalent: Implications for Redox Systems Biology. Bioscience Reports *35*, e00173.

Masuoka, N., Wakimoto, M., Ubuka, T., and Nakano, T. (1996). Spectrophotometric Determination of Hydrogen Peroxide: Catalase Activity and Rates of Hydrogen Peroxide Removal by Erythrocytes. Clinica Chimica Acta. International Journal of Clinical Chemistry *254*, 101-112.

Matsumura, T., Okamoto, K., Iwahara, S.-I., Hori, H., Takahashi, Y., Nishino, T., and Abe, Y. (2008). Dimer-Oligomer Interconversion of Wild-Type and Mutant Rat 2-Cys Peroxiredoxin: Disulfide Formation at Dimer-Dimer Interfaces Is Not Essential for Decamerization. The Journal of Biological Chemistry *283*, 284-293.

Mieyal, J.J., Gallogly, M.M., Qanungo, S., Sabens, E.A., and Shelton, M.D. (2008). Molecular Mechanisms and Clinical Implications of Reversible Protein S-Glutathionylation. Antioxidants & Redox Signaling *10*, 1941-1988.

Mishra, S., and Imlay, J. (2012). Why Do Bacteria Use So Many Enzymes to Scavenge Hydrogen Peroxide? Archives of Biochemistry and Biophysics *525*, 145-160.

Morais, M., Giuseppe, P., Souza, T., Alegria, T., Oliveira, M., Netto, L., and Murakami, M. (2015). How Ph Modulates the Dimer-Decamer Interconversion of 2-Cys Peroxiredoxins from the Prx1 Subfamily. The Journal of Biological Chemistry *290*, 8582-8590.

Munhoz, D.C., and Netto, L.E. (2004). Cytosolic Thioredoxin Peroxidase I and Ii Are Important Defenses of Yeast against Organic Hydroperoxide Insult: Catalases and Peroxiredoxins Cooperate in the Decomposition of H2o2 by Yeast. The Journal of Biological Chemistry *279*, 35219-35227.

Nagy, P., Karton, A., Betz, A., Peskin, A.V., Pace, P., O'reilly, R.J., Hampton, M.B., Radom, L., and Winterbourn, C.C. (2011). Model for the Exceptional Reactivity of Peroxiredoxins 2 and 3 with Hydrogen Peroxide: A Kinetic and Computational Study. The Journal of Biological Chemistry *286*, 18048-18055.

Nelson, K.J., and Parsonage, D. (2011). Measurement of Peroxiredoxin Activity. Current Protocols in Toxicology *Chapter 7*, Unit 7.10.

Nelson, K.J., Parsonage, D., Hall, A., Karplus, P.A., and Poole, L.B. (2008). Cysteine Pk(a) Values for the Bacterial Peroxiredoxin Ahpc. Biochemistry *47*, 12860-12868.

Nishiyama, A., Masutani, H., Nakamura, H., Nishinaka, Y., and Yodoi, J. (2001). Redox Regulation by Thioredoxin and Thioredoxin-Binding Proteins. IUBMB Life *52*, 29-33.

O'neill, J.S., and Reddy, A.B. (2011). Circadian Clocks in Human Red Blood Cells. Nature *469*, 498-503.

Ogusucu, R., Rettori, D., Munhoz, D.C., Netto, L.E., and Augusto, O. (2007). Reactions of Yeast Thioredoxin Peroxidases I and Ii with Hydrogen Peroxide and Peroxynitrite: Rate Constants by Competitive Kinetics. Free Radical Biology and Medicine *42*, 326-334.

Olivier, B.G., Rohwer, J.M., and Hofmeyr, J.H. (2005). Modelling Cellular Systems with Pysces. Bioinformatics *21*, 560-561.

Olry, A., Boschi-Muller, S., and Branlant, G. (2004). Kinetic Characterization of the Catalytic Mechanism of Methionine Sulfoxide Reductase B from Neisseria Meningitidis. Biochemistry *43*, 11616-11622.

Padayachee, L., and Pillay, C.S. (2015). The Thioredoxin System and Not the Michaelis-Menten Equation Should Be Fitted to Substrate Saturation Datasets from the Thioredoxin Insulin Assay. Redox Report, 10.1179/1351000215y.0000000024.

Park, B.G., Yoo, C.I., Kim, H.T., Kwon, C.H., and Kim, Y.K. (2005). Role of Mitogen-Activated Protein Kinases in Hydrogen Peroxide-Induced Cell Death in Osteoblastic Cells. Toxicology *215*, 115-125.

Park, J., Lee, S., Lee, S., and Kang, S.W. (2014). 2-Cys Peroxiredoxins: Emerging Hubs Determining Redox Dependency of Mammalian Signaling Networks. International Journal of Cell Biology *2014*, 715867.

Park, J.W., Piszczek, G., Rhee, S.G., and Chock, P.B. (2011). Glutathionylation of Peroxiredoxin I Induces Decamer to Dimers Dissociation with Concomitant Loss of Chaperone Activity. Biochemistry *50*, 3204-3210.

Parsonage, D., Youngblood, D.S., Sarma, G.N., Wood, Z.A., Karplus, P.A., and Poole, L.B. (2005). Analysis of the Link between Enzymatic Activity and Oligomeric State in Ahpc, a Bacterial Peroxiredoxin(,). Biochemistry *44*, 10.1021/bi050448i.

Paulo, E., Garcia-Santamarina, S., Calvo, I.A., Carmona, M., Boronat, S., Domenech, A., Ayte, J., and Hidalgo, E. (2014). A Genetic Approach to Study H2o2 Scavenging in Fission Yeast--Distinct Roles of Peroxiredoxin and Catalase. Molecular Microbiology *92*, 246-257.

Perkins, A., Nelson, K.J., Parsonage, D., Poole, L.B., and Karplus, P.A. (2015). Peroxiredoxins: Guardians against Oxidative Stress and Modulators of Peroxide Signaling. Trends in Biochemical Sciences *40*, 435-445.

Peskin, A.V., Dickerhof, N., Poynton, R.A., Paton, L.N., Pace, P.E., Hampton, M.B., and Winterbourn, C.C. (2013). Hyperoxidation of Peroxiredoxins 2 and 3: Rate Constants for the Reactions of the Sulfenic Acid of the Peroxidatic Cysteine. The Journal of Biological Chemistry *288*, 14170-14177.

Pham-Huy, L.A., He, H., and Pham-Huy, C. (2008a). Free Radicals, Antioxidants in Disease and Health. International Journal of Biomedical Science *4*, 89-96.

Pham-Huy, L.A., He, H., and Pham-Huy, C. (2008b). Free Radicals, Antioxidants in Disease and Health. International Journal of Biomedical Science *4*, 89-96.

Pillay, C.S., Hofmeyr, J.H., Olivier, B.G., Snoep, J.L., and Rohwer, J.M. (2009). Enzymes or Redox Couples? The Kinetics of Thioredoxin and Glutaredoxin Reactions in a Systems Biology Context. Biochemical Journal *417*, 269-275.

Pillay, C.S., Hofmeyr, J.H., and Rohwer, J.M. (2011). The Logic of Kinetic Regulation in the Thioredoxin System. BMC Systems Biology *5*, 15.

Poole, L.B., Hall, A., and Nelson, K.J. (2011). Overview of Peroxiredoxins in Oxidant Defense and Redox Regulation. Current Protocols in Toxicology *Chapter 7*, Unit7.9.

Poynton, R.A., and Hampton, M.B. (2014). Peroxiredoxins as Biomarkers of Oxidative Stress. Biochimica et Biophysica Acta *1840*, 906-912.

Rabilloud, T., Berthier, R., Vincon, M., Ferbus, D., Goubin, G., and Lawrence, J.J. (1995). Early Events in Erythroid Differentiation: Accumulation of the Acidic Peroxidoxin (Prp/Tsa/Nkef-B). Biochemical Journal *312*, 699-705.

Radjainia, M., Venugopal, H., Desfosses, A., Phillips, Amy j., Yewdall, N.A., Hampton, Mark b., Gerrard, Juliet a., and Mitra, Alok k. (2015). Cryo-Electron Microscopy Structure of Human Peroxiredoxin-3 Filament Reveals the Assembly of a Putative Chaperone. Structure *23*, 912-920.

Ragu, S., Dardalhon, M., Sharma, S., Iraqui, I., Buhagiar-Labarchède, G., Grondin, V., Kienda, G., Vernis, L., Chanet, R., Kolodner, R.D.*, et al.* (2014). Loss of the Thioredoxin Reductase Trr1 Suppresses the Genomic Instability of Peroxiredoxin Tsa1 Mutants. PLoS ONE *9*, e108123.

Randall, L.M., Ferrer-Sueta, G., and Denicola, A. (2013). Peroxiredoxins as Preferential Targets in H2o2-Induced Signaling. Methods in Enzymology *527*, 41-63.

Rhee, S.G., Woo, H.A., Kil, I.S., and Bae, S.H. (2012). Peroxiredoxin Functions as a Peroxidase and a Regulator and Sensor of Local Peroxides. J Biol Chem *287*, 4403-4410.

Ristow, M., Zarse, K., Oberbach, A., Kloting, N., Birringer, M., Kiehntopf, M., Stumvoll, M., Kahn, C.R., and Bluher, M. (2009). Antioxidants Prevent Health-Promoting Effects of Physical Exercise in Humans. Proceedings of the National Academy of Sciences of the United States of America *106*, 8665-8670.

Sambrook, J., and Russell, D.W. (2006). Preparation of Plasmid DNA by Alkaline Lysis with Sds: Minipreparation. Cold Spring Harbor Protocols *2006*, pdb.prot4084.

Sayin, V.I., Ibrahim, M.X., Larsson, E., Nilsson, J.A., Lindahl, P., and Bergo, M.O. (2014). Antioxidants Accelerate Lung Cancer Progression in Mice. Science Translational Medicine *6*, 221ra215.

Schumacker, P.T. (2006). Reactive Oxygen Species in Cancer Cells: Live by the Sword, Die by the Sword. Cancer Cell *10*, 175-176.

Seaver, L.C., and Imlay, J.A. (2001). Alkyl Hydroperoxide Reductase Is the Primary Scavenger of Endogenous Hydrogen Peroxide in Escherichia Coli. Journal of Bacteriology *183*, 7173-7181.

Segel, I.H. (2013). Enzyme Kinetics. In Encyclopedia of Biological Chemistry, W.J. Lennarz, and M.D. Lane, eds. (Waltham: Academic Press), pp. 216-220.

Seo, M.S., Kang, S.W., Kim, K., Baines, I.C., Lee, T.H., and Rhee, S.G. (2000). Identification of a New Type of Mammalian Peroxiredoxin That Forms an Intramolecular Disulfide as a Reaction Intermediate. Journal of Biological Chemistry

275, 20346-20354.

Siddique, Y.H., Ara, G., and Afzal, M. (2012). Estimation of Lipid Peroxidation Induced by Hydrogen Peroxide in Cultured Human Lymphocytes. Dose-Response *10*, 1-10.

Sivashanmugam, A., Murray, V., Cui, C., Zhang, Y., Wang, J., and Li, Q. (2009). Practical Protocols for Production of Very High Yields of Recombinant Proteins Using Escherichia Coli. Protein Science *18*, 936-948.

Sobotta, M.C., Liou, W., Stocker, S., Talwar, D., Oehler, M., Ruppert, T., Scharf, A.N., and Dick, T.P. (2015). Peroxiredoxin-2 and Stat3 Form a Redox Relay for H2o2 Signaling. Nature Chemical Biology *11*, 64-70.

Soethoudt, M., Peskin, A.V., Dickerhof, N., Paton, L.N., Pace, P.E., and Winterbourn, C.C. (2014). Interaction of Adenanthin with Glutathione and Thiol Enzymes: Selectivity for Thioredoxin Reductase and Inhibition of Peroxiredoxin Recycling. Free Radical Biology and Medicine *77*, 331-339.

Speranza, M.L., Ronchi, S., and Minchiotti, L. (1973). Purification and Characterization of Yeast Thioredoxin Reductase. Biochimica et Biophysica Acta *327*, 274-281.

Tachibana, T., Okazaki, S., Murayama, A., Naganuma, A., Nomoto, A., and Kuge, S. (2009). A Major Peroxiredoxin-Induced Activation of Yap1 Transcription Factor Is Mediated by Reduction-Sensitive Disulfide Bonds and Reveals a Low Level of Transcriptional Activation. The Journal of Biological Chemistry *284*, 4464-4472.

Tairum, C.A., Jr., De Oliveira, M.A., Horta, B.B., Zara, F.J., and Netto, L.E. (2012). Disulfide Biochemistry in 2-Cys Peroxiredoxin: Requirement of Glu50 and Arg146 for the Reduction of Yeast Tsa1 by Thioredoxin. The Journal of Molecular Biology *424*, 28-41.

Tanaka, T., Nakamura, H., Nishiyama, A., Hosoi, F., Masutani, H., Wada, H., and Yodoi, J. (2000). Redox Regulation by Thioredoxin Superfamily; Protection against Oxidative Stress and Aging. Free Radical Research *33*, 851-855.

Trotter, E.W., Rand, J.D., Vickerstaff, J., and Grant, C.M. (2008). The Yeast Tsa1 Peroxiredoxin Is a Ribosome-Associated Antioxidant. The Biochemical Journal *412*, 73-80.

Trujillo, M., Mauri, P., Benazzi, L., Comini, M., De Palma, A., Flohe, L., Radi, R., Stehr, M., Singh, M., Ursini, F.*, et al.* (2006). The Mycobacterial Thioredoxin Peroxidase Can Act as a One-Cysteine Peroxiredoxin. The Journal of Biological Chemistry *281*, 20555-20566.

Turanov, A.A., Su, D., and Gladyshev, V.N. (2006). Characterization of Alternative Cytosolic Forms and Cellular Targets of Mouse Mitochondrial Thioredoxin Reductase. The Journal of Biological Chemistry *281*, 22953-22963.

Urig, S., Lieske, J., Fritz-Wolf, K., Irmler, A., and Becker, K. (2006). Truncated Mutants of Human Thioredoxin Reductase 1 Do Not Exhibit Glutathione Reductase Activity. FEBS Letters *580*, 3595-3600.

Veal, E., and Day, A. (2011). Hydrogen Peroxide as a Signaling Molecule. Antioxidant & Redox Signaling *15*, 147-151.

Veal, E.A., Day, A.M., and Morgan, B.A. (2007). Hydrogen Peroxide Sensing and Signaling. Molecular Cell *26*, 1-14.

Veal, E.A., Ross, S.J., Malakasi, P., Peacock, E., and Morgan, B.A. (2003). Ybp1 Is Required for the Hydrogen Peroxide-Induced Oxidation of the Yap1 Transcription Factor. Journal of Biological Chemistry *278*, 30896-30904.

Wang, T., Tamae, D., Lebon, T., Shively, J.E., Yen, Y., and Li, J.J. (2005). The Role of Peroxiredoxin Ii in Radiation-Resistant Mcf-7 Breast Cancer Cells. Cancer Research *65*, 10338-10346.

Watson, W.H., Pohl, J., Montfort, W.R., Stuchlik, O., Reed, M.S., Powis, G., and Jones, D.P. (2003). Redox Potential of Human Thioredoxin 1 and Identification of a Second Dithiol/Disulfide Motif. Journal of Biological Chemistry *278*, 33408-33415.

Weidinger, A., and Kozlov, A.V. (2015). Biological Activities of Reactive Oxygen and Nitrogen Species: Oxidative Stress Versus Signal Transduction. Biomolecules *5*, 472-484.

Williams Jr, C.H. (1976). 3 Flavin-Containing Dehydrogenases. In The Enzymes, D.B. Paul, ed. (Academic Press), pp. 89-173.

Winterbourn, C.C. (2008). Reconciling the Chemistry and Biology of Reactive Oxygen Species. Nature Chemical Biology *4*, 278-286.

Winterbourn, C.C., and Hampton, M.B. (2008). Thiol Chemistry and Specificity in Redox Signaling. Free Radical Biology and Medicine *45*, 549-561.

Wittig, I., Braun, H.P., and Schagger, H. (2006). Blue Native Page. Nature Protocols *1*, 418-428.

Woo, H.A., Yim, S.H., Shin, D.H., Kang, D., Yu, D.Y., and Rhee, S.G. (2010). Inactivation of Peroxiredoxin I by Phosphorylation Allows Localized H(2)O(2) Accumulation for Cell Signaling. Cell *140*, 517-528.

Wood, P.M. (1988). The Potential Diagram for Oxygen at Ph 7. The Biochemical Journal *253*, 287-289.

Wood, Z.A., Poole, L.B., and Karplus, P.A. (2003a). Peroxiredoxin Evolution and the Regulation of Hydrogen Peroxide Signaling. Science *300*, 650-653.

Wood, Z.A., Schroder, E., Robin Harris, J., and Poole, L.B. (2003b). Structure, Mechanism and Regulation of Peroxiredoxins. Trends in Biochemical Sciences *28*, 32-40.

Young, I.S., and Woodside, J.V. (2001). Antioxidants in Health and Disease. Journal of Clinical Pathology *54*, 176-186.

Appendix

Table of Contents

1. Core computational Models

1.1 Peroxiredoxin Activity Models with Core Parameters

```
#Core Peroxiredoxin Activity Model - Ping-pong enzyme model

FIX: NADPH NADP H2O2 H2O

R1: NADPH + TrxSS = NADP + TrxSH
(kcat1*TR*(NADPH/Knadph)*(TrxSS/K1trxss))/((1+NADPH/Knadph)*(1
+TrxSS/K1trxss))

R2: TrxSH + H2O2 = TrxSS + H2O
(kcat2*Prx*(TrxSH/Ktrxsh)*(H2O2/K1h2o2))/((H2O2/K1h2o2)+(TrxSH
/Ktrxsh)+((TrxSH/Ktrxsh)*(H2O2/K1h2o2)))
#Kinetic Parameters = units in µM, s-1 and µM-1 s-1

kcat1 =1
TR = 1
Knadph = 1
K1trxss = 1

kcat2 = 1
Prx = 1
Ktrxsh = 1
K1h2o2 = 1

#Species concentrations - units in µM

NADPH = 1
NADP = 1
TrxSS = 0.5
TrxSH = 0.5
H2O2 = 1
H2O = 1
```

```
#Core Peroxiredoxin Activity Model - Redox couple monomer
model

FIX: NADPH NADP H2O2 H2O

R1: NADPH + TrxSS = NADP + TrxSH
(kcat1*TR*(NADPH/Knadph)*(TrxSS/K1trxss))/((1+NADPH/Knadph)*(1
+TrxSS/K1trxss))

R2: H2O2 + PrxSH = H2O + PrxSS
k2*H2O2*PrxSH

R3: PrxSS + TrxSH = PrxSH + TrxSS
k3*PrxSS*TrxSH

#Kinetic Parameters = units in µM, s-1 and µM-1 s-1

kcat1 =1
TR = 1
Knadph = 1
K1trxss = 1

k2 = 1

k3 = 1

#Species concentrations - units in µM

NADPH = 1
NADP = 1
TrxSS = 0.5
TrxSH = 0.5
H2O2 = 1
H2O = 1
PrxSH = 0.5
PrxSS = 0.5
```

```
#Core Peroxiredoxin Activity Model - Redox couple homodimer
model

FIX: NADPH NADP H2O2 H2O

R1: NADPH + TrxSS = NADP + TrxSH
(kcat1*TR*(NADPH/Knadph)*(TrxSS/K1trxss))/((1+NADPH/Knadph)*(1
+TrxSS/K1trxss))

R2: PrxSHPrxSH + H2O2 = PrxSSPrxSH + H2O
k2*PrxSHPrxSH*H2O2*2

R3: PrxSSPrxSH + H2O2 = PrxSSPrxSS + H2O
k2*PrxSSPrxSH*H2O2

R4: PrxSSPrxSS + TrxSH = PrxSSPrxSH + TrxSS
k3*PrxSSPrxSS*TrxSH*2

R5: PrxSSPrxSH + TrxSH = PrxSHPrxSH + TrxSS
k3*PrxSSPrxSH*TrxSH

#Kinetic Parameters = units in µM, s-1 and µM-1 s-1
#Species concentrations - units in µM

kcat1 = 1
TR = 1
Knadph = 1
K1trxss = 1


k2 = 1
k3 = 1

#Kinetic Parameters = units in µM, s-1 and µM-1 s-1
#Species concentrations - units in µM

NADPH = 1
NADP = 1
TrxSS = 0.5
TrxSH = 0.5
H2O2 = 1
H2O = 1
PrxSHPrxSH = 0.33
PrxSSPrxSH = 0.33
PrxSSPrxSS = 0.34
```

1.2 Modelling Scripts

```
#Core modelling of the peroxiredoxin system

#import the operating system
import os
#tell opertaing system get the current working directory (cwd)
and call the cwd backupdir
backupdir = os.getcwd()
#call programmes needed by PySCeS to work
import numpy
import scipy
import pylab
import pysces
import time

#tell PySCeS to look for the psc files in the current folder.
pysces.PyscesModel.MODEL_DIR=backupdir
pysces.PyscesModel.OUTPUT_DIR=backupdir
#tell opertaing system to work in the current directory
os.chdir(backupdir)
#need to call the plotting programme called matplotlib and
pylab.
#from pylab get stuff to doplotting
from pylab import figure, ioff, plt, subplots_adjust, rcParams
rcParams['mathtext.fontset']='stixsans'
pylab.rc('font', serif='Ariel')
from matplotlib.pyplot import*
#from numpy import arrange

matplotlib.rcParams.update({'font.size':12}c)
pylab.rc('xtick', labelsize = 12)
pylab.rc('ytick', labelsize = 12)
pylab.rc('ytick.major', pad = 12)
pylab.rc('ytick.minor', pad = 12)
pylab.rc('axes', labelsize = 12)
#from matplot lib get everything (*)
from matplotlib.pyplot import *

m=pysces.model('prxpingcore')
m.doStateShow()
m.scan_in = 'TR'
m.scan_out=['J_R1', 'Prx', 'TrxSH_ss', 'TrxSS_ss']
scan_range = scipy.linspace(0.01, 10, 200)
m.Scan1(scan_range)
g=m.scan_res
n=pysces.model('prxredoxcore')
n.doStateShow()
n.scan_in = 'TR'
```

```
n.scan_out=['J_R1', 'PrxSH_ss', 'PrxSS_ss', 'TrxSH_ss',
'TrxSS_ss']
scan_range = scipy.linspace(0.01, 10, 200)
n.Scan1(scan_range)
h=n.scan_res
o=pysces.model('prxdimercore')
o.doStateShow()
o.scan_in = 'TR'
o.scan_out=['J_R1', 'PrxSHPrxSH_ss', 'PrxSSPrxSS_ss',
'PrxSSPrxSH_ss', 'TrxSH_ss', 'TrxSS_ss']
scan_range = scipy.linspace(0.01, 10, 200)
o.Scan1(scan_range)
i=o.scan_res

m=pysces.model('prxpingcore')
m.doStateShow()
m.scan_in = 'H2O2'
m.scan_out=['J_R1', 'Prx', 'TrxSH_ss', 'TrxSS_ss']
scan_range = scipy.linspace(0.01, 1, 200)
m.Scan1(scan_range)
xx=m.scan_res

n=pysces.model('prxredoxcore')
n.doStateShow()
n.scan_in = 'H2O2'
n.scan_out=['J_R1', 'PrxSH_ss', 'PrxSS_ss', 'TrxSH_ss',
'TrxSS_ss']
scan_range = scipy.linspace(0.01, 1, 200)
n.Scan1(scan_range)
yy=n.scan_res

o=pysces.model('prxdimercore')
o.doStateShow()
o.scan_in = 'H2O2'
o.scan_out=['J_R1', 'PrxSHPrxSH_ss', 'PrxSSPrxSS_ss',
'PrxSSPrxSH_ss', 'TrxSH_ss', 'TrxSS_ss']
scan_range = scipy.linspace(0.01, 1, 200)
o.Scan1(scan_range)
zz=o.scan_res

m=pysces.model('prxpingcore')
m.doStateShow()
m.scan_in = 'H2O2'
m.scan_out=['J_R1', 'Prx', 'TrxSH_ss', 'TrxSS_ss']
scan_range = scipy.linspace(0.01, 100, 200)
m.Scan1(scan_range)
x=m.scan_res

n=pysces.model('prxredoxcore')
n.doStateShow()
n.scan_in = 'H2O2'
```

```
n.scan_out=['J_R1', 'PrxSH_ss', 'PrxSS_ss', 'TrxSH_ss',
'TrxSS_ss']
scan_range = scipy.linspace(0.01, 100, 200)
n.Scan1(scan_range)
y=n.scan_res

o=pysces.model('prxdimercore')
o.doStateShow()
o.scan_in = 'H2O2'
o.scan_out=['J_R1', 'PrxSHPrxSH_ss', 'PrxSSPrxSS_ss',
'PrxSSPrxSH_ss', 'TrxSH_ss', 'TrxSS_ss']
scan_range = scipy.linspace(0.01, 100, 200)
o.Scan1(scan_range)
z=o.scan_res

m=pysces.model('prxpingcore')
m.TrxSH_init =1
m.TrxSS_init =0
m.doStateShow()
m.scan_in = 'TrxSH_init'
m.scan_out=['J_R1', 'Prx', 'TrxSH_ss', 'TrxSS_ss']
scan_range = scipy.linspace(0.01, 10, 200)
m.Scan1(scan_range)
r=m.scan_res
n=pysces.model('prxredoxcore')
n.TrxSH_init =1
n.TrxSS_init =0
n.doStateShow()
n.scan_in = 'TrxSH_init'
n.scan_out=['J_R1', 'PrxSH_ss', 'PrxSS_ss', 'TrxSH_ss',
'TrxSS_ss']
scan_range = scipy.linspace(0.01, 10, 200)
n.Scan1(scan_range)
s=n.scan_res

o=pysces.model('prxdimercore')
o.TrxSH_init =1
o.TrxSS_init =0
o.doStateShow()
o.scan_in = 'TrxSH_init'
o.scan_out=['J_R1', 'PrxSHPrxSH_ss', 'PrxSSPrxSS_ss',
'PrxSSPrxSH_ss', 'TrxSH_ss', 'TrxSS_ss']
scan_range = scipy.linspace(0.01, 10, 200)
o.Scan1(scan_range)
t=o.scan_res

m=pysces.model('prxpingcore')
m.doStateShow()
m.scan_in = 'Prx'
m.scan_out=['J_R1', 'Prx', 'TrxSH_ss', 'TrxSS_ss']
scan_range = scipy.linspace(0.01, 10, 200)
```

```
m.Scan1(scan_range)
aa=m.scan_res

n=pysces.model('prxredoxcore')
n.PrxSH_init =1
n.PrxSS_init =0
n.doStateShow()
n.scan_in = 'PrxSH_init'
n.scan_out=['J_R1', 'PrxSH_ss', 'PrxSS_ss', 'TrxSH_ss',
'TrxSS_ss']
scan_range = scipy.linspace(0.01, 10, 200)
n.Scan1(scan_range)
bb=n.scan_res

o=pysces.model('prxdimercore')
o.PrxSHPrxSH_init =1
o.PrxSSPrxSS_init =0
o.PrxSSPrxSH_init =0
o.doStateShow()
o.scan_in = 'TrxSH_init'
o.scan_out=['J_R1', 'PrxSHPrxSH_ss', 'PrxSSPrxSS_ss',
'PrxSSPrxSH_ss', 'TrxSH_ss', 'TrxSS_ss']
scan_range = scipy.linspace(0.01, 10, 200)
o.Scan1(scan_range)
cc=o.scan_res

#Start the plotting
ioff()
fig=figure()

#Linear Plots
#plot of the change in flux of all models as thioredoxin
reductase increases
ax = subplot(4,4,1)
ax.plot(g[:,0],g[:,1], 'k-', label='Rate')
ax.plot(h[:,0],h[:,1], 'r-', label='Rate')
ax.plot(i[:,0],i[:,1], 'b-', label='Rate')
ax.set_xlabel(r' Thioredoxin Reductase($\mu$M)')
ax.set_ylabel(r' Flux ($\mu$M s $^{-1}$)')

#plot of the change in flux of all models as hydrogen peroxide
increases
ax = subplot(4,4,3)
ax.plot(xx[:,0],xx[:,1], 'k-', label='Rate')
ax.plot(yy[:,0],yy[:,1], 'r-', label='Rate')
ax.plot(zz[:,0],zz[:,1], 'b-', label='Rate')
ax.set_xlabel(r'Hydrogen Peroxide ($\mu$M)')
ax.set_ylabel(r' Flux ($\mu$M s $^{-1}$)')

#plot of the change in flux of all models as thioredoxin
increases
```

```
ax = subplot(4,4,2)
ax.plot(r[:,0],r[:,1], 'k-', label='Rate')
ax.plot(s[:,0],s[:,1], 'r-', label='Rate')
ax.plot(t[:,0],t[:,1], 'b-', label='Rate')
ax.set_xlabel(r' Thioredoxin ($\mu$M)')
ax.set_ylabel(r' Flux ($\mu$M s $^{-1}$)')

#plot of the change in flux of all models as peroxiredoxin
increases
ax = subplot(4,4,4)
ax.plot(aa[:,0],aa[:,1], 'k-', label='Rate')
ax.plot(bb[:,0],bb[:,1], 'r-', label='Rate')
ax.plot(cc[:,0],cc[:,1], 'b-', label='Rate')
ax.set_xlabel(r' Peroxiredoxin ($\mu$M)')
ax.set_ylabel(r' Flux ($\mu$M s $^{-1}$)')

#Log Plots
#plot of the change in flux of all models as thioredoxin
reductase increases
ax = subplot(4,4,5)
ax.loglog(g[:,0],g[:,1], 'k-', label='Rate')
ax.loglog(h[:,0],h[:,1], 'r-', label='Rate')
ax.loglog(i[:,0],i[:,1], 'b-', label='Rate')
ax.set_xlabel(r' Thioredoxin Reductase($\mu$M)')
ax.set_ylabel(r' Flux ($\mu$M s $^{-1}$)')

#plot of the change in flux of all models as hydrogen peroxide
increases
ax = subplot(4,4,7)
ax.loglog(x[:,0],x[:,1], 'k-', label='Rate')
ax.loglog(y[:,0],y[:,1], 'r-', label='Rate')
ax.loglog(z[:,0],z[:,1], 'b-', label='Rate')
ax.set_xlabel(r'Hydrogen Peroxide ($\mu$M)')
ax.set_ylabel(r' Flux ($\mu$M s $^{-1}$)')

#plot of the change in flux of all models as thioredoxin
increases
ax = subplot(4,4,6)
ax.loglog(r[:,0],r[:,1], 'k-', label='Rate')
ax.loglog(s[:,0],s[:,1], 'r-', label='Rate')
ax.loglog(t[:,0],t[:,1], 'b-', label='Rate')
ax.set_xlabel(r' Thioredoxin ($\mu$M)')
ax.set_ylabel(r' Flux ($\mu$M s $^{-1}$)')

#plot of the change in flux of all models as peroxiredoxin
increases
ax = subplot(4,4,8)
ax.loglog(aa[:,0],aa[:,1], 'k-', label='Rate')
ax.loglog(bb[:,0],bb[:,1], 'r-', label='Rate')
ax.loglog(cc[:,0],cc[:,1], 'b-', label='Rate')
ax.set_xlabel(r' Peroxiredoxin ($\mu$M)')
```

```
ax.set_ylabel(r' Flux ($\mu$M s $^{-1}$)')

subplots_adjust(wspace=0.6)
subplots_adjust(hspace=0.6)

pylab.savefig('Flux Analysis.png')
fig.show()
```

2. Realistic Computational Modelling

2.1 Human erythrocyte peroxiredoxin 2

2.1.1 Model Files

```
#Realistic modelling of the peroxiredoxin system-Human
Peroxiredoxin 2

#Ping-pong enzyme model

FIX: NADPH NADP H2O2 H2O

R1: NADPH + TrxSS = NADP + TrxSH
(kcat1*TR*(NADPH/Knadph)*(TrxSS/K1trxss))/((1+NADPH/Knadph)*(1
+TrxSS/K1trxss))

R2: TrxSH + H2O2 = TrxSS + H2O
(kcat2*Prx*(TrxSH/Ktrxsh)*(H2O2/K1h2o2))/((H2O2/K1h2o2)+(TrxSH
/Ktrxsh)+((TrxSH/Ktrxsh)*(H2O2/K1h2o2)))

#Kinetic Parameters = units in µM, s-1 and µM-1 s-1

kcat1 =25.78
TR = 1
Knadph = 6
K1trxss = 1.83

kcat2 = 13.2
Prx = 0.5
Ktrxsh = 3.24
K1h2o2 = 0.7

#Species concentrations - units in µM

NADPH = 200
NADP = 1
TrxSS = 1
TrxSH = 1
H2O2 = 30
H2O = 1
```

```
#Realistic modelling of the peroxiredoxin system-Human
Peroxiredoxin 2

#Redox couple monomer model

FIX: NADPH NADP H2O2 H2O

R1: NADPH + TrxSS = NADP + TrxSH
(kcat1*TR*(NADPH/Knadph)*(TrxSS/K1trxss))/((1+NADPH/Knadph)*(1
+TrxSS/K1trxss))

R2: H2O2 + PrxSH = H2O + PrxSS
k2*H2O2*PrxSH

R3: PrxSS + TrxSH = PrxSH + TrxSS
k3*PrxSS*TrxSH

#Kinetic Parameters = units in µM, s-1 and µM-1 s-1

kcat1 =25.78
TR = 1
Knadph = 6
K1trxss = 1.83

k2 = 100

k3 = 0.074

#Species concentrations - units in µM

NADPH = 200
NADP = 1
TrxSS = 1
TrxSH = 1
H2O2 = 30
H2O = 1
PrxSH = 0.25
PrxSS = 0.25
```

```
#Realistic modelling of the peroxiredoxin system-Human
Peroxiredoxin 2

#Redox couple homodimer model

FIX: NADPH NADP H2O2 H2O

R1: NADPH + TrxSS = NADP + TrxSH
(kcat1*TR*(NADPH/Knadph)*(TrxSS/K1trxss))/((1+NADPH/Knadph)*(1
+TrxSS/K1trxss))

R2: PrxSHPrxSH + H2O2 = PrxSSPrxSH + H2O
k2*PrxSHPrxSH*H2O2*2

R3: PrxSSPrxSH + H2O2 = PrxSSPrxSS + H2O
k2*PrxSSPrxSH*H2O2

R4: PrxSSPrxSS + TrxSH = PrxSSPrxSH + TrxSS
k3*PrxSSPrxSS*TrxSH*2

R5: PrxSSPrxSH + TrxSH = PrxSHPrxSH + TrxSS
k3*PrxSSPrxSH*TrxSH

#Kinetic Parameters = units in µM, s-1 and µM-1 s-1

kcat1 =25.78
TR = 1
Knadph = 6
K1trxss = 1.83


k2 = 100
k3 = 0.074

#Species concentrations - units in µM

NADPH = 200
NADP = 1
TrxSS = 1
TrxSH = 1
H2O2 = 30
H2O = 1
PrxSHPrxSH = 0.1667
PrxSSPrxSH = 0.1667
PrxSSPrxSS = 0.1667
```

2.1.2 *In vitro* Dataset

```
#Human peroxiredoxin 2 in vitro dataset (hprx.txt)- from
PlotDigitizer

# "[hTrx]"     "V"

0.18518007 0.001532415
0.8454714 0.021095108
1.1396866 0.02812719
1.4713523 0.03454971
1.7673641 0.03761227
2.100412  0.04098131
2.395318  0.046486653
2.7654018 0.05016218
3.3959813 0.053234957
4.6558967 0.062128637
6.582322  0.07684436
9.81634   0.07724846
```

2.1.3 Data Fitting Scripts

```
#Fitting of the models to the human peroxiredoxin 2 in vitro
dataset
#using Python Notebook

%pylab inline
import scipy as sp
import os
backupdir = os.getcwd()
import pysces
import time
import numpy
pysces.PyscesModel.MODEL_DIR=backupdir
pysces.PyscesModel.OUTPUT_DIR=backupdir
os.chdir(backupdir)


pylab.rc('xtick', labelsize = 12)
pylab.rc('ytick', labelsize = 12)
pylab.rc('ytick.major', pad = 12)
pylab.rc('ytick.minor', pad = 12)
pylab.rc('axes', labelsize = 12)

from pylab import figure, ioff, plt, subplots_adjust, rcParams
rcParams['mathtext.fontset']='stixsans'
pylab.rc('font', serif='Ariel')

from matplotlib.pyplot import*
#from numpy import arange
matplotlib.rcParams.update({'font.size':12})

#from matplot lib get everything (*)
from matplotlib.pyplot import *

#Ping-pong enzyme model fitting

fd = numpy.loadtxt('hprx.txt')

m=pysces.model('hprxping')
m.TrxSH_init = 0.01
m.TrxSS_init = 0
m.doStateShow()
m.SetQuiet()
m.scan_in='TrxSH_init'
m.scan_out=['J_R1']
scan_range=np.linspace(0.01, 10, 200)
m.Scan1(scan_range)
m.Scan1Plot()
aa=m.scan_res
```

```
# generate model data for fit conditions
def genmodeldata(xrange, kcat1, kcat2, K1h2o2):

    m.kcat1 = kcat1
    m.kcat2 = kcat2
    m.K1h2o2 = K1h2o2

    m.scan_in = 'TrxSH_init'
    m.scan_out = ['J_R1']
    m.Scan1(xrange)
    return m.scan_res[:,1]

#using curve_fit
def fitexp(expdata, p0):
    df = len(expdata)-len(p0)
    ydata = expdata[:,1]
    xdata = expdata[:,0]
    SStot = sum((ydata - np.mean(ydata))**2)   # sum of
squares of distance of data from mean
    cfit = sp.optimize.curve_fit(genmodeldata, xdata, ydata,
p0, full_output=1)
    pfit = cfit[0]
    cov_x = cfit[1]
    fin_residuals = cfit[2]['fvec']
    SSQ = sum((fin_residuals)**2)
    SE = np.sqrt(np.diag(cov_x))
    SD = np.sqrt(SSQ/len(fin_residuals))
    Rsq = 1.0-SSQ/SStot
    return {'pfit':pfit, 'SE':SE, 'SSQ':SSQ, 'SD':SD,
'Rsq':Rsq, 'df':df, 'cov_x':cov_x, 'cfit':cfit}
p0 = np.copy(( m.kcat1, m.kcat2, m.K1h2o2 ))
curvefit = fitexp(fd, p0)
print "parameters:\t", curvefit['pfit']
print "errors:\t\t", curvefit['SE']
print "SD:\t\t", curvefit['SD']
print "Rsquared:\t", curvefit['Rsq']

def plotfit(expdata, p0, label):
    curvefit = fitexp(expdata, p0)
    params =  curvefit['pfit']
    err = curvefit['SE']
    exp_x = expdata[:,0]
    exp_y = expdata[:,1]
    model_x = np.linspace(1, exp_x[-1], 100)
    model_y = genmodeldata(model_x, *params)
    plt.plot(exp_x, exp_y, 'o',label=label)
    plt.plot(model_x, model_y, '-',label='model')
    plt.xlabel('[Trx] ($\mu$M)')
    plt.ylabel('Rate ($\mu$M.s$^{-1}$)')
    plt.legend(loc='best')
```

```
    plt.xlim(0,1.05*exp_x[-1])
    print "parameters:"
    print 'kcat1:  ', curvefit['pfit'][0], ' +- ',
curvefit['SE'][0]
    print 'kcat2:  ', curvefit['pfit'][1], ' +- ',
curvefit['SE'][1]
    print 'k1h2o2 : ', curvefit['pfit'][2], ' +- ',
curvefit['SE'][2]
    print 'Rsquared:', curvefit['Rsq']


plotfit( fd, p0, 'hprx')
print '-----------------------------------'



# Redox couple monomer model fitting

n=pysces.model('hprxredox')
n.TrxSH_init = 0.01
n.TrxSS_init = 0
n.doStateShow()
n.SetQuiet()
n.scan_in='TrxSH_init'
n.scan_out=['J_R1']
scan_range=np.linspace(0.01, 10, 200)
n.Scan1(scan_range)
n.Scan1Plot()
bb=n.scan_res

# generate model data for fit conditions
def genmodeldata(xrange, kcat1, k2, k3):

    n.kcat1 = kcat1
    n.k2 = k2
    n.k3 = k3

    n.scan_in = 'TrxSH_init'
    n.scan_out = ['J_R1']
    n.Scan1(xrange)
    return n.scan_res[:,1]

#using curve_fit
def fitexp(expdata, p0):
    df = len(expdata)-len(p0)
    ydata = expdata[:,1]
    xdata = expdata[:,0]
    SStot = sum((ydata - np.mean(ydata))**2)   # sum of
squares of distance of data from mean
    cfit = sp.optimize.curve_fit(genmodeldata, xdata, ydata,
p0, full_output=1)
```

```
    pfit = cfit[0]
    cov_x = cfit[1]
    fin_residuals = cfit[2]['fvec']
    SSQ = sum((fin_residuals)**2)
    SE = np.sqrt(np.diag(cov_x))
    SD = np.sqrt(SSQ/len(fin_residuals))
    Rsq = 1.0-SSQ/SStot
    return {'pfit':pfit, 'SE':SE, 'SSQ':SSQ, 'SD':SD,
'Rsq':Rsq, 'df':df, 'cov_x':cov_x, 'cfit':cfit}
p0 = np.copy((n.kcat1, n.k2, n.k3 ))
curvefit = fitexp(fd,p0)
print "parameters:\t", curvefit['pfit']
print "errors:\t\t", curvefit['SE']
print "SD:\t\t", curvefit['SD']
print "Rsquared:\t", curvefit['Rsq']

def plotfit(expdata, p0, label):
    curvefit = fitexp(expdata, p0)
    params =  curvefit['pfit']
    err = curvefit['SE']
    exp_x = expdata[:,0]
    exp_y = expdata[:,1]
    model_x = np.linspace(1, exp_x[-1], 100)
    model_y = genmodeldata(model_x, *params)
    plt.plot(exp_x, exp_y, 'o',label=label)
    plt.plot(model_x, model_y, '-',label='model')
    plt.xlabel('[Trx] ($\mu$M)')
    plt.ylabel('Rate ($\mu$M.s$^{-1}$)')
    plt.legend(loc='best')
    plt.xlim(0,1.05*exp_x[-1])
    print "parameters:"
    print 'kcat1: ', curvefit['pfit'][0], ' +- ',
curvefit['SE'][0]
    print 'k2:      ', curvefit['pfit'][1], ' +- ',
curvefit['SE'][1]
    print 'k3:  ', curvefit['pfit'][2], ' +- ',
curvefit['SE'][2]
    print 'Rsquared:', curvefit['Rsq']


plotfit(fd, p0, 'hprx')
print '----------------------------------'

#Redox couple homodimer model fitting

o=pysces.model('hprxdimer')
o.TrxSH_init = 0.01
o.TrxSS_init = 0
o.doStateShow()
o.SetQuiet()
o.scan_in='TrxSH_init'
```

```
o.scan_out=['J_R1']
scan_range=np.linspace(0.01, 10, 200)
o.Scan1(scan_range)
o.Scan1Plot()
cc=o.scan_res

# generate model data for fit conditions
def genmodeldata(xrange, kcat1, k2, k3):

    o.kcat1 = kcat1
    o.k2 = k2
    o.k3 = k3

    o.scan_in = 'TrxSH_init'
    o.scan_out = ['J_R1']
    o.Scan1(xrange)
    return o.scan_res[:,1]

#using curve_fit
def fitexp(expdata, p0):
    df = len(expdata)-len(p0)
    ydata = expdata[:,1]
    xdata = expdata[:,0]
    SStot = sum((ydata - np.mean(ydata))**2)   # sum of
squares of distance of data from mean
    cfit = sp.optimize.curve_fit(genmodeldata, xdata, ydata,
p0, full_output=1)
    pfit = cfit[0]
    cov_x = cfit[1]
    fin_residuals = cfit[2]['fvec']
    SSQ = sum((fin_residuals)**2)
    SE = np.sqrt(np.diag(cov_x))
    SD = np.sqrt(SSQ/len(fin_residuals))
    Rsq = 1.0-SSQ/SStot
    return {'pfit':pfit, 'SE':SE, 'SSQ':SSQ, 'SD':SD,
'Rsq':Rsq, 'df':df, 'cov_x':cov_x, 'cfit':cfit}
p0 = np.copy((o.kcat1, o.k2, o.k3 ))
curvefit = fitexp(fd,p0)
print "parameters:\t", curvefit['pfit']
print "errors:\t\t", curvefit['SE']
print "SD:\t\t", curvefit['SD']
print "Rsquared:\t", curvefit['Rsq']

def plotfit(expdata, p0, label):
    curvefit = fitexp(expdata, p0)
    params =  curvefit['pfit']
    err = curvefit['SE']
    exp_x = expdata[:,0]
    exp_y = expdata[:,1]
    model_x = np.linspace(1, exp_x[-1], 100)
    model_y = genmodeldata(model_x, *params)
```

```
    plt.plot(exp_x, exp_y, 'o',label=label)
    plt.plot(model_x, model_y, '-',label='model')
    plt.xlabel('[Trx] ($\mu$M)')
    plt.ylabel('Rate ($\mu$M.s$^{-1}$)')
    plt.legend(loc='best')
    plt.xlim(0,1.05*exp_x[-1])
    print "parameters:"
    print 'kcat1: ', curvefit['pfit'][0], ' +- ',
curvefit['SE'][0]
    print 'k2:      ', curvefit['pfit'][1], ' +- ',
curvefit['SE'][1]
    print 'k3:  ', curvefit['pfit'][2], ' +- ',
curvefit['SE'][2]
    print 'Rsquared:', curvefit['Rsq']

plotfit(fd, p0, 'hprx')
print '----------------------------------'
```

2.1.4 Flux Control Analysis

```
#Flux control analysis of the human peroxiredoxin 2 activity
models

#import the operating system
import os
#tell opertaing system get the current working directory (cwd)
and call the cwd backupdir
backupdir = os.getcwd()
#programmes needed by PySCeS to work
import numpy
import scipy
import pylab
import pysces
import time
#tell PySCeS to look for the psc files in the current folder.
pysces.PyscesModel.MODEL_DIR=backupdir
pysces.PyscesModel.OUTPUT_DIR=backupdir

pylab.rc('xtick', labelsize = 12)
pylab.rc('ytick', labelsize = 12)
pylab.rc('ytick.major', pad = 12)
pylab.rc('ytick.minor', pad = 12)
pylab.rc('axes', labelsize = 12)

#tell opertaing system to work in the current directory
os.chdir(backupdir)

#need to call the plotting programme called matplotlib and
pylab.
#from pylab get stuff to doplotting
from pylab import figure, ioff, plt, subplots_adjust, rcParams
rcParams['mathtext.fontset']='stixsans'
pylab.rc('font', family='serif')
pylab.rc('font', serif='Ariel')

from matplotlib.pyplot import*
#from numpy import arange
matplotlib.rcParams.update({'font.size':12})

#from matplot lib get everything (*)
from matplotlib.pyplot import *

#unfitted human peroxiredoxin 2 models

m=pysces.model('hprxping')
m.doStateShow()
m.doMca()
m.showCC()
a= m.scan_res
```

```
n=pysces.model('hprxredox')
n.doStateShow()
n.doMca()
n.showCC()
b = n.scan_res

o=pysces.model('hprxdimer')
o.doStateShow()
o.doMca()
o.showCC()
c = o.scan_res

#fitted human peroxiredoxin 2 models

m=pysces.model('hprxpingfit')
m.doStateShow()
m.doMca()
m.showCC()
a= m.scan_res

n=pysces.model('hprxredoxfit')
n.doStateShow()
n.doMca()
n.showCC()
b = n.scan_res

o=pysces.model('hprxdimerfit')
o.doStateShow()
o.doMca()
o.showCC()
c = o.scan_res
```

Table S1 Comparison of flux control coefficients for each reaction in the peroxiredoxin activity models fitted to the human peroxiredoxin 2 dataset.

Reactions	Flux Control Coefficients
	Ping-Pong Enzyme Model
1	$C_{R1}^{JR1} = 0.232$ $C_{R2}^{JR1} = 0.768$
2	$C_{R1}^{JR2} = 0.232$ $C_{R2}^{JR2} = 0.768$
	Redox Couple Monomer Model
1	$C_{R1}^{JR1} = 0.232$ $C_{R2}^{JR1} = 0.313$ $C_{R3}^{JR1} = 0.455$
2	$C_{R1}^{JR2} = 0.232$ $C_{R2}^{JR2} = 0.313$ $C_{R3}^{JR2} = 0.455$
3	$C_{R1}^{JR3} = 0.232$ $C_{R2}^{JR3} = 0.313$ $C_{R3}^{JR3} = 0.455$
	Redox Couple Homodimer Model
1	$C_{R1}^{JR1} = 0.771$ $C_{R2}^{JR1} = 0.001$ $C_{R3}^{JR1} = 0.010$ $C_{R4}^{JR1} = 0.207$ $C_{R5}^{JR1} = 0.010$
2	$C_{R1}^{JR2} = 1.54$ $C_{R2}^{JR2} = -0.001$ $C_{R3}^{JR2} = -0.977$ $C_{R4}^{JR2} = -0.492$ $C_{R5}^{JR2} = 0.928$

3	C_{R1}^{JR3}= 0.733 C_{R2}^{JR3} = 0.001 C_{R1}^{JR2}= 0.060 C_{R4}^{JR3}= 0.242 C_{R5}^{JR3}= -0.035
4	C_{R1}^{JR4} = 0.733 C_{R2}^{JR4} = 0.001 C_{R3}^{JR4} = 0.060 C_{R4}^{JR4} = 0.242 C_{R5}^{JR4}= -0.035
5	C_{R1}^{JR5}= 1.54 C_{R2}^{JR5}= -0.001 C_{R3}^{JR5}= -0.977 C_{R5}^{JR4}= -0.492 C_{R5}^{JR5}= 0.928

2.2 *Caulobacter crescentus* peroxiredoxin

2.2.1 Model Files

```
#Realistic modelling - C. crescentus periplasmic peroxiredoxin

#Ping-pong enzyme model

FIX: NADPH NADP H2O2 H2O

R1: NADPH + TrxSS = NADP + TrxSH
(kcat1*TR*(NADPH/Knadph)*(TrxSS/K1trxss))/((1+NADPH/Knadph)*(1
+TrxSS/K1trxss))

R2: TrxSH + H2O2 = TrxSS + H2O
(kcat2*Prx*(TrxSH/Ktrxsh)*(H2O2/K1h2o2))/((H2O2/K1h2o2)+(TrxSH
/Ktrxsh)+((TrxSH/Ktrxsh)*(H2O2/K1h2o2)))

#Kinetic Parameters = units in µM, s-1 and µM-1 s-1

kcat1 = 22.75
TR = 0.5
Knadph = 1.2
K1trxss = 2.8

kcat2 = 73
Prx = 0.5
Ktrxsh = 24
K1h2o2 = 106

#Species concentrations - units in µM

NADPH = 100
NADP = 1
TrxSS = 4
TrxSH = 4
H2O2 = 150
H2O = 1
```

#Realistic modelling - *C. crescentus* periplasmic peroxiredoxin

#Redox couple monomer enzyme model

FIX: NADPH NADP H2O2 H2O

R1: NADPH + TrxSS = NADP + TrxSH
(kcat1*TR*(NADPH/Knadph)*(TrxSS/K1trxss))/((1+NADPH/Knadph)*(1
+TrxSS/K1trxss))

R2: H2O2 + PrxSH = H2O + PrxSS
k2*H2O2*PrxSH

R3: PrxSS + TrxSH = PrxSH + TrxSS
k3*PrxSS*TrxSH

#Kinetic Parameters = units in µM, s-1 and µM-1 s-1

kcat1 = 22.75
TR = 0.5
Knadph = 1.2
K1trxss = 2.8

k2 = 0.74

k3 = 3

#Species concentrations - units in µM

NADPH = 100
NADP = 1
TrxSS = 4
TrxSH = 4
H2O2 = 30
H2O = 1
PrxSH = 0.25
PrxSS = 0.25

```
#Realistic modelling - C. crescentus periplasmic peroxiredoxin

#Redox couple homodimer model

FIX: NADPH NADP H2O2 H2O

R1: NADPH + TrxSS = NADP + TrxSH
(kcat1*TR*(NADPH/Knadph)*(TrxSS/K1trxss))/((1+NADPH/Knadph)*(1
+TrxSS/K1trxss))

R2: PrxSHPrxSH + H2O2 = PrxSSPrxSH + H2O
k2*PrxSHPrxSH*H2O2*2

R3: PrxSSPrxSH + H2O2 = PrxSSPrxSS + H2O
k2*PrxSSPrxSH*H2O2

R4: PrxSSPrxSS + TrxSH = PrxSSPrxSH + TrxSS
k3*PrxSSPrxSS*TrxSH*2

R5: PrxSSPrxSH + TrxSH = PrxSHPrxSH + TrxSS
k3*PrxSSPrxSH*TrxSH

#Kinetic Parameters = units in µM, s-1 and µM-1 s-1

kcat1 = 22.75
TR = 0.5
Knadph = 1.2
K1trxss = 2.8


k2 = 0.74
k3 = 3

#Species concentrations - units in µM

NADPH = 100
NADP = 1
TrxSS = 4
TrxSH = 4
H2O2 = 30
H2O = 1
PrxSHPrxSH = 0.167
PrxSSPrxSH = 0.167
PrxSSPrxSS = 0.167
```

2.2.2 *In vitro* Dataset

```
# C. crescentus periplasmic peroxiredoxin dataset(pprx.txt)-
from #PlotDigitizer

# "[H2O2]"     "V"

10.699877 0.039947545
26.50682  0.0685985
50.146397 0.102454417
102.45166 0.148446217
201.31421 0.169207383
300.43314 0.222976167
500.51273 0.233225883
752.8099  0.278175333
1002.9143  0.269272517
```

2.2.3 Data Fitting Scripts

```
#Fitting of the models to the C. crescentus periplasmic
peroxiredoxin #in vitro dataset

#using Python Notebook


%pylab inline
import scipy as sp
import os
backupdir = os.getcwd()
import pysces
import time
import numpy
pysces.PyscesModel.MODEL_DIR=backupdir
pysces.PyscesModel.OUTPUT_DIR=backupdir
os.chdir(backupdir)

pylab.rc('xtick', labelsize = 12)
pylab.rc('ytick', labelsize = 12)
pylab.rc('ytick.major', pad = 12)
pylab.rc('ytick.minor', pad = 12)
pylab.rc('axes', labelsize = 12)

from pylab import figure, ioff, plt, subplots_adjust, rcParams
rcParams['mathtext.fontset']='stixsans'
pylab.rc('font', serif='Ariel')

from matplotlib.pyplot import*
#from numpy import arange
matplotlib.rcParams.update({'font.size':12})

#from matplot lib get everything (*)
from matplotlib.pyplot import *

fd = numpy.loadtxt('pprx.txt')

#Ping-pong enzyme model fitting

m=pysces.model('pprxping')
m.doStateShow()
m.SetQuiet()
m.scan_in='H2O2'
m.scan_out=['J_R1']
scan_range=np.linspace(0.01, 1000, 200)
m.Scan1(scan_range)
m.Scan1Plot()
s=m.scan_res
```

```
# generate model data for fit conditions
def genmodeldata(xrange, kcat2, Ktrxsh):


    m.kcat2 = kcat2
    m.Ktrxsh = Ktrxsh

    m.scan_in = 'H2O2'
    m.scan_out = ['J_R1']
    m.Scan1(xrange)
    return m.scan_res[:,1]
#using curve_fit
def fitexp(expdata, p0):
    df = len(expdata)-len(p0)
    ydata = expdata[:,1]
    xdata = expdata[:,0]
    SStot = sum((ydata - np.mean(ydata))**2)   # sum of
squares of distance of data from mean
    cfit = sp.optimize.curve_fit(genmodeldata, xdata, ydata,
p0, full_output=1)
    pfit = cfit[0]
    cov_x = cfit[1]
    fin_residuals = cfit[2]['fvec']
    SSQ = sum((fin_residuals)**2)
    SE = np.sqrt(np.diag(cov_x))
    SD = np.sqrt(SSQ/len(fin_residuals))
    Rsq = 1.0-SSQ/SStot
    return {'pfit':pfit, 'SE':SE, 'SSQ':SSQ, 'SD':SD,
'Rsq':Rsq, 'df':df, 'cov_x':cov_x, 'cfit':cfit}

p0 = np.copy(( m.kcat2, m.Ktrxsh ))
curvefit = fitexp(fd, p0)
print "parameters:\t", curvefit['pfit']
print "errors:\t\t", curvefit['SE']
print "SD:\t\t", curvefit['SD']
print "Rsquared:\t", curvefit['Rsq']
def plotfit(expdata, p0, label):
    curvefit = fitexp(expdata, p0)
    params =  curvefit['pfit']
    err = curvefit['SE']
    exp_x = expdata[:,0]
    exp_y = expdata[:,1]
    model_x = np.linspace(1, exp_x[-1], 100)
    model_y = genmodeldata(model_x, *params)
    plt.plot(exp_x, exp_y, 'o',label=label)
    plt.plot(model_x, model_y, '-',label='model')
    plt.xlabel('[Hydrogen Peroxide] ($\mu$M)')
    plt.ylabel('Rate ($\mu$M.s$^{-1}$)')
    plt.legend(loc='best')
    plt.xlim(0,1.05*exp_x[-1])
    print "parameters:"
```

```
    print 'kcat2:  ', curvefit['pfit'][0], ' +- ',
curvefit['SE'][0]
    print 'ktrxsh:  ', curvefit['pfit'][1], ' +- ',
curvefit['SE'][1]
    print 'Rsquared:', curvefit['Rsq']


plotfit( fd, p0, 'pprx')
print '----------------------------------'

#Redox couple monomer model fitting

n=pysces.model('pprxredox')
n.doStateShow()
n.SetQuiet()
n.scan_in='H2O2'
n.scan_out=['J_R1']
scan_range=np.linspace(0.01, 1000, 200)
n.Scan1(scan_range)
n.Scan1Plot()
t=n.scan_res

# generate model data for fit conditions
def genmodeldata(xrange, k2,  k3):

    n.k2 = k2
    n.k3 = k3

    n.scan_in = 'H2O2'
    n.scan_out = ['J_R1']
    n.Scan1(xrange)
    return n.scan_res[:,1]

#using curve_fit
def fitexp(expdata, p0):
    df = len(expdata)-len(p0)
    ydata = expdata[:,1]
    xdata = expdata[:,0]
    SStot = sum((ydata - np.mean(ydata))**2)   # sum of
squares of distance of data from mean
    cfit = sp.optimize.curve_fit(genmodeldata, xdata, ydata,
p0, full_output=1)
    pfit = cfit[0]
    cov_x = cfit[1]
    fin_residuals = cfit[2]['fvec']
    SSQ = sum((fin_residuals)**2)
    SE = np.sqrt(np.diag(cov_x))
    SD = np.sqrt(SSQ/len(fin_residuals))
    Rsq = 1.0-SSQ/SStot
    return {'pfit':pfit, 'SE':SE, 'SSQ':SSQ, 'SD':SD,
'Rsq':Rsq, 'df':df, 'cov_x':cov_x, 'cfit':cfit}
```

```
p0 = np.copy((n.k2, n.k3 ))
curvefit = fitexp(fd,p0)
print "parameters:\t", curvefit['pfit']
print "errors:\t\t", curvefit['SE']
print "SD:\t\t", curvefit['SD']
print "Rsquared:\t", curvefit['Rsq']

def plotfit(expdata, p0, label):
    curvefit = fitexp(expdata, p0)
    params =  curvefit['pfit']
    err = curvefit['SE']
    exp_x = expdata[:,0]
    exp_y = expdata[:,1]
    model_x = np.linspace(1, exp_x[-1], 100)
    model_y = genmodeldata(model_x, *params)
    plt.plot(exp_x, exp_y, 'o',label=label)
    plt.plot(model_x, model_y, '-',label='model')
    plt.xlabel('[Hydrogen Peroxide] ($\mu$M)')
    plt.ylabel('Rate ($\mu$M.s$^{-1}$)')
    plt.legend(loc='best')
    plt.xlim(0,1.05*exp_x[-1])
    print "parameters:"
    print 'k2: ', curvefit['pfit'][0], ' +- ',
curvefit['SE'][0]
    print 'k3:  ', curvefit['pfit'][1], ' +- ',
curvefit['SE'][1]
    print 'Rsquared:', curvefit['Rsq']


plotfit(fd, p0, 'pprx)
print '----------------------------------'

#Redox couple homodimer model fitting

o=pysces.model('pprxdimer')
o.doStateShow()
o.SetQuiet()
o.scan_in='H2O2'
o.scan_out=['J_R1']
scan_range=np.linspace(0.01, 1000, 200)
o.Scan1(scan_range)
o.Scan1Plot()
u=o.scan_res

# generate model data for fit conditions
def genmodeldata(xrange, k2, k3):

    o.k2 = k2
    o.k3 = k3

    o.scan_in = 'H2O2'
```

```
    o.scan_out = ['J_R1']
    o.Scan1(xrange)
    return o.scan_res[:,1]

#using curve_fit
def fitexp(expdata, p0):
    df = len(expdata)-len(p0)
    ydata = expdata[:,1]
    xdata = expdata[:,0]
    SStot = sum((ydata - np.mean(ydata))**2)   # sum of
squares of distance of data from mean
    cfit = sp.optimize.curve_fit(genmodeldata, xdata, ydata,
p0, full_output=1)
    pfit = cfit[0]
    cov_x = cfit[1]
    fin_residuals = cfit[2]['fvec']
    SSQ = sum((fin_residuals)**2)
    SE = np.sqrt(np.diag(cov_x))
    SD = np.sqrt(SSQ/len(fin_residuals))
    Rsq = 1.0-SSQ/SStot
    return {'pfit':pfit, 'SE':SE, 'SSQ':SSQ, 'SD':SD,
'Rsq':Rsq, 'df':df, 'cov_x':cov_x, 'cfit':cfit}
p0 = np.copy((o.k2, o.k3 ))
curvefit = fitexp(fd,p0)
print "parameters:\t", curvefit['pfit']
print "errors:\t\t", curvefit['SE']
print "SD:\t\t", curvefit['SD']
print "Rsquared:\t", curvefit['Rsq']
def plotfit(expdata, p0, label):
    curvefit = fitexp(expdata, p0)
    params =  curvefit['pfit']
    err = curvefit['SE']
    exp_x = expdata[:,0]
    exp_y = expdata[:,1]
    model_x = np.linspace(1, exp_x[-1], 100)
    model_y = genmodeldata(model_x, *params)
    plt.plot(exp_x, exp_y, 'o',label=label)
    plt.plot(model_x, model_y, '-',label='model')
    plt.xlabel('[Hydrogen Peroxide] ($\mu$M)')
    plt.ylabel('Rate ($\mu$M.s$^{-1}
$)')
    plt.legend(loc='best')
    plt.xlim(0,1.05*exp_x[-1])
    print "parameters:"
    print 'k2:      ', curvefit['pfit'][0], ' +- ',
curvefit['SE'][0]
    print 'k3:  ', curvefit['pfit'][1], ' +- ',
curvefit['SE'][1]
    print 'Rsquared:', curvefit['Rsq']

plotfit(fd, p0, 'pprx)
```

```
print '-----------------------------------'
```

2.2.4 Flux Control Analysis

```
#Flux control analysis of the C. crescentus periplasmic
peroxiredoxin #models

#import the operating system
import os
#tell opertaing system get the current working directory (cwd)
and call the cwd backupdir
backupdir = os.getcwd()
#programmes needed by PySCeS to work
import numpy
import scipy
import pylab
import pysces
import time
#tell PySCeS to look for the psc files in the current folder.
pysces.PyscesModel.MODEL_DIR=backupdir
pysces.PyscesModel.OUTPUT_DIR=backupdir

pylab.rc('xtick', labelsize = 12)
pylab.rc('ytick', labelsize = 12)
pylab.rc('ytick.major', pad = 12)
pylab.rc('ytick.minor', pad = 12)
pylab.rc('axes', labelsize = 12)

#tell opertaing system to work in the current directory
os.chdir(backupdir)

#need to call the plotting programme called matplotlib and
pylab.
#from pylab get stuff to doplotting
from pylab import figure, ioff, plt, subplots_adjust, rcParams
rcParams['mathtext.fontset']='stixsans'
pylab.rc('font', family='serif')
pylab.rc('font', serif='Ariel')

from matplotlib.pyplot import*
#from numpy import arange
matplotlib.rcParams.update({'font.size':12})

#from matplot lib get everything (*)
from matplotlib.pyplot import *

#unfitted C. crescentus periplasmic peroxiredoxin models

m=pysces.model('pprxping')
m.doStateShow()
m.doMca()
m.showCC()
a= m.scan_res
```

```
n=pysces.model('pprxredox')
n.doStateShow()
n.doMca()
n.showCC()
b = n.scan_res

o=pysces.model('pprxdimer')
o.doStateShow()
o.doMca()
o.showCC()
c = o.scan_res

#fitted C. crescentus periplasmic peroxiredoxin models


m=pysces.model('pprxpingfit')
m.doStateShow()
m.doMca()
m.showCC()
a= m.scan_res

n=pysces.model('pprxredoxfit')
n.doStateShow()
n.doMca()
n.showCC()
b = n.scan_res

o=pysces.model('pprxdimerfit')
o.doStateShow()
o.doMca()
o.showCC()
c = o.scan_res
```

Table S2 Comparison of flux control coefficients for each reaction in the peroxiredoxin activity models with *C. crescentus* and *E. coli* peroxiredoxin parameters from the literature and parameters determined by data fitting to *C. crescentus* peroxiredoxin dataset.

Reactions	Flux Control Coefficients
	Ping-Pong Enzyme Model
1	$C_{R1}^{JR1} = 0.0001$ $C_{R1}^{JR1} = 0.9999$
2	$C_{R1}^{JR2} = 0.0001$ $C_{R2}^{JR2} = 0.9999$
	Redox Couple Monomer Model
1	$C_{R1}^{JR1} = 0.003$ $C_{R2}^{JR1} = 0.413$ $C_{R3}^{JR1} = 0.584$
2	$C_{R1}^{JR1} = 0.003$ $C_{R2}^{JR1} = 0.413$ $C_{R3}^{JR1} = 0.584$
3	$C_{R1}^{JR1} = 0.003$ $C_{R2}^{JR1} = 0.413$ $C_{R3}^{JR1} = 0.584$
	Redox Couple Homodimer Model
1	$C_{R1}^{JR1} = 0.003$ $C_{R2}^{JR1} = 0.171$ $C_{R3}^{JR1} = 0.242$ $C_{R4}^{JR1} = 0.342$ $C_{R5}^{JR1} = 0.242$
2	$C_{R1}^{JR2} = 0.007$ $C_{R2}^{JR2} = 0.170$ $C_{R3}^{JR2} = -0.345$ $C_{R4}^{JR2} = 0.341$

	$C_{R5}^{JR2} = 0.827$
3	$C_{R1}^{JR3} = 0.001$ $C_{R2}^{JR3} = 0.171$ $C_{R3}^{JR3} = 0.656$ $C_{R4}^{JR3} = 0.343$ $C_{R5}^{JR3} = -0.172$
4	$C_{R1}^{JR} = 0.001$ $C_{R2}^{JR4} = 0.171$ $C_{R3}^{JR4} = 0.656$ $C_{R4}^{JR4} = 0.343$ $C_{R5}^{JR4} = -0.172$
5	$C_{R1}^{JR5} = 0.007$ $C_{R2}^{JR5} = 0.170$ $C_{R3}^{JR5} = -0.345$ $C_{R4}^{JR5} = 0.341$ $C_{R5}^{JR5} = 0.827$

2.3 *Saccharomyces cerevisiae* Tsa1 peroxiredoxin

2.3.1 Model Files

```
#Realistic modelling - TSA1 S. cerevisiae peroxiredoxin

#Ping-pong enzyme model

FIX: NADPH NADP H2O2 H2O

R1: NADPH + TrxSS = NADP + TrxSH
(kcat1*TR*(NADPH/Knadph)*(TrxSS/K1trxss))/((1+NADPH/Knadph)*(1
+TrxSS/K1trxss))

R2: TrxSH + H2O2 = TrxSS + H2O
(kcat2*Prx*(TrxSH/Ktrxsh)*(H2O2/K1h2o2))/((H2O2/K1h2o2)+(TrxSH
/Ktrxsh)+((TrxSH/Ktrxsh)*(H2O2/K1h2o2)))


#Kinetic Parameters = uM and s-1

kcat1 = 66
TR = 0.5
Knadph = 1.2
K1trxss = 4.4

kcat2 = 0.31
Ktrxsh =  25.5
K1h2o2 = 12

Prx = 1

#Species concentrations

NADPH = 150
NADP = 1
TrxSS = 2.5
TrxSH = 2.5
H2O2 = 30
H2O = 1
```

```
#Realistic modelling - TSA1 S. cerevisiae peroxiredoxin

#Redox couple monomer model

#Yeast Peroxiredoxin Modelling

#Model of the peroxiredoxin system with peroxiredoxin modelled
as a redox couple

FIX: NADPH NADP H2O2 H2O

R1: NADPH + TrxSS = NADP + TrxSH
(kcat1*TR*(NADPH/Knadph)*(TrxSS/K1trxss))/((1+NADPH/Knadph)*(1
+TrxSS/K1trxss))

R2: H2O2 + PrxSH = H2O + PrxSS
k2*H2O2*PrxSH

R3: PrxSS + TrxSH = PrxSH + TrxSS
k3*PrxSS*TrxSH

#Kinetic Parameters = uM and min

kcat1 = 66
TR = 0.5
Knadph = 1.2
K1trxss = 4.4

#approximated by kcat/km

k2 = 22
k3 = 3

#Species concentrations

NADPH = 150
NADP = 1
TrxSS = 2.5
TrxSH = 2.5
H2O2 = 30
H2O = 1
PrxSH = 0.5
PrxSS = 0.5
```

```
#Realistic modelling - TSA1 S. cerevisiae peroxiredoxin

#Redox couple homodimer model

#Yeast Peroxiredoxin Modelling

#Model of the peroxiredoxin system with peroxiredoxin modeled
as a homodimer redox couple

FIX: NADPH NADP H2O2 H2O

R1: NADPH + TrxSS = NADP + TrxSH
(kcat1*TR*(NADPH/Knadph)*(TrxSS/K1trxss))/((1+NADPH/Knadph)*(1
+TrxSS/K1trxss))

R2: PrxSHPrxSH + H2O2 = PrxSSPrxSH + H2O
k2*PrxSHPrxSH*H2O2*2

R3: PrxSSPrxSH + H2O2 = PrxSSPrxSS + H2O
k2*PrxSSPrxSH*H2O2

R4: PrxSSPrxSS + TrxSH = PrxSSPrxSH + TrxSS
k3*PrxSSPrxSS*TrxSH*2

R5: PrxSSPrxSH + TrxSH = PrxSHPrxSH + TrxSS
k3*PrxSSPrxSH*TrxSH

#Kinetic Parameters = uM and s

kcat1 = 66
TR = 0.5
Knadph = 1.2
K1trxss = 4.4

#approximated by kcat/km

k2 = 22
k3 = 3


#Species concentrations

NADPH = 150
NADP = 1
TrxSS = 2.5
TrxSH = 2.5
H2O2 = 30
H2O = 1
PrxSHPrxSH = 0.33
PrxSSPrxSH = 0.33
PrxSSPrxSS = 0.34
```

2.3.2 *In vitro* Datasets

1. 150 μM NADPH, 0.5 μM thioredoxin reductase, 30 μM hydrogen peroxide in a reaction buffer pH 7.0 at varying thioredoxin (0-15 μM) and peroxiredoxin 1 μM peroxiredoxin

```
# "[Trx]"  "V"
0     0.0051
0.1   0.0339
0.5   0.0457
1     0.0694
2.5   0.1153
5     0.1366
10    0.1381
15    0.1406
```

2. 150 μM NADPH, 0.5 μM thioredoxin reductase, 30 μM hydrogen peroxide in a reaction buffer pH 7.0 at varying thioredoxin (0-15 μM) and peroxiredoxin 2 μM peroxiredoxin

```
# "[Trx]"  "V"
0     0.0021
0.1   0.0539
0.5   0.0892
1     0.1539
2.5   0.1892
5     0.2344
10    0.2525
   15 0.2550
```

3. 150 μM NADPH, 0.5 μM thioredoxin reductase, 30 μM hydrogen peroxide in a reaction buffer pH 7.0 at varying thioredoxin (0-15 μM) and peroxiredoxin 0.5 μM peroxiredoxin

```
# "[Trx]"  "V"
0     0.00104
0.1   0.02157
0.5   0.02972
1     0.03414
2.5   0.04032
5     0.04301
10    0.04489
15    0.04592
```

2.3.3 Blue Native Page of TSA1

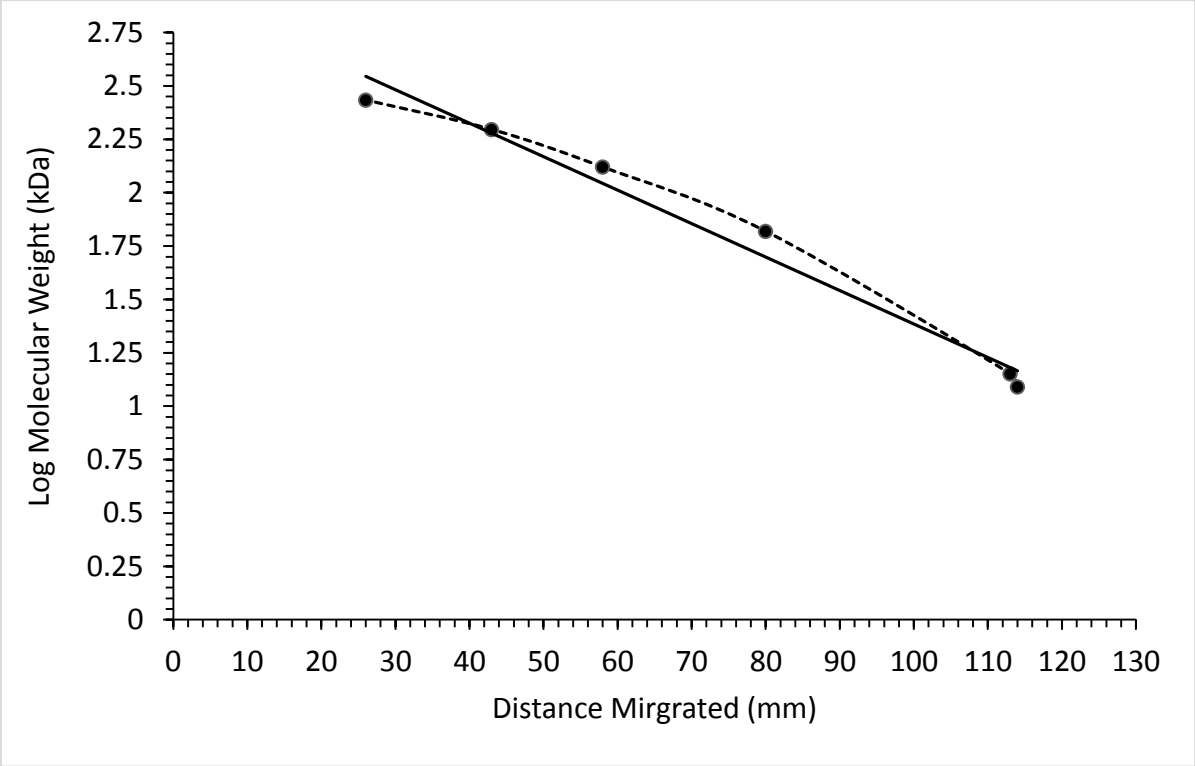

Figure S1 Standard curve for molecular weight sizing of native peroxiredoxin on a BN-PAGE 4-13% gradient gel using the molecular weight kit for non-denaturing PAGE (Sigma).